THE ADOPTION OF LASER MELTING TECHNOLOGY FOR THE MANUFACTURE OF FUNCTIONALLY GRADED COBALT CHROME ALLOY FEMORAL STEMS

Kevin Brian Hazlehurst BEng (Hons)

A thesis submitted in partial fulfilment of the requirements of the University of Wolverhampton for the degree of Doctor of Philosophy

July 2014

This work or any part thereof has not previously been presented in any form to the University or to any other body whether for the purposes of assessment, publication or for any other purpose (unless otherwise indicated). Save for any express acknowledgments, references and/or bibliographies cited in the work, I can confirm that the intellectual content of the work is the result of my own efforts and of no other person.

Signature ……

Date ……

Abstract

Total Hip Arthroplasty (THA) is an orthopaedic procedure that is performed to reduce pain and restore the functionality of hip joints that are affected by degenerative diseases. The outcomes of THA are generally good. However, the stress shielding of the periprosthetic femur is a factor that can contribute towards the premature loosening of the femoral stem. In order to improve the stress shielding characteristics of metallic femoral stems, stiffness configurations that offer more flexibility should be considered.

This research has investigated the potential of more flexible and lightweight cobalt chromium molybdenum (CoCrMo) femoral stems that can be manufactured using Selective Laser Melting (SLM). Square pore cellular structures with compressive properties that are similar to human bone have been presented and incorporated into femoral stems by utilising fully porous and functionally graded designs.

A three dimensional finite element model has been developed to investigate and compare the load transfer to the periprosthetic femur when implanted with femoral stems offering different stiffness configurations. It was shown that the load transfer was improved when the properties of the square pore cellular structures were incorporated into the femoral stem designs.

Factors affecting the manufacturability and production of laser melted femoral stems have been investigated. A femoral stem design has been proposed for cemented or cementless fixation. Physical testing has shown that a functionally graded stem can be repeatedly manufactured using SLM, which was 48% lighter and 60% more flexible than a traditional CoCrMo prosthesis.

The research presented in this thesis has provided an early indication of utilising SLM to manufacture lightweight CoCrMo femoral stems with levels of flexibility that have the potential to reduce stress shielding in the periprosthetic femur.

Acknowledgements

Firstly, I would like to thank Dr Chang Jiang Wang and Prof Mark Stanford for their supervision, guidance and support that they offered throughout the duration of this research. Their encouragement and expertise in orthopaedic biomechanics and additive layer manufacturing was crucial for the successful completion of this project. I would also like to thank Prof Kevin Kibble for his advice and for providing the financial support to enable my attendance at conferences.

I am extremely grateful to Mr Iain Lyall for arranging the manufacture of the components and test samples that were essential for the completion of this project. Thanks must also go to Mr Colin Durnall and Mr James Stamps for their assistance in sample preparation and in realising the physical tests.

I would like to acknowledge the Faculty of Science and Engineering at the University of Wolverhampton for their financial support and for providing me with the opportunity to study for this prestigious award.

I would like to thank all my family, especially my patient wife Samantha, for providing financial and emotional support and for believing in me throughout my years of study. Finally, I would like to dedicate this thesis to my son Todd, who I hope to make proud by studying for this award.

Table of Contents

List of Figures

List of Tables

Nomenclature

APDL	Ansys Parametric Design Language
ALM	Additive Layer Manufacturing
BWm	Body Weight metres
CAD	Computer Aided Design
CMM	Co-ordinate Measuring Machine
CoCrMo	Cobalt Chromium Molybdenum
CT	Computed Tomography
DMLS	Direct Metal Laser Sintering
EBM	Electron Beam Melting
EDM	Electro Discharge Machining
EOS	Electro Optical Systems
FDS	Fully Dense Stem
FEA	Finite Element Analysis
FGM	Functionally Graded Material
GPC	Functionally graded femoral stem with axially graded stiffness
GPS	Fully porous femoral stem with axially graded stiffness
HA	Hydroxyapatite

LENS^{TM}	Laser Engineered Net Shaping
µCT	Micro Computed Tomography
OPC	Functionally graded stem with orthotropic material properties
OPS	Fully porous femoral stem with orthotropic material properties
PC	Functionally graded femoral stem with uniform stiffness
PS	Fully porous femoral stem with uniform stiffness
PMMA	Polymethylmethacrylate
RM	Rapid Manufacturing
RP	Rapid Prototyping
SED	Strain Energy Density
SEM	Scanning Electron Microscope
SLM	Selective Laser Melting
STL	Standard Tessellation Language
THA	Total Hip Arthroplasty
UHMWPE	Ultra High Molecular Weight Polyethylene

Glossary

Anteversion	The angular difference between the femoral neck axis and the transcondylar axis of the knee
Arthroplasty	A surgical procedure that replaces a damaged joint with artificial components
Distal	Anatomically located far from the joint attachment
Diaphysis	Shaft of a long bone
Epiphysis	The end of a long bone that contains cancellous bone
In vitro	Experiments or observations performed in a controlled environment outside a living organism
In vivo	Experiments or observations performed within a living organism
Metaphysis	Transitional region of the bone where the diaphysis and epiphysis form
Necrosis	The death of a tissue due to a lack of blood supply
Osteoarthritis	A degenerative joint disease that can cause pain, swelling, stiffness and ultimately, a change in bone structure.
Periprosthetic	A region local to the prosthesis
Prosthesis	An artificial substitute for a missing body part
Proximal	Anatomically located local to the joint attachment

Chapter 1 Introduction

1.1 Background

Total Hip Arthroplasty (THA) is an orthopaedic procedure that is performed to reduce pain and to restore the functionality of hip joints that are affected with degenerative diseases such as osteoarthritis. THA involves the surgical removal of the head and neck of the proximal femur and the cartilage and subchondral bone in the acetabulum. A new joint is then created by inserting a metallic femoral stem and cup into the medullar of the femur and the acetabulum respectively. Across England, Wales and Northern Ireland in 2012 there were 76,448 cases of primary THA performed, with an additional 10,040 cases of revision surgery required (National Joint Registry, 2013). This figure represents a 16% increase in revision rates when compared to the previous year. Additionally, it is considered that with younger and more active individuals requiring THA, revision rates could continue to rise due to an increased life expectancy. Due to these trends, it has been discussed that the prospect of revision surgery should be considered as a factor when referring patients for primary THA (Parsons and Sonnabend, 2004).

Postoperatively, the load transfer to the proximal femur is reduced following the insertion of metallic femoral stems that are much stiffer than the bone that they replace. This change to the mechanical loading environment of the femur promotes a phenomenon known as stress shielding. This phenomenon causes a reduction in periprosthetic bone density, which is especially prevalent in the proximal-medial femur (Karachalios *et al.,* 2004). Stress shielding can contribute to the premature failure of THA through mechanisms such as aseptic loosening, stem migration and periprosthetic bone fractures, all of which promote the need for revision surgery (Kroger *et al.,* 1998).

Therefore, it would be beneficial if femoral stems could be manufactured with characteristics that would assist in the reduction or elimination of stress shielding.

Over 20 years ago, it was theoretically proposed that more flexible femoral stems could alleviate stress shielding and help to preserve periprosthetic bone stock (Huiskes *et al*., 1992; Kuiper and Huiskes, 1997). More recently, it was suggested that stiffness-matching strategies between the femoral stem and the host bone should be investigated for future designs (Ebrahimi *et al*., 2012). However, it is considered that limitations associated with the traditional manufacturing methods have restricted the investigation of stiffness matching strategies for biocompatible alloys.

For THA, femoral stems are either monoblock or modular in design. Monoblock stems are manufactured from cobalt chrome alloys in a single piece, whereas modular stems often consist of a titanium alloy femoral stem that is mechanically connected to a cobalt chrome head by using a taper junction. The elastic modulus of the titanium alloy Ti-6Al-4V is approximately half that of cobalt chromium molybdenum (CoCrMo) and is often preferred in this instance for reducing stress shielding in periprosthetic bone. Additionally, modular stems offer the patient and surgeon some degree of customisation with respect to leg length, offset and version (Sporer and Paprosky, 2006). However, concerns are associated with modular designs due to the mechanical failure of the taper junction (Sotereanos *et al*., 2013) and because of fretting corrosion (Viceconti *et al*. 1997). Metal on metal wear debris can be released from the taper junction and this has been linked to the identification of adverse soft tissue reactions (Langton *et al*., 2012). The subsequent release of cobalt and chromium ions into the blood stream has been considered to promote the aseptic loosening of orthopaedic implants (Gruber *et al*., 2007). Therefore, when considering the problems associated with modular designs, it would be beneficial if alternative monoblock femoral stem designs were available.

1.2 Problem statement

The introduction of metal powder based Additive Layer Manufacturing (ALM) systems such as Selective Laser Melting (SLM) and Electron Beam Melting (EBM) have provided capabilities to manufacture components from a single alloy with tailored mechanical properties. Therefore, orthopaedic implants can be manufactured with mechanical properties that are much closer to those of human bone, when compared to traditional metallic implants (Harrysson *et al.*, 2008; Murr *et al*., 2010; Bertol *et al*., 2010; Parthasarathy *et al*., 2011). The mechanical properties of femoral stems can be tailored by incorporating porous cellular structures into their designs. The potential application of porous titanium alloy femoral stems has been investigated using numerical methods. Finite Element Analysis (FEA) has been performed and a reduction in the stress shielding of periprosthetic bone was observed (Harrysson *et al*., 2008; Yan *et al*., 2011; Arabnejad Khanoki and Pasini, 2013). Literature investigating the mechanical behaviour and characteristics of titanium alloy open cellular structures manufactured using ALM is readily available. However, the mechanical behaviour and characteristics of CoCrMo cellular structures manufactured using SLM is not currently fully understood.

The School of Engineering at the University of Wolverhampton possesses several powder based ALM systems, including the EOSINT M270 Xtended Direct Metal Laser Melting machine. This machine has the ability to produce near net shape components from biocompatible alloys such as CoCrMo and Ti-6Al-4V. Given this, it was assumed that this manufacturing facility could be utilised to realise alternative designs for lightweight CoCrMo femoral stems, which offer more desirable stiffness characteristics when compared to traditional bulk metallic implants. Hence, this enabled the investigation of stiffness configurations that can potentially alleviate stress shielding in the periprosthetic femur.

1.3 Research aim and objectives

The overall aim of this research was to propose alternative designs for CoCrMo femoral stems that can be manufactured using SLM. The femoral stems should exhibit clinically suitable design characteristics and offer stiffness configurations that will reduce stress shielding in the periprosthetic femur. The design proposals were justified from the results that were observed when adopting a combination of physical testing and numerical analysis.

The main objective of the research presented was to investigate the mechanical behaviour and manufacturability of laser melted CoCrMo femoral stems with varying stiffness configurations. This was achieved through the following specific objectives:

- Investigate the compressive behaviour of laser melted square pore CoCrMo cellular structures, which were designed with varying density in order to provide mechanical properties that are much closer to those of human bone.
- Investigate the load transfer to the periprosthetic femur using three dimensional finite element analysis. CoCrMo femoral stems offering more flexible stiffness configurations were considered that utilised fully porous and functionally graded designs.
- Investigate the flexural behaviour of functionally graded and fully dense CoCrMo femoral stems when subjected to cantilever bending. Physical and numerical methods were utilised to determine the stiffness of the different designs.
- Investigate the factors that can affect the manufacturability and mechanical behaviour of laser melted CoCrMo femoral stems.

1.4 Structure of the thesis

This thesis is composed of nine chapters, with the content as follows:

Chapter 1 states the background, research question and the aim and objectives.

Chapters 2 and 3 comprise the literature review and present the basis for the work presented. Firstly, the fundamental topics associated with THA are discussed. Then ALM is introduced, where the advantages and limitations of utilising ALM for orthopaedic applications are presented. Finally, studies that have produced or modelled additive manufactured femoral stems have been critically evaluated within the context of the aim and objectives of this work.

Chapter 4 investigates the compressive properties of laser melted square pore CoCrMo cellular structures of varying volumetric porosity. Physical test data was compared to an analytical model and numerical results that were obtained using the finite element method.

Chapter 5 uses the finite element method to investigate the load transfer to the periprosthetic femur. The mechanical properties of square pore cellular structures were utilised to create fully porous and functionally graded CoCrMo femoral stems. Ten different stiffness configurations were analysed and compared to a fully dense stem, which was used as a benchmark for comparison throughout.

Chapter 6 investigates the flexural characteristics of functionally graded and fully dense CoCrMo femoral stems when subjected to cantilever bending. Physical test data was compared to numerical results obtained using the finite element method.

Chapter 7 investigates and discusses factors that are associated with the manufacturability and mechanical behaviour of laser melted CoCrMo femoral stems.

The investigation included residual stress, internal structural defects, orientation of the cellular structure and part with respect to the build platform and the removal of unprocessed and partially melted powder particles.

Chapter 8 proposes cemented and cementless femoral stem designs based upon the results and observations from the work undertaken.

Chapter 9 states the conclusions of this work and indicates the areas for future research.

1.5 Original contribution to knowledge

The original contributions to the body of knowledge from this research are:

- The compressive properties of laser melted square pore CoCrMo cellular structures were investigated, in order to provide structures that exhibit similar stiffness and strength characteristics when compared to the human femur.
- The finite element method was used to investigate the load transfer to the periprosthetic femur when implanted with CoCrMo femoral stems that incorporate the mechanical properties of laser melted square pore cellular structures.
- The flexural behaviour of functionally graded CoCrMo femoral stems was investigated, in order to provide lightweight femoral stems that exhibit more flexibility than a traditional fully dense prosthesis.
- The influence of the strut size and porosity of laser melted square pore CoCrMo cellular structures was investigated in relation to the repeatable mechanical behaviour of functionally graded CoCrMo femoral stems.

- Factors relating to the manufacturability of laser melted CoCrMo femoral stems have been identified and critically evaluated within the context of producing functionally graded designs.

The above points collectively contribute to the body of knowledge. However, it is considered that this is an original investigation into the adoption of laser melting technology for the manufacture of functionally graded cobalt chrome alloy femoral stems.

Chapter 2 Total Hip Arthroplasty (THA)

2.1 Introduction

This chapter introduces the fundamental topics associated with THA. Firstly, the anatomy and loading of the hip joint are described, along with characteristics and mechanical properties of human bone. Femoral stem materials, designs and methods of fixation are also described. Lastly, the mechanisms of femoral stem failure are presented.

2.2 The hip joint

2.2.1 Anatomy and physiology

The hip joint, scientifically referred to as the acetabulofemoral joint is a ball and socket joint formed by the femoral head and the acetabulum of the pelvis. The pelvis consists of three bones that fuse together in early adulthood; these are the ilium, ischium and pubis. The proximal portion of the femur consists of the femoral head that is spherical in shape, a cylindrical femoral neck and two bony landmarks that are used for muscle attachment, referred to as the greater and lesser trochanters. The anatomy of the proximal femur is shown in Figure 2.1.

In a healthy hip joint, cartilage covers the top of the femoral head and the acetabulum. The cartilage provides shock absorption and a free moving articulating joint with a smooth surface. Three ligaments provide stability in the hip joint; these are the iliofemoral, pubofemoral and the ischiofemoral ligaments. The iliofemoral ligament connects the ilium to the femur and provides the main constraint on the hip joint. The ischiofemoral ligament joins the ischium to the femur on the posterior side of the joint. The pubofemoral ligament connects the pubis and the femur, also blending in with the iliofemoral ligament.

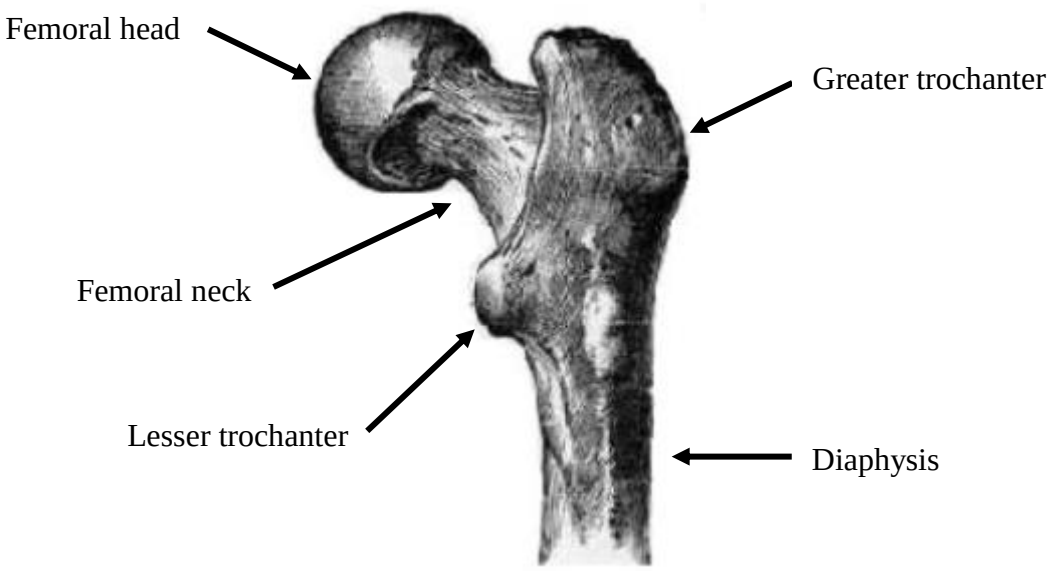

Figure 2.1 Anatomy of the proximal femur (Wheeless, 2011).

The muscles of the hip joint are numerous and many muscles are often involved to provide any single movement of the joint. The movements of the hip joint are flexion, extension, abduction, adduction, rotation and circumduction, all of which are described in terms of the anatomical planes of the human body, which are shown in Figure 2.2.

- Flexion is the movement of the femur in the sagittal plane in the anterior direction, whereas extension is the movement of the femur in the posterior direction.
- Abduction is the movement of the femur in the frontal plane laterally, whereas adduction is the movement of the femur medially.
- Rotation of the hip joint is a rotating action of the anterior surface of the femur in its longitudinal axis. Medial rotation occurs internally towards the body and lateral rotation is a movement away from the body.
- Circumduction is a combination of flexion, extension, abduction and adduction.

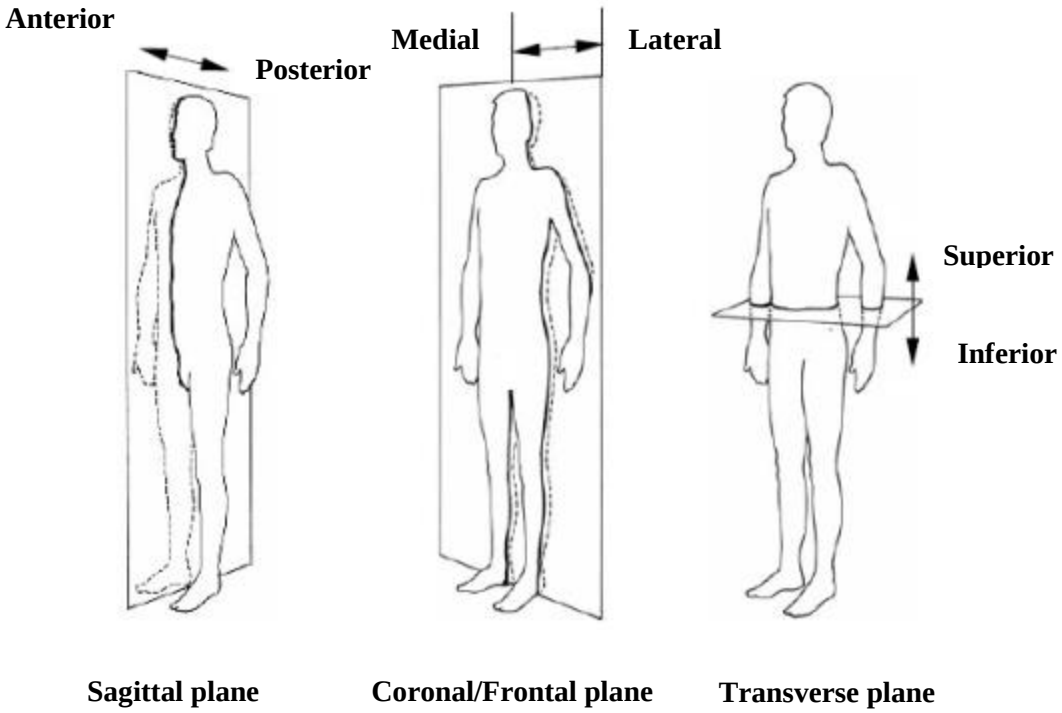

Figure 2.2 Anatomical planes of the human body (Shi, 2007).

The main muscles associated with the common movements of the hip joint have been described by Thompson and Floyd (2011), where flexion is controlled by the ilopsoas and pectineus, and extension is controlled by the gluteus maximus. Abduction is controlled by the gluteus minimus and medius, and adduction is controlled by the bevis, longus and magnus.

2.2.2 Forces on the hip joint

Hip joint forces need to be quantified in order to perform physical experiments or numerical analysis in a realistic and accurate manor. The loading of the hip joint was initially studied using simplified muscle models and optimisation techniques based upon gait analysis data (Crowninshield *et al*., 1978; Pedersen *et al*., 1987). However, the most accurate method for determining the magnitude of hip joint forces is by using instrumented prostheses. Bergmann *et al.* (1988) utilised a telemetrised femoral stem to

measure hip joint forces and to some extent instigated in vivo measurement. Since then, instrumented implants have been utilised to measure hip joint forces when performing general daily activities. It is evident that the magnitude of hip joint forces varies in accordance to the level of activities that are being performed by the individual (Bergmann *et al*., 1993; Bergmann *et al*., 2001; Heller *et al*., 2001). It has been approximated that the hip joint is subjected to in excess of 1 million gait cycles every year (Morlock *et al*., 2001). When walking normally in the single stance phase of gait, the average peak hip joint reaction force has been reported to be in the region of 2.5 times body weight (Bergmann *et al*., 2001). Heller *et al.* (2005) developed a validated musculoskeletal model in order to provide a more accurate representation of in vivo loading conditions and reported that the abductor muscle generated a peak force of approximately one's own body weight when walking.

2.3 The structure and mechanical properties of bone

The quality and quantity of bone available for orthopaedic implantation is an important factor that can determine the success of joint arthroplasty (Wirth *et al*., 2011). Therefore, in order to investigate the performance of orthopaedic implants, the characteristics and mechanics of human bone need to be understood.

Bones form the major component of the human musculoskeletal system, and their duty is to support body weight, resist mechanical loading, perform motion and protect the body's internal organs. In addition to this, bones are important for calcium metabolism and for providing space to allow the generation of blood cells.

Bone is a material with a matrix consisting of both organic and inorganic components. The organic component of bone is primarily made up of collagen; this defines the bones shape and helps to contribute to the resistance of tensile loading. The inorganic

components are hydroxyapatites, typically consisting of calcium phosphates that provide resistance against compressive loading.

The human skeleton consists of two types of bone, cortical and cancellous or trabecular bone. The differentiation between these two types of bone is based upon density and porosity. It is thought that the transition between cortical and cancellous bone occurs at approximately 30% porosity (Brown *et al*., 1998). In the human skeleton, cortical bone is generally found where the applied mechanical stresses are higher and cancellous bone where the stresses are lower.

Figure 2.3 shows a cross section of a natural proximal femur, where the distribution of the cortical and cancellous bone can be observed. The individual trabeculae of the cancellous bone are naturally aligned to optimise the load transfer from the femoral head and neck to the diaphysis or shaft of the femur. The diaphysis of the femur consists of a hollow cylindrical cross section of cortical bone, which transfers the load from the hip to the knee.

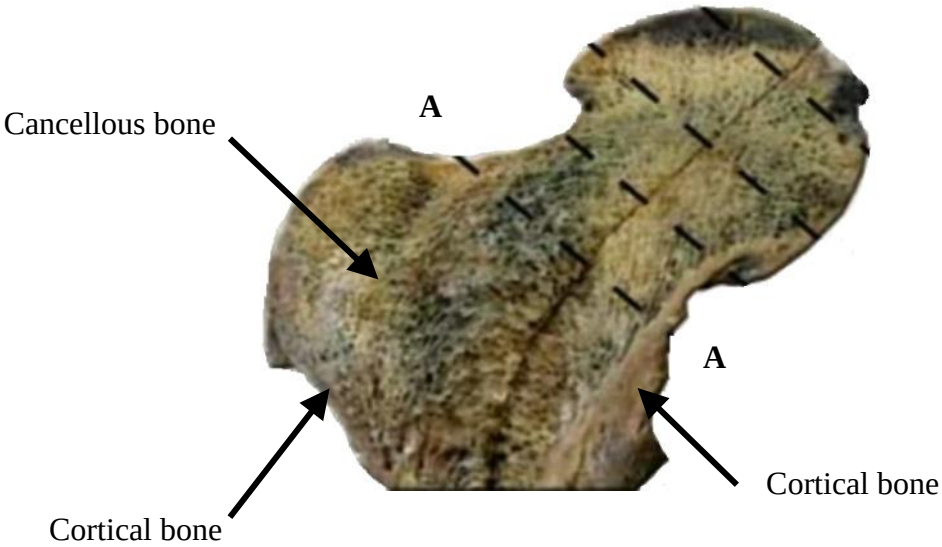

Figure 2.3 The frontal cross section of a natural proximal femur (McMinn, 2012).

2.3.1 Mechanical properties of bone

Bones must be strong enough to ensure that fractures do not occur under events of what can be classed as normal physiological loading. The mechanical properties of bone are dependent upon the presence of the mineral phase within the materials matrix. The mineral content and microstructure of bone are distributed in a heterogeneous manner, and the stress-strain laws of cortical and cancellous bone are sensitive to the bones porosity and microstructural alignment. The elastic modulus of femoral cortical bone has been reported to be 17 GPa in the longitudinal direction and 11.5 GPa in the transverse direction (Reilly and Burstein, 1975). The values presented in Table 2.1 show that cortical bone is a material that exhibits anisotropic behaviour.

Table 2.1 Mechanical properties of cortical bone (Reilly and Burstein, 1975).

Mechanical Property	Longitudinal axis	Transverse axis
Youngs modulus (GPa)	17	11.5
Ultimate tensile strength (MPa)	133	51
Ultimate compressive strength (MPa)	193	133
Ultimate strain (%)	3.1	0.7

The anisotropy in cortical bone is caused by the alignment of osteons along the longitudinal axis of long bones such as the femur, whereas, the anisotropy of cancellous bone is determined by the orientation of the individual trabecular. The elastic modulus of cancellous bone is less predictable than cortical bone and can vary between 0.1 GPa and 4.5 GPa dependent upon anatomical location (Turner *et al*., 1990).

2.4 Bone remodelling theory

Bone is a vascular structure that responds to both hormonal and mechanical signals, meaning that bone can functionally adapt to the environment that it is located within. Therefore, bone adjusts its mass and architecture according to the mechanical loading that it is subjected to (Huiskes *et al*., 2000). For this reason, bone remodelling has become a key topic of consideration associated with the design, analysis and performance of femoral stems.

Wolff (1986) introduced the theory known as 'Wolff's Law', stating that bone changes and adapts according to the mechanical stresses and strains applied to it, meaning that new bone forms where it is needed and resorbs where it is not needed. The physical changes in bone take place slowly due to the action of bone cells. The formation of osteoblasts results in bone apposition (formation of bone) and osteoclasts results in bone resorption (removal of bone). This phenomenon of bone constantly changing is described as bone remodelling and can be described by either external or internal remodelling. External remodelling is measured by a change in the geometry of the bone and internal remodelling is measured by a change in bone mineral density, and hence porosity.

Following the initial work by Wolff, there have been numerous studies performed on bone remodelling. Cowin and Hegedus (1976) developed one of the first mathematical models describing how bone remodelling could be predicted based upon general continuum mechanical principles. Further work in this area was performed by Huiskes *et al.* (1987) and Weinans *et al.* (1992) who described bone remodelling mathematically by using the finite element method. In both cases, finite element models were used to predict bone resorption in the femur by using Strain Energy Density (SED) as the mechanical stimulus for feedback. This enabled the determination of bone shape and

density adaptions in response to mechanical loading scenarios. The method of using SED as the mechanical stimulus to simulate bone remodelling is common within the literature (Huiskes *et al*., 1992; Kuiper and Huiskes, 1997; Yan *et al*., 2011; Gong *et al*., 2012; Arabnejad Khanoki and Pasini, 2013).

Where SED is equivalent to $u = \frac{1}{2}\sigma.\varepsilon$, when σ is the stress tensor and ε is the strain tensor. From this relationship, it can be observed that an increase in stress within the periprosthetic bone is favourable for increasing the mechanical stimulus and hence bone remodelling.

2.5 Femoral stem materials

Materials that are used for orthopaedic applications are commonly referred to as biomaterials. Any materials that are selected for orthopaedic applications must be biocompatible and be able to withstand the mechanical loads applied to them during daily activities. It is considered that biomaterials need to be able to resist damage from the human body, whilst not subjecting any damage to the body itself. Orthopaedic implants are typically manufactured from three groups of materials, these being metals, polymers and ceramics. Total joint arthroplasties are commonly formed with a combination of two or more of these material groups.

Polymers are often utilised for the articulating surface of the acetabular component that is used in THA. The most common polymer used for articulates is UHMWPE (Ultra High Molecular Weight Polyethylene), which is a highly cross-linked form of polyethylene that possesses good wear characteristics and a low coefficient of friction. For this research, the focus has been applied to metals that are specifically used for the manufacture of femoral stems.

2.5.1 Metals

Stainless steel was one of the first metals to be used in orthopaedics, and the alloy 316L is the most commonly utilised. Over recent years, the use of this alloy for joint replacement has diminished slowly due to it having a lower strength and less resistance to corrosion when compared to other biocompatible metals. However, from an economic perspective this alloy is superior to others and is utilised for fracture fixation devices, screws and intramedullary nails (Gil *et al*., 2006).

The other common metals used for femoral stems are titanium and cobalt chrome based alloys. Titanium alloys were originally developed primarily for use in the aerospace industry and are now frequently utilised for biomedical applications. The most common titanium alloy used in orthopaedics is Ti-6Al-4V. This alloy has become a popular material for orthopaedic implants because it is less dense and more flexible than other implantable alloys. Generally, titanium and its alloys are preferred to other alloys such as cobalt chrome and stainless steel for orthopaedic applications due to their superior biocompatibility, flexibility, specific strength and corrosion resistance (Niinomi, 2002). Despite this, there are problems associated with the use of titanium alloys in terms of their poor wear characteristics and notch sensitivity. Hence, the applications of titanium alloys are limited to where the importance of wear resistance is minimal.

The most common cobalt chrome based alloy used for the manufacture of femoral stems is cobalt chromium molybdenum (CoCrMo). This alloy can be utilised in a cast or wrought form, with the latter often being preferred for orthopaedic applications, due to its superior strength and toughness (Marti, 2000). CoCrMo is considered the strongest, hardest and most fatigue resistant of all the metals used for load bearing implants, but its relatively high elastic modulus of around 200 GPa is nearly twice that of Ti-6Al-4V. This can create a stiffness mismatch with femoral cortical bone to the order of twelve

times. This stiffness mismatch promotes the stress shielding phenomenon, which is described in Section 2.8.3. Therefore, implant stiffness is critical if metallic alloys are to be used and minimum levels of stress shielding are to be attained (Niinomi, 2008).

2.5.2 Functionally graded and composite materials

The concept of a Functionally Graded Material (FGM) is to create a composite by grading the microstructure of a material, or to vary the microstructure of one material to another across a specific gradient (Bever and Duwez, 1972).

From a medical perspective, the concept of functional gradation is common in living tissue such as bone. Bone possesses a stiff dense outer structure (cortical bone) with a composition that gradually changes to a less stiff porous internal structure (cancellous bone). Hence, in order to optimise an orthopaedic implants response to external loading it has previously been hypothesised that the optimal structure should have a similar gradation to bone (Pompe *et al*., 2003).

Functionally graded and composite femoral stems have been theoretically investigated using the finite element method. Simoes and Marques (2005) proposed a stem with a CoCrMo core that was encased by a flexible composite material. Whereas, Boudeau *et al.* (2012) proposed an alternative design consisting of a carbon fibre reinforced polyetheretherketone composite material. Both of these studies indicated that the load transfer to the proximal femur was improved by the introduction of more flexible stiffness configurations. Gong *et al.* (2012) used a simplified two dimensional axisymmetric finite element model and mathematical optimisation techniques to investigate the performance of a titanium alloy-hydroxyapatite functionally graded material. It was observed that the elastic modulus of the stem could be axially graded so that it was stiffer proximally whilst having a much lower elastic modulus distally. This resulted in a reduction in proximal stress shielding without compromising the bone-

implant interface stability. More recently, Oshkour *et al.* (2014) investigated stainless steel-hydroxyapatite and titanium alloy-hydroxyapatite functionally graded femoral stems, where a 22% increase in SED was observed in the proximal femur.

The above studies have highlighted the potential of utilising functionally graded and composite materials. However, it may be considered that the introduction of more flexible femoral stems for clinical use has been delayed due to limitations that have been associated with traditional manufacturing processes, and due to the higher costs that have historically been associated with the production of functionally graded and composite materials.

2.6 Femoral stem designs

2.6.1 Historical developments

It is believed that the first THA was performed by Philip Wiles in 1938, using stainless steel components (Wiles, 1958). A femoral stem was mechanically fixed to the outside of the femur as shown in Figure 2.4. However, the results were unsatisfactory in this instance as the fixings that were used for attachment purposes fractured or became loose (Wiles, 1958). In the 1950's, Kenneth McKee started implanting monoblock Thomson femoral stems. Stainless steel components were used initially and a high incidence of loosening was observed after a one year review (McKee and Watson-Farrah, 1966). Following this, alternative materials were considered for the manufacture of femoral stems. In 1953, a modified Thomson prosthesis with a smaller femoral head was manufactured completely from a cobalt chrome alloy and this performed well in comparison to its stainless steel counterparts (McKee and Watson-Farrah, 1966). Ring (1968) then introduced what is thought to be the first cementless components for THA. However, in the 1970's, although the McKee and Ring prostheses continued to function

well, they were replaced with designs that were generated by Sir John Charnley (Gomez and Morcuende, 2005).

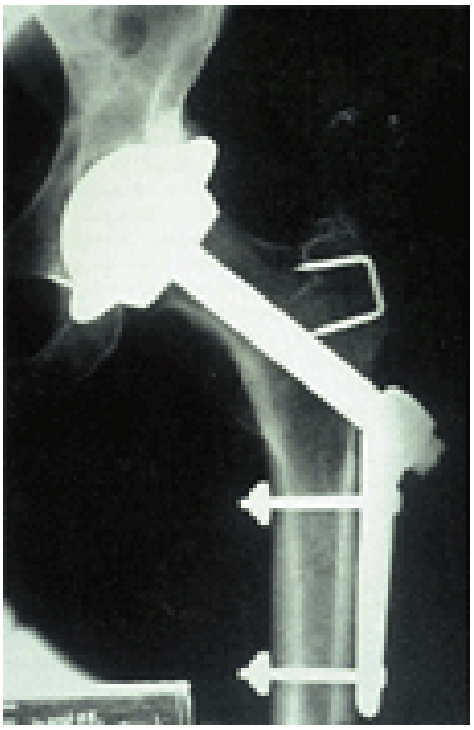

Figure 2.4 Radiograph showing the early THA by Philip Wiles (Wiles, 1958).

2.6.2 Current trends

The selection of femoral stems for THA is ultimately determined by the preference of the orthopaedic surgeon and there is a vast selection of cemented and cementless implants available globally. Trends have been reported in the National Joint Registry for England, Wales and Northern Ireland describing the most popular cemented and cementless femoral stems that are used for primary THA. The Exeter V40 stem is the most favoured cemented prosthesis and has dominated selection for the past 10 years (National Joint Registry, 2013). The most popular cementless stem is the Depuy Corail fully hydroxyapatite coated titanium alloy stem. This stem has been used in over 40% of the cementless arthroplasties performed over the past 5 years across England, Wales and Northern Ireland (National Joint Registry, 2013).

2.6.3 Modular versus monoblock femoral stems

The design of femoral stems has varied historically and to date has been dependent upon the implant manufacturer (Mai *et al*., 2010). To simplify matters femoral stems are described as either monoblock, where the stem and head is a single piece, or modular, where the stem and the head are separate components that are interlocked mechanically by a taper junction, as shown in Figure 2.5. Titanium alloys are often chosen as the preferred material for modular femoral stems, due to the materials relatively low stiffness, and are often coupled with a cobalt chrome or ceramic femoral head. However, the poor wear characteristics of titanium alloys rule out any applications for articulation and therefore monoblock stems are generally manufactured from cobalt chrome alloys.

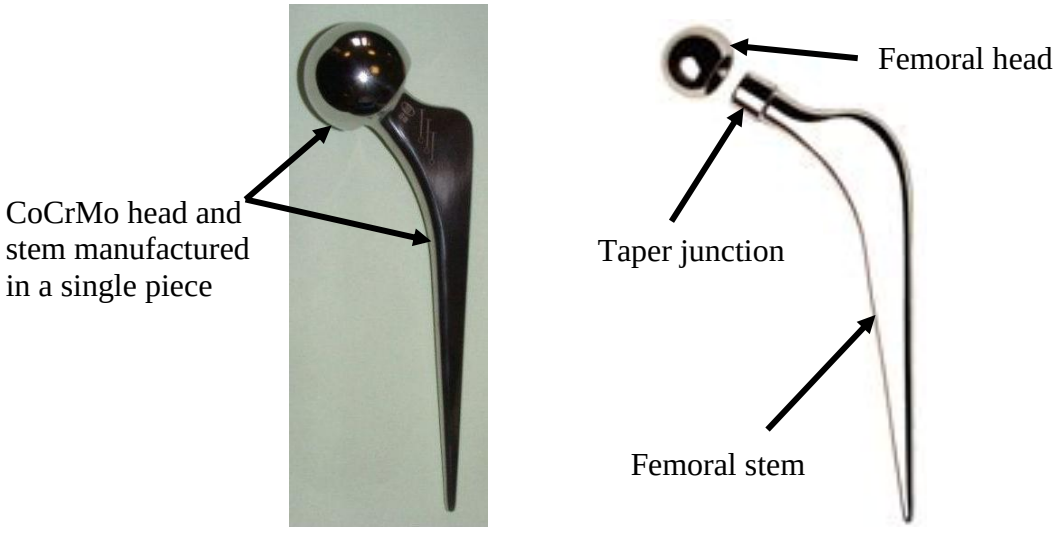

Figure 2.5 (a) A femoral stem with a monoblock design (Cash *et al*., 2010) (b) A femoral stem with a modular design (Stryker, 2013).

Modular stems offer the patient adjustment and some degree of customisation with respect to femoral head offset, version and leg length (Sporer and Paprosky, 2006). In

contrast to this, recent concerns have been associated with modular designs due to the mechanical failure of the taper junction (Sotereanos *et al*., 2013) and due to the identification of adverse soft tissue reactions that have been linked to the metal on metal wear debris that is released from the taper junction (Langton *et al*., 2012).

2.7 Femoral stem fixation

2.7.1 Cemented fixation

Femoral stems can be cemented into place using the acrylic polymethylmethacrylate (PMMA), which is mixed during surgery and is used to create a bond between the implant and the bone itself. This method of fixation is successful for older less active individuals, with post-operative survivorship rates of up to 20 years being reported (Kavanaugh *et al*., 1994; Smith *et al*., 1998). A caveat is that heat is generated during the curing stage of the PMMA and this can promote a condition called thermal necrosis, which can damage the periprosthetic tissue and compromise the stability of the implant.

2.7.2 Cementless fixation and bone ingrowth

Cementless fixation is where the femoral stem is press fitted into the bone in order to establish biological fixation through bone ingrowth. This method of fixation has historically been preferred for younger, more active individuals who possess adequate bone stock for the procedure (Dorr *et al*., 1990). Contrary to this, a more recent study has indicated that cementless fixation has the potential to be a safe, viable option in patients over the age of 75 years old (Meftah *et al*., 2013). Femoral stems that are used for cementless fixation require a rough or porous surface in order to encourage bone ingrowth during the healing progress.

Porous substrates have historically been used to provide biological fixation at the bone-implant interface. Roughened titanium, cobalt chrome or titanium beads, plasma

sprayed titanium and the depositing of bioactive materials such as hydroxyapatite (HA) have been applied to the surface of femoral stems. HA coated implants generally achieve good results; with Aebli *et al.* (2003) describing that HA coated implants form a bond with the host bone that can be compared to the strength of cortical bone. Despite this, there are concerns with using HA coatings in terms of the brittleness of the material, the strength of bond between the HA and the metal implant, and due to the condition of the bone-implant interface following the resorption of the HA coating (Manley *et al*., 1998). The resorption of the HA coating can be problematic, as over time the coating can be replaced by new bone on the implant surface and the mechanical interlocking between the HA and the bone may be negligible (Geesink *et al*., 1988).

2.7.3 Comparison between cemented and cementless fixation

Hearn *et al.* (1995) commented that cemented and cementless femoral stems used in THA performed equally well, and that the enthusiasm for moving towards cementless fixation was justified. Mont *et al.* (1999), in their 5-year follow up study also found that the performance of cementless femoral stems was comparable to cemented stems. In contrast to this, Weidenhielm *et al.* (1995) found that cemented stems performed well past 14 years, whereas cementless stems failed at around 5 years. However, the stems compared in this study were different in material and geometry, which could have been a possible limitation. More recently, cemented femoral stems were found to have a 12-year survival rate of 98.3% (Aubault *et al.*, 2013). Additionally, during a minimum of 10 years follow up study a survival rate of 97.2% was observed at 16 years for cementless prostheses (Hwang *et al*., 2012).

When comparing femoral stem fixation, it is still not clear from the reviewed literature which method yields optimal results. However, current trends are favouring cementless fixation (National Joint Registry, 2013). This trend is shown in Figure 2.6, where it can

be observed that the cross over from cemented to cementless fixation took place in 2009. This indicates that cementless fixation of femoral stems is currently the preferred choice in the UK.

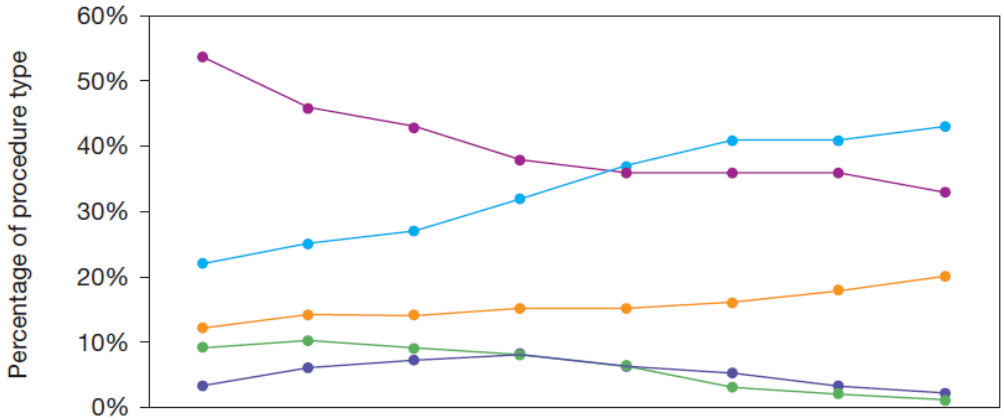

Year	2005	2006	2007	2008	2009	2010	2011	2012
Cemented	54%	46%	43%	38%	36%	36%	36%	33%
Cementless	22%	25%	27%	32%	37%	41%	41%	43%
Hybrid	12%	14%	14%	15%	15%	16%	18%	20%
Resurfacing	9%	10%	9%	8%	6%	3%	2%	1%
Large head metal-on-metal (≥36mm)	3%	6%	7%	8%	6%	5%	3%	2%

Figure 2.6 Types of THA procedures that have been performed in England, Wales and Northern Ireland between 2005 and 2012 (National Joint Registry, 2013).

2.8 Failure of femoral stem fixation

From an engineering perspective, the failure of THA is caused by the mechanical failure of implanted components or through the failure of fixation. There are also surgical complications such as infection, blood clots and nerve damage that need to be considered. However, these cannot be improved from an engineering perspective; therefore, they have not been focussed upon in this research.

The failure of femoral stem fixation is multifactorial; however, it can be thought that aseptic loosening is the main contributor. Aseptic loosening can be caused through

implant wear debris, induced relative micro motion at the bone-implant interface and through the stress shielding of the periprosthetic bone.

2.8.1 Wear debris

In THA, UHWMPE is often used as the bearing surface for the acetabulum. The articulating motion of the hip joint causes polymeric wear debris to be generated through fretting or fragmentation. These sub-micron particles can cause an inflammatory reaction within the periprosthetic tissues known as osteolysis. The UHWMPE wear debris attracts a cell type known as a macrophage that should digest the particles that are generated; however, the wear debris cause these cells to die and release other enzymes and chemicals into the human body. These enzymes and chemicals can cause the progressive failure of the periprosthetic bone and result in the loosening and eventual failure of the arthroplasty.

In addition to polymeric wear debris, the deposition of cobalt and chromium ions in the blood stream can result in aseptic loosening and can cause necrosis of the bone and surrounding soft tissue (Gruber *et al*., 2007). Adverse soft tissue reactions have been linked to the metal on metal wear debris that is released from the taper junction, this being prevalent in large head metal on metal modular designs (Langton *et al*., 2012).

2.8.2 Micro-motion at the bone implant interface

Micro-motions are the relative displacements that occur between the surface of an orthopaedic implant and the bone. The magnitudes of these displacements are relevant to the physiological loads that are applied to the implanted joint. It is thought that once the micro-motions reach a threshold value in the region of 100 μm – 200 μm, the biological fixation of the implant will become compromised, and fibrous tissue will be formed at the bone-implant interface, as opposed to new bone (Pilliar *et al*., 1986;

Maloney *et al*., 1989). This fibrous tissue has inferior mechanical properties when compared to bone and therefore contributes to the premature loosening of implants.

The stability between the bone and the implant can be classified into primary and secondary stability. Primary stability refers to the stability at the bone-implant interface immediately after implantation and depends entirely upon mechanical factors (Viceconti *et al*., 2000). Secondary stability describes the biological stability of the implant when bone ingrowth as occurred. From the literature, it is evident that poor primary stability contributes to the failure of fixation for cementless implants used in THA (Maloney *et al*., 1989; Phillips *et al,* 1990). Hence, it is important to establish sound primary stability in order to achieve adequate secondary stability through full bone ingrowth at the bone-implant interface.

From a clinical perspective, the two main factors that contribute to the stability of an orthopaedic implant is the quality and quantity of the host bone, and the surgical fit of the implant. Wirth *et al.* (2011) confirmed that implant stability is directly affected by the microstructural quality of the periprosthetic cancellous bone. Bertollo *et al.* (2011) studied the effect of surgical fit on implant shear strength for porous titanium and found that the average shear strength at cortical and cancellous bone sites was superior in press fit and line on line fits when compared to a 1mm clearance fit. This shows that creating initial contact at the interface is critical in order to promote bone ingrowth and optimise secondary stability.

2.8.3 Stress shielding

Stress shielding is a phenomenon that is associated with all forms of joint arthroplasty and is especially prevalent in the replacement of load bearing joints such as the hip and knee. Following THA, the load transfer to the proximal femur is reduced when femoral stems having a substantially higher stiffness than the bone are inserted. Hence, the

femoral stem carries part of the load that was previously fully carried by the bone. This causes a reduction in the stress distributed in the remaining host bone, meaning that the periprosthetic bone will become insufficiently loaded and will not remodel. Stress shielding in this instance can ultimately affect the longevity of THA and thus, promote the need for revision surgery (Whiteside, 1989).

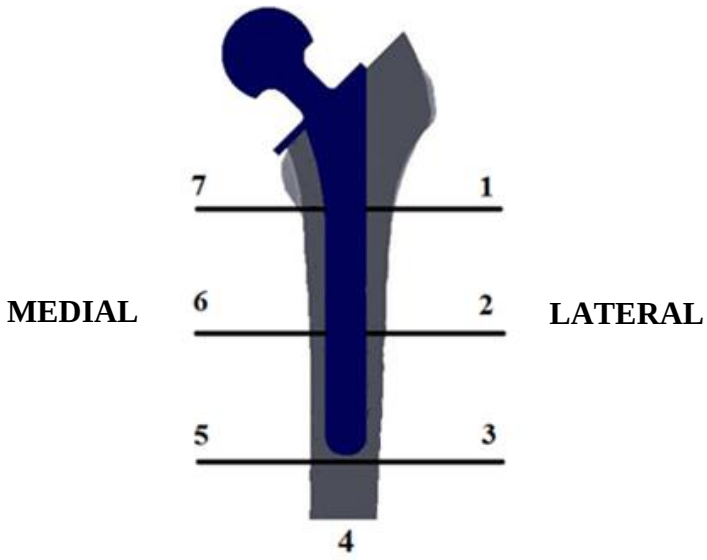

Figure 2.7 Gruens zones for measuring periprosthetic bone density (Gruen, 1979).

Stress shielding can also contribute to the premature failure of THA through stem migration and fractures in the periprosthetic bone (Kroger *et al*., 1998). Stress shielding following THA is especially prevalent in the proximal-medial femur and the region that corresponds to the calcar and lesser trochanter of the femur is often worse affected (Karachalios *et al*., 2004; Stiehl, 2009). In clinical situations, radiographic evaluations are performed to examine and quantify the effects of stress shielding by separating the femur into what are referred as Gruen's zones as shown in Figure 2.7. These zones are used to measure periprosthetic bone density following THA and therefore provide indications of where stress shielding is occurring (Gruen *et al*., 1979).

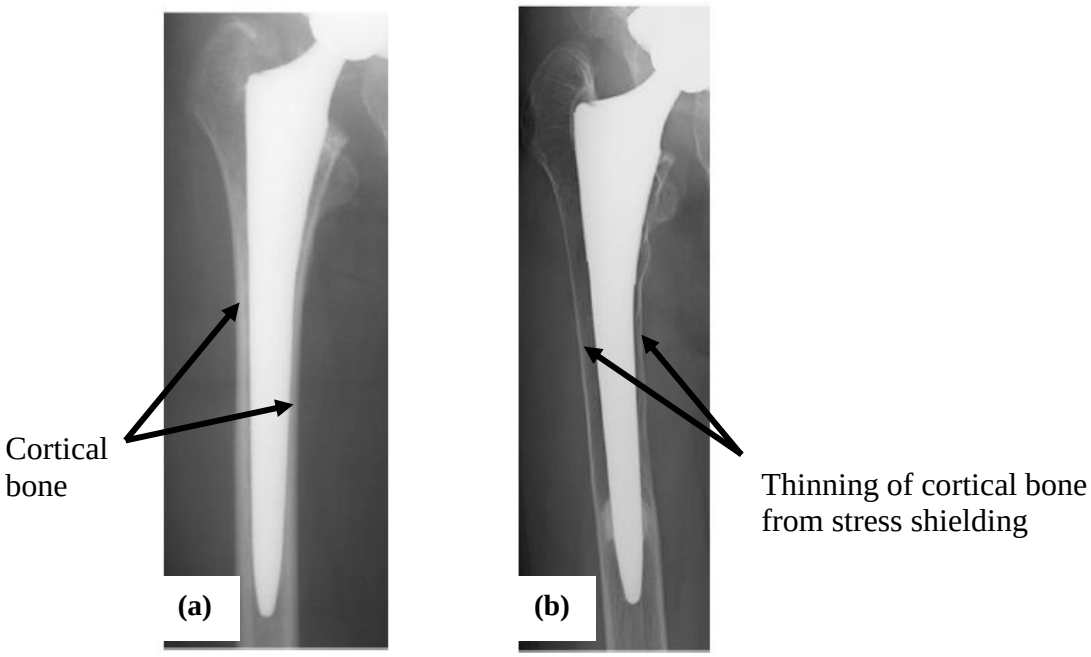

Figure 2.8 Radiographs showing the stress shielding phenomenon following THA. (a) Radiograph at 1 month following surgery (b) Radiograph at 5 years following surgery, where severe stress shielding is evident (Nishino *et al*., 2013).

Figure 2.8 shows the radiographs of a 52-year-old woman who underwent THA using a cementless titanium alloy modular femoral stem. In this instance, severe thinning of the cortical bone was evident at 5 years following surgery (Nishino *et al*., 2013).

Using Figure 2.8 as an example, it can be assumed that revision surgery would be difficult in this instance due to the poor quality of the periprosthetic bone stock. Therefore, it is evident that periprosthetic stress shielding is an ongoing phenomenon that can affect the longevity of femoral stems and the success of subsequent revision surgeries. It is considered that in order to help alleviate stress shielding, more flexible femoral stems should be investigated (Ebrahimi *et al*., 2012).

Chapter 3 Additive Layer Manufacturing (ALM) for orthopaedic applications

3.1 Introduction

This chapter introduces the potential of utilising metal powder based Additive Layer Manufacturing (ALM) systems for the production of orthopaedic implants. The advantages and limitations of ALM technologies are described in relation to this research topic. The mechanical behaviour and finite element modelling of additive manufactured cellular structures are considered and discussed. Finally, physical and numerical studies that have investigated the mechanical behaviour and performance of functionally graded and porous femoral stems manufactured using ALM are critically evaluated in order to provide the basis for this research.

3.2 Additive Layer Manufacturing (ALM)

ALM refers to a group of technologies that can produce prototypes or final production components of near net shape, from three-dimensional CAD models by using a layer-by-layer build process. ALM techniques were developed in the late 1980's and since then new technologies have evolved in this area. Originally, ALM was seen as a method of rapid prototyping (RP) for polymeric components but in recent years, an improvement in ALM has enabled these processes to be classified as rapid manufacturing (RM) technologies (Levy *et al*., 2003).

ALM offers a capability to realise the designs of polymeric or metallic components virtually irrespective of their geometric complexity, with reduced capital investment and waste. Murr *et al.* (2009) commented that up to 80% of the material from which knee implants were conventionally machined from was converted into scrap, whereas with ALM the unprocessed powder can be reused for future work. The flexibility and unique

capabilities of ALM have attracted interest from the aerospace, automotive and medical sectors through providing simplified supply chains and reduced lead times. In contrast with traditional manufacturing processes, ALM offers the exploration of manufacture led design as opposed to design led manufacture.

ALM technologies can be categorised by: liquid based, solid based and powder based systems. For this research, the metal powder-based systems of Electron Beam Melting (EBM) and more specifically Selective Laser Melting (SLM) are of interest.

3.2.1 Electron Beam Melting (EBM)

EBM is a process that was developed by ARCAM in the United States and the technology consists of building parts out of metal powders on a layer-by-layer basis. EBM uses a high-powered electron beam to selectively melt and fuse together the metallic powder. With EBM, components are manufactured in a vacuum system at an elevated temperature. It is thought that this provides a clean and predictable build environment for producing components that are free from residual stresses (Parthasarathy *et al*., 2010).

3.2.2 Selective Laser Melting (SLM)

SLM was introduced in 1994 by the German company Electro Optical Systems (EOS) by using the trade name of Direct Metal Laser Sintering (DMLS). This additive manufacturing technology is considered the first to be capable of producing metal parts from a powder in a single melting process. A schematic of the SLM process is shown in Figure 3.1. The process starts with a metal powder with a particulate size ranging typically between 10 µm and 60 µm. Components are then built in layers with a thickness of between 20 µm to 40 µm, by using an optically guided laser beam to

selectively melt and fuse together the powder until the required geometry has been created.

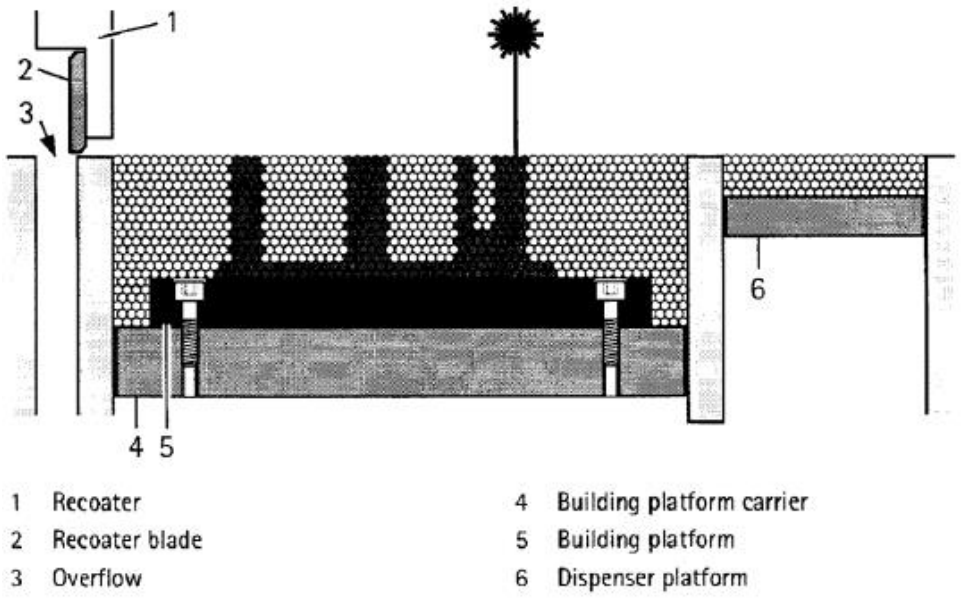

Figure 3.1 Diagram of the SLM process (Electro Optical Systems, 2005).

Upon completion of the manufacturing process, the build plate is removed from the machine and wire Electro Discharge Machining (EDM) is used to remove the components from the build plate. The components are then subjected to post processing operations in order to remove support structures and improve the surface finish as required.

3.3 Limitations of ALM

The published literature and data describing the mechanical behaviour and structural integrity of metallic components manufactured using ALM is limited when compared to more conventional manufacturing processes. Therefore, there is still a certain degree of uncertainty associated with ALM in relation to the repeatability and reliability of the process. It is thought that this uncertainty maybe partially attributed to ALM being an emerging technology when compared to more established methods of manufacturing.

Topics that have been identified for consideration when relating ALM to the manufacture of orthopaedic implants are surface finish, unsupported/downward facing surfaces and residual stress.

3.3.1 Surface finish

Components that are manufactured using SLM and EBM are characterised by having a somewhat rough surface finish in their as-built condition. The poor surface finish can be partially attributed to the "stair step" effect, which involves the stepped approximation of component layers that consist of curved or inclined surfaces (Strano *et al*., 2013). Surface defects can also occur through the laser induced balling phenomenon, where by discontinuities in scan tracks can increase surface roughness and limit the capability to build sharp geometries (Mumtaz and Hopkinson, 2009). In order to improve the surface finish of components manufactured using SLM, parametric studies have been performed to investigate the effects of altering the machines operating parameters.

Gu and Shen (2009) concluded that increasing laser power and reducing the scan speed and layer thickness helped to alleviate the balling phenomenon, when processing stainless steel using SLM. Whereas, Bacchewar *et al.* (2007) described that layer thickness and laser power were parameters that influenced the surface finish of upward and downward facing surfaces respectively. Logically, it was also described that in order to negate the effects of "stair stepping", the layer thickness should be reduced (Strano *et al*., 2013).

The hip joint can be dynamically loaded with in excess of 1 million gait cycles every year (Morlock *et al*., 2001). Therefore, the fatigue strength of additive manufactured alloys is a critical factor that could affect the longevity and reliability of femoral stems. The bulk mechanical properties and fatigue characteristics of the additive manufactured cobalt chrome alloy EOS Cobalt Chrome MP1 are comparable to other traditional forms

of production (Electro Optical Systems, 2010). However, to obtain a smooth “as built” surface finish when using ALM is difficult. Therefore, long and costly post processing methods are often needed to attain an adequate surface finish in order to optimise the fatigue characteristics of additive manufactured components.

3.3.2 Downward facing surfaces

The concern of downward facing or unsupported surfaces is inherent with the ALM of metals, because unlike polymers, the metal powder cannot support itself in the powder bed during the build process. Generally, it is recommended is that any surface with an angle of less than 45 degrees with respect to the build platform should be supported with sacrificial structures that are removed upon completion of the build process. In contrast with this general design rule, Emmelmann *et al.* (2011) successfully manufactured cylindrical titanium alloy struts with a length of 5 mm using SLM at build angles below 45 degrees. However, it was observed that as the build angle decreased, the strut diameter increased due to the attachment of partially melted particles that were introduced through the dissipation of heat. In agreement with this, Parthasarathy *et al.* (2011) manufactured porous titanium components using EBM with unsupported surfaces that were parallel to the build platform. From the literature it is evident that unsupported surfaces with an angle below 45 degrees respective to the build platform can be built using ALM, however, the dimensional accuracy, surface finish and mechanical properties will be affected (Emmelmann *et al*., 2011; Parthasarathy *et al*., 2011).

3.3.3 Residual stress

Residual stresses are self-equilibrating and exist in a body that has no external loads or constraints applied to it and are still present in a body when all sources of external load have been removed. It has been described that laser based manufacturing processes

create thermally induced residual stresses, due to the large temperature gradients that are inherent with such processes (Mercelis and Kruth, 2006).

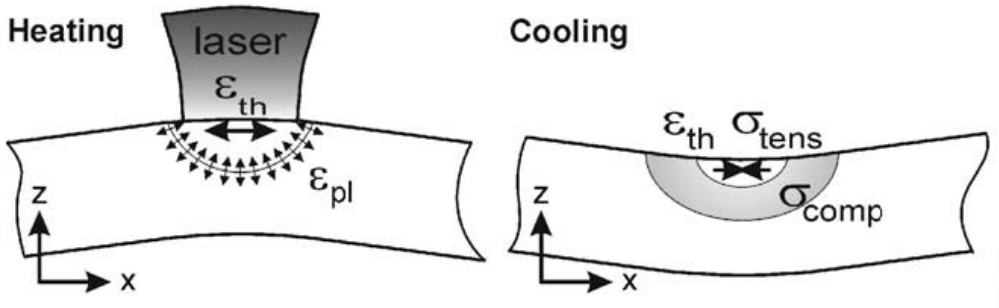

Figure 3.2 The potential effect of the temperature gradient mechanism on part deformation (Kruth *et al*., 2004).

The rapid temperature cycles in SLM create steep temperature gradients in the component layers and this induces thermal stresses that are present during and after the build (Roberts *et al*., 2009). The temperature gradient mechanism relative to part deformation has been described by Kruth *et al.* (2004) and is shown in Figure 3.2. Residual stresses can ultimately affect the dimensional accuracy and mechanical properties of components manufactured using SLM through a combination of deformation and warping.

3.4 The potential of ALM for orthopaedic applications

Femoral stems that offer more flexible stiffness configurations when compared to their bulk metallic counterparts have shown a potential to reduce stress shielding and therefore contribute towards improving implant longevity, through preserving periprosthetic bone (Kuiper and Huiskes, 1997; Simoes and Marques, 2005; Yan *et al*., 2011; Gong et *al*., 2012; Boudeau *et al*., 2012; Arabnejad Khanoki and Pasini, 2013). More recently, it has been reiterated that stiffness-matching strategies between the

femoral stem and the host bone should be investigated for future designs (Ebrahimi *et al*., 2012).

ALM has provided an opportunity to investigate stiffness-matching strategies between orthopaedic implants and the host bone. Using ALM to manufacture orthopaedic implants offers the ability to produce customised lightweight components with tailored mechanical properties from a single alloy (Murr *et al*., 2010; Bertol *et al*., 2010). In addition, the design of single alloy orthopaedic implants that can reduce the effects of periprosthetic stress shielding can be realised. From the literature, different approaches have been considered in order to tailor the mechanical properties of components manufactured using ALM.

3.4.1 Altering process parameters

A change in the mechanical properties of components has been observed through altering the process parameters of ALM systems. SLM machines are intelligent pieces of equipment that house complex systems and there are a significant number of process parameters that can be adjusted. However, the three main parameters that are usually altered are the laser power, scan speed and step over distance of the laser beam.

Stamp *et al.* (2009) produced a porous structure by modifying the scan strategy on the machine, so that the powder was exposed with a 90 degree rotation in relation to the previous layer. In this instance, the step over distance of the laser was specified so there was no overlap and this resulted in an interconnected porous structure with rectangular pores. Additionally, Wang *et al.* (2010) introduced porosity into titanium components using SLM with pore sizes ranging between 200 µm – 500 µm. The authors observed that as the scan speed increased from 0.01 m/s to 0.03 m/s the porosity increased. Although, when the scan speed was set at 0.05 m/s the porosity within the components decreased again.

Espana *et al.* (2010) investigated the use of Laser Engineered Net Shaping (LENS^{TM}) to produce conceptual designs of porous functionally graded CoCrMo femoral stems. The observations from the work were:

- Porosity increases with decreasing laser power.
- Porosity increases with increasing scan speed.
- Porosity increases with increasing powder feed rate.

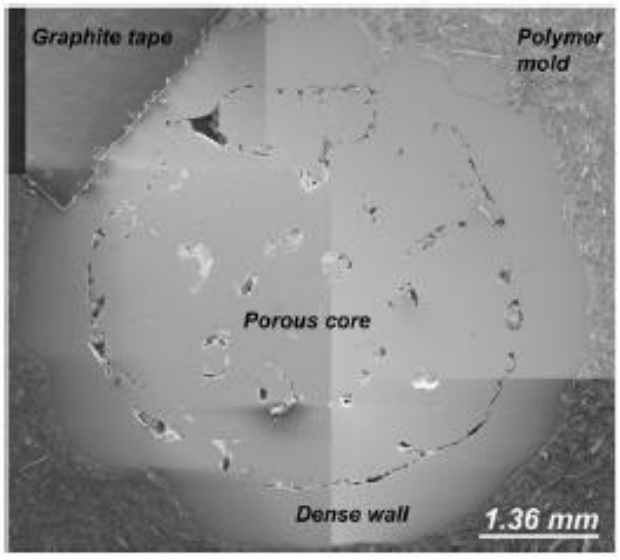

Figure 3.3 CoCrMo alloy sample produced by LENS^{TM} with a dense outer skin and porous core (Espana *et al.*, 2010).

Additionally, the results from the authors' physical tests indicate that the elastic modulus of the CoCrMo porous components produced by LENS^{TM} could be varied between 33 GPa and 43 GPa, which is much lower than the modulus of wrought CoCrMo, which is in the region of 200 GPa. However, it is considered that this methodology should be used with caution, as the parts that are produced are not fully dense and heterogeneities will be present within the materials microstructure, as shown in Figure 3.3. This could have a detrimental effect on the mechanical properties, structural integrity and hence the performance of components. For this reason, the

design and manufacture of porous cellular structures is considered a more suitable alternative. Cellular structures with homogenised mechanical properties offer a more reliable opportunity for modifying the stiffness of components manufactured using ALM.

3.5 Cellular structures

Cellular structures are solids that are comprised of an interconnected network of solid struts or plates, which are assembled in an order to provide lightweight porous structures (Gibson and Ashby, 1997). The work of Webber and White (1972) was one of the early studies to investigate the use of porous materials for biomedical applications by using graded composites to aid bone ingrowth into the implant. Since this early work, research has mainly investigated the use of metallic open cellular structures to establish the long-term biological fixation of orthopaedic implants and tissue scaffolds. Additionally, it has been considered that closed cell porous metals could be utilised to manufacture flexible, lightweight femoral stems for either cemented or cementless fixation (Ryan *et al.*, 2006). However, the successful application of open or closed cellular metals for orthopaedic applications is dependent upon the availability of capable and reliable manufacturing processes.

3.5.1 Gibson and Ashby's model

Gibson and Ashby (1997) considered that the most important characteristic of a cellular structure is its relative density. To demonstrate this, they proposed an equation to estimate the elastic modulus of a three-dimensional square pore cellular structure where:

$$\frac{E^*}{E_s} = C\left(\frac{\rho^*}{\rho_s}\right)^2 \tag{3.1}$$

Here E^* is the elastic modulus of the cellular structure, E_s is the elastic modulus of the solid, C is an experimentally derived constant dependent upon the unit cell geometry, ρ^* is the density of the cellular solid and ρ_s is the density of the solid. Similarly, an equation was also proposed to estimate the yield strength of a three-dimensional cellular structure where:

$$\frac{\sigma^*}{\sigma_{ys}} = C\left(\frac{\rho^*}{\rho_s}\right)^{\frac{3}{2}} \tag{3.2}$$

Here σ^* and σ_{ys} are the yield strengths of the cellular structure and solid respectively. Equations 3.1 and 3.2 have been useful for providing an analytical comparison with experimental and numerical studies that have investigated the stiffness and strength of additive manufactured cellular structures (Cansizoglu *et al*., 2008; Parthasarathy *et al*., 2010; Murr *et al*., 2010).

3.5.2 Mechanical behaviour of additive manufactured cellular structures

ALM possesses a capability to manufacture open and closed cellular structures from common biomedical alloys such Ti-6Al-4V and CoCrMo. A unit cell approach is utilised to design porous structures with a regular geometry by using three-dimensional Computer Aided Design (CAD) software. Cubes, cylinders, truncated octahedrons, truncated cubes, truncated cuboctahedrons, triangular prisms, rectangular prisms, octagonal prisms and rhombic dodecahedras can be chosen to construct cellular structures using unit cells (Cheah *et al*., 2003).

ALM technologies can produce porous structures with stiffness and strength characteristics that are closer to human bone, when compared to the bulk material properties of the alloys themselves (Murr *et al*., 2010). The mechanical behaviour of titanium alloy open cellular structures has been more thoroughly researched. Harrysson

et al. (2008) investigated the compressive and flexural properties of rhombic dodecahedron cellular structures manufactured using EBM with cell sizes varying between 3 mm and 12 mm, as shown in Figure 3.4. The stiffness and strength of the cellular structures were dependent upon the volumetric porosity. Compressive modulus values of between 12 MPa and 60 MPa were reported, which are considerably lower than the modulus of Ti-6Al-4V, which is in the region of 110 GPa. Additionally, Cansizoglu *et al.* (2008) found that cellular structures with hexagonal pores exhibited elastic moduli values ranging between 50 MPa and 225 MPa when subjected to uniaxial compression, with the majority of the specimens showing brittle failure.

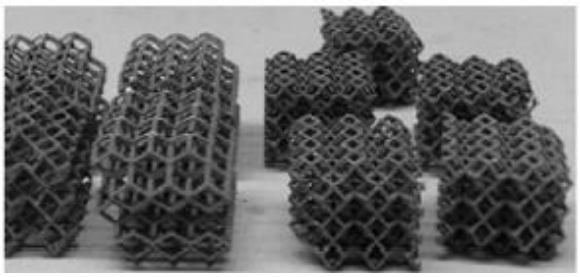

Figure 3.4 Titanium alloy cellular structures manufactured using EBM (Harrysson *et al.*, 2008).

In contrast to this, stiffer, square pore cellular structures with a volumetric porosity ranging between 50% and 70% were manufactured using EBM that exhibited elastic modulus values of between 0.57 GPa and 2.92 GPa. It was also observed that the densities of such structures were similar to the bone that they would potentially be replacing (Parthasarathy *et al.*, 2010). Similar square pore structures were subjected to shearing forces and no obvious weakness was evident between the connecting layers (Parthasarathy *et al.*, 2011). More recently, the compressive properties of square pore titanium alloy cellular structures manufactured using EBM and SLM were compared (Sallica-Leva *et al.*, 2013). The results showed that the laser-melted components provided higher mechanical properties when compared to the parts manufactured using

EBM. This was attributed to microstructural differences and variations in operating parameters that were observed between the two technologies.

A small sample of the literature has investigated the mechanical behaviour of additive manufactured cellular structures when subjected to cyclic loading conditions. When performing compression fatigue testing on titanium alloy cellular structures, the fatigue strength was found to increase with an increasing relative density (Li *et al.*, 2012). Whereas Brenne *et al*. (2013) investigated the cyclic behaviour of square pore titanium alloy cellular structures when subjected to uniaxial and four point bending loading conditions. Areas of high strain local to the applied load were observed within the struts and it was evident that the fatigue strength and energy absorption of the structures were improved when the components were heat-treated.

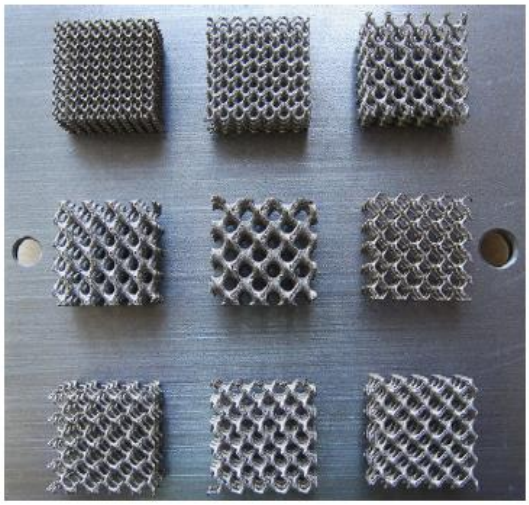

Figure 3.5 Laser melted stainless steel cellular structures (Yan *et al.*, 2012).

The mechanical properties of cellular structures manufactured from other biocompatible alloys are not as well described within the literature when compared to titanium alloys. Yan *et al.* (2012) evaluated the compressive properties of cellular structures manufactured from 316 L stainless steel, as shown in Figure 3.5. It was observed that the density of the individual struts was higher when smaller unit cells were used.

Additionally, the yield strength and elastic modulus was 36% and 27% higher respectively for a 2 mm unit cell size when compared to an 8 mm unit cell. This indicated that the stiffness and strength of the cellular structures decreased with an increase in volumetric porosity. Rivera *et al.* (2011) investigated the mechanical properties of a laser melted CoCrMo open cellular structure, which would facilitate bone ingrowth into an acetabular cup. A structure with a pore size of 0.50 mm was proposed that possessed similar mechanical properties to commercially available tantalum and titanium alloys.

3.5.3 Finite element modelling of cellular structures

In order to reduce the need for time consuming and expensive physical testing, it is considered beneficial to use the finite element method to model and predict the mechanical behaviour of cellular structures. However, the high temperature melting and solidification of the metal powder that occurs with ALM can cause strut curvature and corrugation, thus providing structures with minor geometric irregularities and an uneven surface finish (Parthasarathy *et al.*, 2010). In contrast to this, finite element models simulate the ideal situation where each individual strut is assumed to have a perfectly smooth and uniform geometry.

Published studies have observed differences between numerical and physical test data relating to the mechanical behaviour of additive manufactured cellular structures. Numerical results overestimated the effective mechanical properties of titanium alloy cellular structures manufactured using EBM with a rhombic dodecahedron unit cell, by a mean factor of 5.65 when subjected to uniaxial compression and three point bending (Harrysson *et al.*, 2008). The compressive properties of titanium alloy square pore cellular structures manufactured using EBM were investigated; similarly, the simulation results overestimated the effective mechanical properties of the structures when

compared to the physical test data (Parthasarathy *et al*., 2011). However, a direct comparative analysis was not performed in this instance. Smith *et al.* (2013) achieved a good correlation between numerical and physical test data for the compressive behaviour of stainless steel 316 L cellular structures but a reverse engineering methodology was needed. Here, the strut diameter was adjusted until the experimental and numerical stress strain relationship correlated. Wieding *et al.* (2013) modelled square pore cellular structures with a non-linear stress strain relationship that was derived from uniaxial compression tests. This still resulted in a 20% overestimation in the computed stiffness values reported from the finite element analysis.

Modelling parameters such as element geometry, mesh density and material modelling could be factors contributing to the difference between numerical and experimental results. However, it is thought that the predominant factor governing the correlation between numerical and physical test results can be attributed to the uneven surface finish creating heterogeneities and deformations within the additive manufactured cellular structures (Harrysson *et al*., 2008; Parthasarathy *et al*., 2010; Parthasarathy *et al*., 2011). This structural variation creates local areas of stress concentration and sites where premature fracture can occur (Simone and Gibson, 1998).

In a recent study, it was described that in order to model the mechanical behaviour of additive manufactured cellular structures accurately, structural variation and heterogeneities should be accounted for (Campoli *et al.*, 2013). In order to create such three dimensional finite element models, techniques such as micro computed tomography (µCT) scanning need to be employed. Ryan *et al.* (2009) investigated the compressive properties of porous titanium alloy bone scaffolds by comparing physical test data with finite element models that were created using three different methods, namely a single unit cell, idealised CAD model and a µCT derived model. The µCT

model provided a closer comparison with the physical test data when compared to the data from the idealised model, where an acceptable 10% increase in the elastic modulus was observed. However, despite the benefits of utilising μCT derived finite element models they are computationally expensive. In this work, approximately 600,000 elements 70 μm in size were used to mesh a model with a small bounding volume of 8 mm × 8 mm × 16 mm. An additional complication here is that the mechanical properties of cellular structures produced using ALM have been shown to be sensitive to their build direction and thus display a small amount of anisotropy (Harrysson *et al*., 2008; Ryan *et al*., 2009). It can be summarised that the finite element modelling of additive manufactured cellular structures is a complex research topic in itself that still requires further work.

3.6 The performance of prostheses manufactured using ALM

Currently, there is a distinct lack of published literature describing the in vivo performance of a fully porous or functionally graded femoral stem manufactured using ALM. This review has had to focus upon the limited number of physical and numerical studies that have been published to date.

Harrysson *et al.* (2008) utilised cellular structures to manufacture porous titanium femoral stems using EBM and a more flexible stem was created that was 78% lighter than its bulk titanium counterpart was. The finite element method was used to investigate the stress distribution in the proximal femur, modelling the porous portion of the stem as a continuum body with physically determined material properties being assigned. Higher stress values were observed in the proximal femur when compared to fully dense titanium and cobalt chrome stems, however this was only evident from a qualitative perspective. Overall, it was summarised that ALM provides a great potential to manufacture customised orthopaedic implants with tailored mechanical properties.

Murr *et al.* (2010) discussed "next generation" functionally graded hip and knee implants that could be customised to the patients' needs by using EBM. Various fully porous and functionally graded titanium alloy designs were presented in the work, as shown in Figure 3.6. Cellular structures with similar mechanical properties to bone were presented, but in all cases, the load transfer to the femur was not considered.

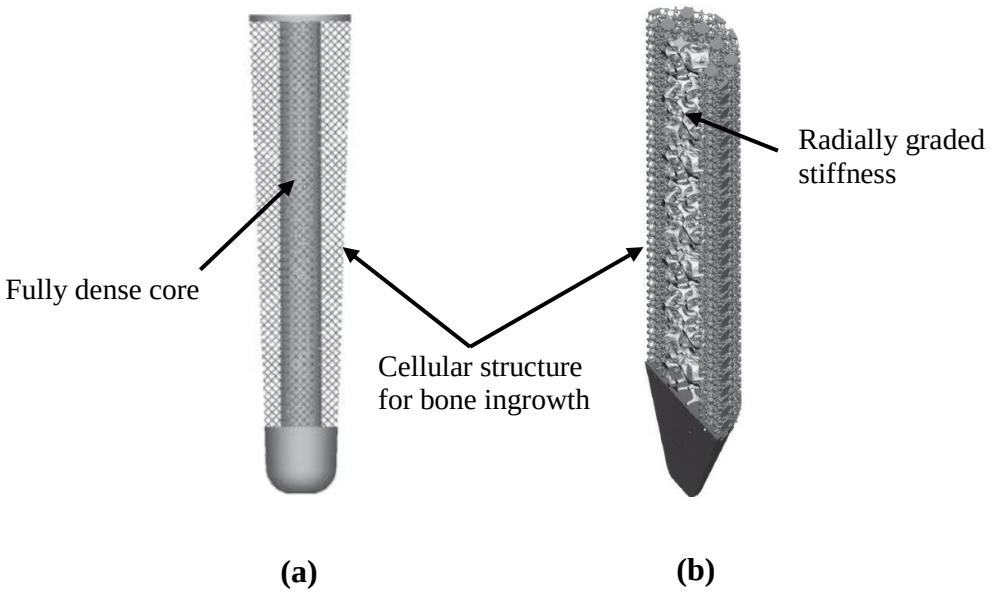

Figure 3.6 Conceptual models of functionally graded components. (a) A tibial component (b) A section of a porous femoral stem (Murr *et al*., 2010).

Espana *et al.* (2010) manufactured a functionally graded CoCrMo femoral stem using an alternative method of ALM called Laser Engineered Net Shaping (LENS^{TM}). The stem consisted of a fully dense outer shell with a more flexible porous core. However, as previously described, from observing a cross sectional image of the part (Figure 3.3) and evaluating the manufacturing technique, it can be claimed that the material is not fully dense as the porosity was created through altering the machines operating parameters.

Yan *et al.* (2011) theoretically investigated the functional adaption of the femur when implanted with porous titanium femoral stems using estimated material properties. The

results indicated that stress shielding was reduced when the properties of the porous titanium were utilised and it was evident that the bone density loss decreased linearly with an increase in porosity of the stem. Future work was suggested to investigate the structural integrity of porous titanium stems, as this was not covered in the work. More recently, Arabnejad Khanoki and Pasini (2013) performed a numerical optimization study using a two-dimensional finite element model of an implanted femur. The fatigue characteristics of a porous functionally graded titanium alloy stem were investigated and optimised to reduce bone resorption and maintain interface stability. A reduction in bone resorption of 53.8% was observed when square pore cellular structures were utilised. The stem was modelled free of defects in this instance, which is questionable as it has been previously discussed that ALM produces cellular structures with local stress raisers, which may be susceptible to crack propagation and fatigue failure. This assumption was based upon that EBM was used to produce proof of concept planar samples of the porous stem where no structural defects were observed. It is logical that no defects were observed in the work, as porosity was only present in one direction and the inspected surface was parallel to the build platform. If a full three-dimensional stem was manufactured with porosity in three axes, it can be assumed that defects and heterogeneities would be present (Harrysson *et al.*, 2008; Parthasarathy *et al*., 2011).

In contrast to numerical analysis, Harrison *et al.* (2013) performed an in vitro study to investigate the micro-motion and frictional characteristics of titanium alloy femoral stems with a porous surface topography. A fully dense femoral stem was manufactured using SLM with a surface topography comprised of an interconnected cellular structure with unique anchoring features. The additive manufactured stem was implanted into an ovine femur and the performance was physically compared with a plasma sprayed titanium stem with an identical geometry. The results showed that the stems manufactured using SLM have the potential to improve the primary stability of the

implant when compared to other traditional surface coatings. In this instance, the authors focussed solely on interface stability and did not consider adapting the stiffness of the femoral stem to reduce stress shielding.

Finite element models that have investigated the performance of porous femoral stems have modelled the cellular structure or porous region as a single continuum body. Material properties have been determined from physical testing (Harrysson *et al*., 2008) or estimated by using Gibson and Ashby's theoretical model (Yan *et al*., 2011). The reasons for using this modelling technique are twofold. Firstly, the finite element method tends to overestimate the stiffness and strength of additive manufactured cellular structures and secondly a vast amount of computing power would be required to model the cellular structures explicitly. Wieding *et al.* (2013) numerically investigated the mechanical stability of porous titanium bone scaffolds that were constructed with square pore cellular structures. A cylindrical bone scaffold that was 30 mm in diameter and height was inserted in order to repair a femur with a large segmental bone defect. It is believed that this is the first study to analyse the mechanical behaviour of cellular structures in a three dimensional capacity. Whilst the finite element model showed a reasonable agreement with the physical tests, by overestimating the stiffness of the scaffolds by approximately 20%, it is considered that to employ the same methodology to femoral stem would be troublesome. Femoral stems are much larger and are more geometrically complex when compared to bone scaffolds. To model the cellular structures of a full femoral stem explicitly when implanted in the femur would be challenging, as the computational power required to construct and solve such a model would be vast.

3.7 Summary and concluding remarks from the literature review

This chapter and the previous one have reviewed the fundamental topics associated with THA and introduced the potential of adopting ALM technologies for orthopaedic applications.

Stress shielding of the periprosthetic femur is an ongoing phenomenon that can have a detrimental effect on the longevity of femoral stems. Alternative materials and design methodologies that will alleviate stress shielding have been considered and theoretically analysed within the literature. Despite this, cobalt chrome and titanium alloys are still commonly used to manufacture monoblock and modular femoral stems respectively.

Over the past 6 years, research has highlighted the potential of utilising ALM for orthopaedic applications. ALM has shown a capability to produce orthopaedic implants from common biomedical alloys with effective mechanical properties that are much closer to human bone. This has been achieved by incorporating cellular structures into implant designs. The mechanical behaviour of additive manufactured cellular structures has been discussed, where it is evident that the stiffness and strength of cellular structures are dependent upon the strut size and volumetric porosity. In addition to this, the finite element modelling of cellular structures has been identified as a complex topic.

Literature investigating the performance of titanium alloy cellular structures and femoral stems manufactured using ALM is ever growing. However, titanium alloy stems need to be utilised in a modular capacity. The recent concerns associated with modular designs, in terms of the mechanical failure and wear of the taper junction have provided justification to investigate alternative CoCrMo monoblock designs that would help to alleviate such problems. Although the positive effect of less stiff implants is

already known, there is no obvious work that has investigated the performance of CoCrMo femoral stems manufactured using SLM.

This thesis will focus upon adopting SLM to realise the designs of CoCrMo femoral stems that are lighter and more flexible when compared to their traditional bulk metallic counterparts. The mechanical behaviour and manufacturability of CoCrMo cellular structures and femoral stems will be investigated through a combination of physical and analytical methods. Thereby, enabling the proposal of innovative designs that have the potential to alleviate stress shielding and contribute towards increasing the longevity of THA.

Chapter 4 The compressive properties of laser melted square pore CoCrMo cellular structures

4.1 Introduction

This chapter investigates the mechanical behaviour of square pore CoCrMo cellular structures that have been manufactured using SLM with a volumetric porosity ranging between 25% and 95%, when subjected to uniaxial compression.

Square pore cellular structures can be manufactured using ALM with mechanical properties that are closer to human bone (Parthasarathy *et al*., 2011). It is considered that such structures can then be utilised to reduce the stiffness of cobalt chrome femoral stems that are used in THA.

Uniaxial compression tests were performed in order to determine the effective stiffness and 0.2% compressive yield strength of the square pore cellular structures. Finite element analysis and the Gibson and Ashby model have been used to form respective numerical and analytical comparisons with the elastic modulus values that were determined from the uniaxial compression tests.

Structural variation has been modelled using the finite element method, in order to investigate the effect that this can have on the stiffness of a cellular structure. This was justified from previous work (Parthasarathy *et al*., 2011; Smith *et al*., 2013) and from observing the as-built condition of the cellular structures that were manufactured.

4.2 Methods

4.2.1 Design and manufacture of the cellular structures

The designs for seven individual square pore cellular structures were generated using the CAD software Solidworks 2012. Individual strut sizes ranging between 0.20 mm and 2.50 mm were considered and contained within 15 mm cubic volumes. The volumetric porosity of the cubes was designed to vary between approximately 25% and 95%, the individual specifications for each cellular structure are presented in Table 4.1.

A typical CAD model of a component showing the configuration of pores is shown in Figure 4.1. The solid model for each structure was exported from the CAD software into Materialise Magics 17.0 software using a Standard Tessellation Language (STL) file format. The components were then positioned on the build platform and slice files of the two dimensional cross sectional geometry were generated for each layer to enable manufacture.

Table 4.1 Characteristics of each cellular structure.

Cellular structure	Strut size (mm)	Pore size (mm)	Designed volumetric porosity (%)
1	0.20	1.44	95.14
2	0.35	1.74	90.85
3	0.50	1.57	82.46
4	1.00	1.80	64.80
5	1.50	1.88	50.00
6	2.00	2.33	45.00
7	2.50	1.67	25.93

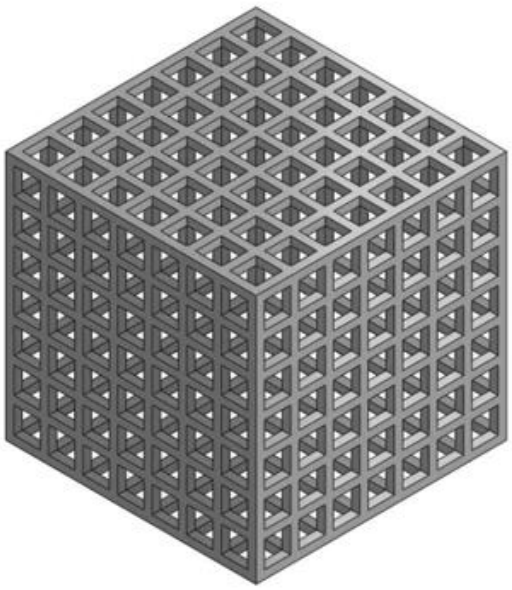

Figure 4.1 A CAD model of Component 3 with a volumetric porosity of 82.46%.

The structures were manufactured from the EOS material, Cobalt Chrome MP1, which is a CoCrMo based super alloy powder that is suitable for medical applications. The powder was sieved to a particle size of no greater than 63 µm and the components were manufactured using an EOSINT M270 Xtended Direct Metal Laser Melting machine.

The machine used a laser with a spot size of 100 µm to selectively melt the powder until the required geometry was fabricated. The components were built in 20 µm layers and the recommended standard process parameters for the material were used. A laser power of 200 W, a laser step over distance of 0.08 mm and a laser scan speed of 800 mm/s were employed. The material processing was performed in a nitrogen based atmosphere with less than 0.1% oxygen present in the build chamber. Upon completion of the build, the components were stress relieved in an argon atmosphere at a temperature of 1050ºC for two hours and left to cool in the furnace. The components were then removed from the build platform using wire EDM.

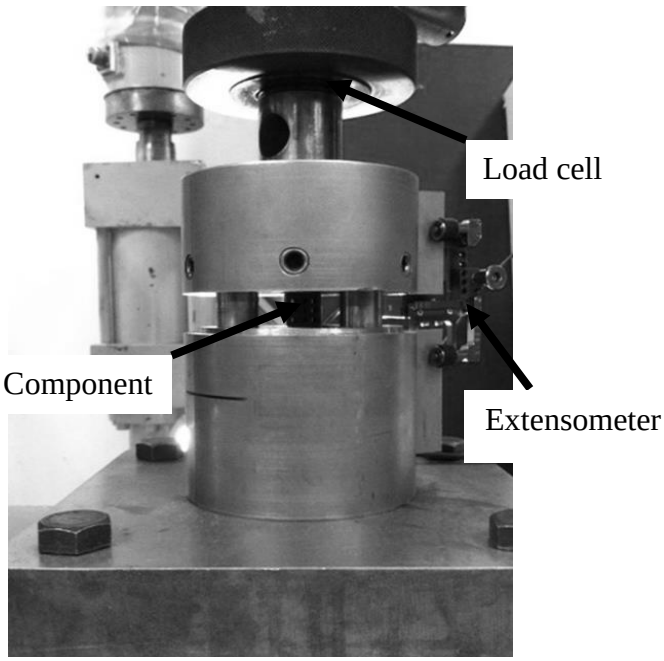

Figure 4.2 Test set up for uniaxial compression testing.

4.2.2 Uniaxial compression tests

Uniaxial compression tests were performed using a Zwick Roell 1474 materials testing machine, with a maximum load capacity of 100 kN. The tests were performed to determine the compressive properties of the cellular structures in the orientation in which they were built. A strain rate of 0.5 mm/min was applied and the displacement was measured using a calibrated digital clip on extensometer, which had an accuracy class of 0.5 according to BS EN ISO 9513:2012. The test set up was designed in accordance with BS ISO 13314:2011, with efforts being made to ensure uniaxial loading by using the machined fixture shown in Figure 4.2. The components were loaded to failure or until the 100 kN load capacity of the machine was reached. The stress strain relationship for each individual component was calculated from the real time force versus displacement data obtained from the test machine. The effective elastic modulus and 0.2% offset yield strength for each sample was determined from the slope of each individual stress strain curve. Four samples for each component were

tested so that a mean value and standard deviation for the effective elastic modulus and 0.2% offset yield strength could be determined.

4.2.3 Finite element modelling

ANSYS 13.0 finite element modelling software was used to predict the effective elastic modulus of the seven individual structures. Comparisons could then be made with the physical test data and analytical predictions. The software was also used to perform a simulation that considered the effect of structural variation and heterogeneities within a cellular structure.

4.2.3.1 Predicting the effective elastic modulus of the cellular structures

Three dimensional finite element models were created in ANSYS 13.0 with an identical geometry to the CAD models that were used for manufacture. Each model was meshed using SOLID 185 four node tetrahedral elements. Mesh sensitivity was studied until further mesh refinement changed the reaction force at the constrained face of the model by 5% or less. This resulted in an element size of 0.20 mm being used in each simulation. A uniform 0.1% compressive strain was applied within the materials elastic limit to the top face of the structure, with the opposite face having its degrees of freedom constrained. Symmetrical boundary conditions were applied in two planes so that the 0.20 mm element size could be utilised with less computational expense. In essence, a quarter of the designed component was modelled in each instance. The CoCrMo alloy was modelled with linear isotropic behaviour, with an elastic modulus of 200 GPa (Electro Optical Systems, 2010), and a Poisson's ratio of 0.3 being assumed. Since the cellular structure was symmetrical in all three principle axes, the elastic modulus could be described by $E_x=E_y=E_z$. Therefore, the effective elastic modulus E_{eff} could be calculated as follows:

$$E_{eff} = \frac{\sigma}{\varepsilon} = \frac{\left(\frac{F_y}{A}\right)}{\left(\frac{\Delta l}{l}\right)} = \frac{F_y}{0.001 \times A} \tag{4.1}$$

Where F_y is the reaction force at the constrained face of the model and A is the cross sectional area of the component.

4.2.3.2 Finite element modelling of structural variation within a cellular structure

The finite element model used in this work, modelled each individual strut with an idealised geometry (Harrysson *et al*., 2008; Parthasarathy *et al*., 2011; Wieding *et al*., 2013). In contrast to this and as discussed previously, additive manufactured cellular structures possess structural variations and a somewhat uneven surface finish. Considering this, Component 3 was selected and modelled with defects in order to investigate what effect this had on the compressive stiffness.

The finite element model was modified by using Ansys Parametric Design Language (APDL) to decrease the stiffness of selected elements to represent irregularity and heterogeneities within the structure. The modified finite element mesh is represented in Figure 4.3. A stiffness value for the defected elements was chosen to be four orders of magnitude less than the elastic modulus of the CoCrMo alloy. In this instance, the full 15 mm cube was modelled with the same element size and boundary conditions as used previously. The adapted model was compared to the ideal model to form a direct comparison of the structures stiffness with and without defects.

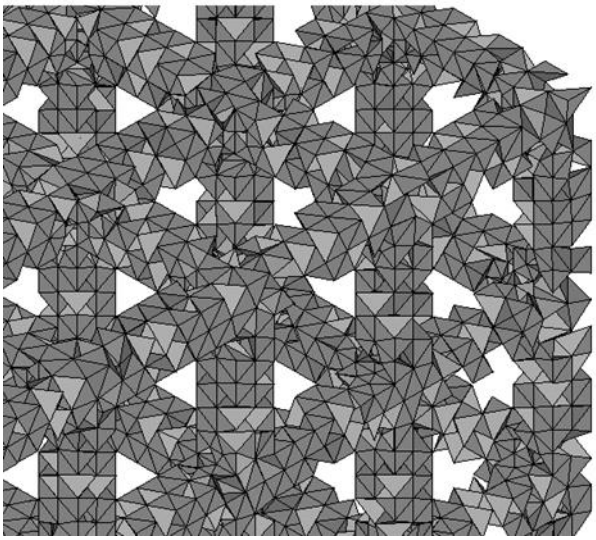

Figure 4.3, The modified finite element model for Component 3. The elements shown have a stiffness of E = 200 GPa. The elements not shown have a decreased stiffness of E = 0.02 GPa.

4.2.4 Analytical prediction of the structural stiffness

In order to obtain an additional comparison with the physical test data, the model proposed by Gibson and Ashby (1997) was utilised. Recalling Equation 3.1, the effective elastic modulus of a cellular structure can be estimated using:

$$\frac{E^*}{E_s} = C\left(\frac{\rho^*}{\rho_s}\right)^2 \tag{3.1}$$

E^* is the elastic modulus of the cellular structure, E_s is the elastic modulus of the solid material, C is a constant that has been experimentally determined to have a value of 1 (Gibson and Ashby, 1997) and ρ^* and ρ_s is the density of the cellular structure and solid material respectively. From Equation 3.1, it is evident that the elastic modulus is dependent upon the relative density, and the relative density can be related to porosity (φ) by:

$$\left(\frac{\rho^*}{\rho_s}\right) = 1 - \varphi \tag{4.2}$$

For convenience, Equation 3.1 can be rewritten to calculate the effective elastic modulus as follows:

$$E_{eff} = E_s \left(1-\varphi\right)^2 \tag{4.3}$$

The above equation has been used to predict the effective stiffness of the square pore cellular structures.

4.3 Results

4.3.1 Design and manufacture of the cellular structures

It has been demonstrated that square pore cellular structures with strut sizes between 0.20 mm and 2.50 mm, having a designed volumetric porosity ranging between 25% and 95% can be manufactured using standard operating parameters for CoCrMo. Figure 4.4 shows a selection of components on the build plate in their as-built form. An uneven surface finish was created similar to previous studies that have used ALM to manufacture metallic cellular structures (Harrysson *et al*., 2008; Murr *et al*., 2010; Parthasarathy *et al*., 2011; Smith *et al*., 2013). From inspection, structural variation was visible on the outer surfaces of the components, and this was more evident with cellular structures possessing a strut size of 0.5 mm or less. An example of this can be observed from Figure 4.5.

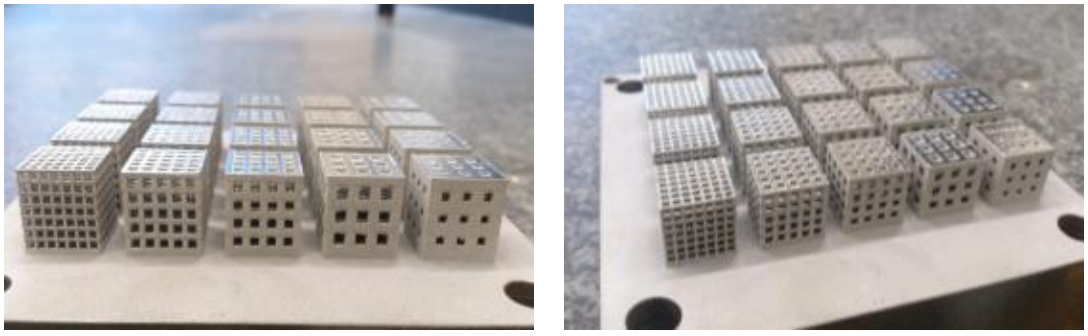

Figure 4.4 Components 3 to 7 in their as-built condition.

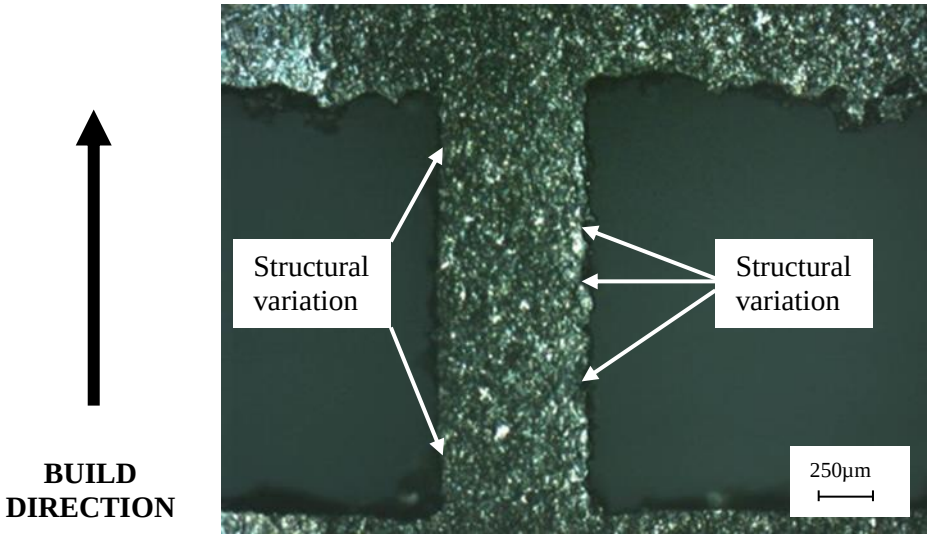

Figure 4.5 Micrograph of a vertical strut on Component 3.

4.3.2 Uniaxial compression tests

The mean compressive properties for each design configuration were calculated from the real time force versus displacement data. The typical stress strain relationship for each structure is compared in Figure 4.6. The effective stiffness and strength were both seen to decrease with increasing porosity. The mean compressive properties are presented in Table 4.2. It is evident that the mean effective elastic modulus varied between 1.06 GPa and 28.59 GPa and the mean compressive yield strength varied between 9.30 MPa and 327.47 MPa dependent upon porosity. The yield strength was not determined for Component 7 because the structure did not exhibit any plastic deformation before the maximum 100 kN load capacity of the test machine was reached.

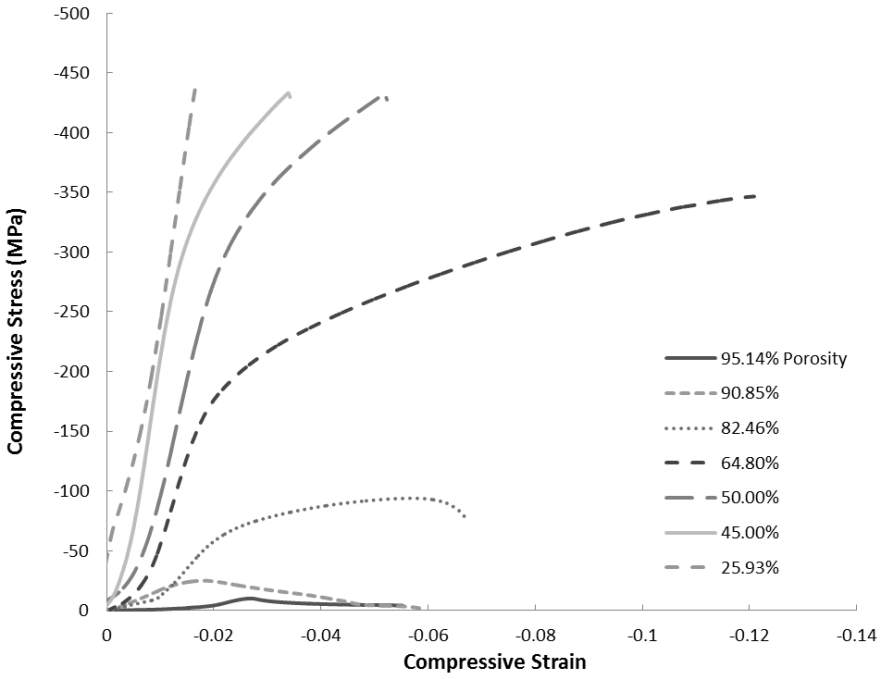

Figure 4.6 Typical experimental stress strain relationship for each structure.

Table 4.2 The mean effective elastic modulus and 0.2% compressive yield strength of each structure from the uniaxial compression tests *(n=4)*.

Component Number	Strut Size (mm)	Designed Volume Based Porosity (%)	Mean Effective Elastic Modulus (GPa)	Mean 0.2% Compressive Yield Strength (MPa)
1	0.20	95.14	1.06 +/- 0.12	9.3+/-0.38
2	0.35	90.85	2.23 +/- 0.38	24.73+/-2.00
3	0.50	82.46	4.79 +/- 0.51	65.43+/-1.82
4	1.00	64.80	13.64+/-0.73	175.15+/-4.37
5	1.50	50.00	17.98+/-1.95	295.72+/-8.80
6	2.00	45.01	25.25+/-3.59	327.47+/-12.00
7	2.50	25.93	28.59+/-3.64	No yielding

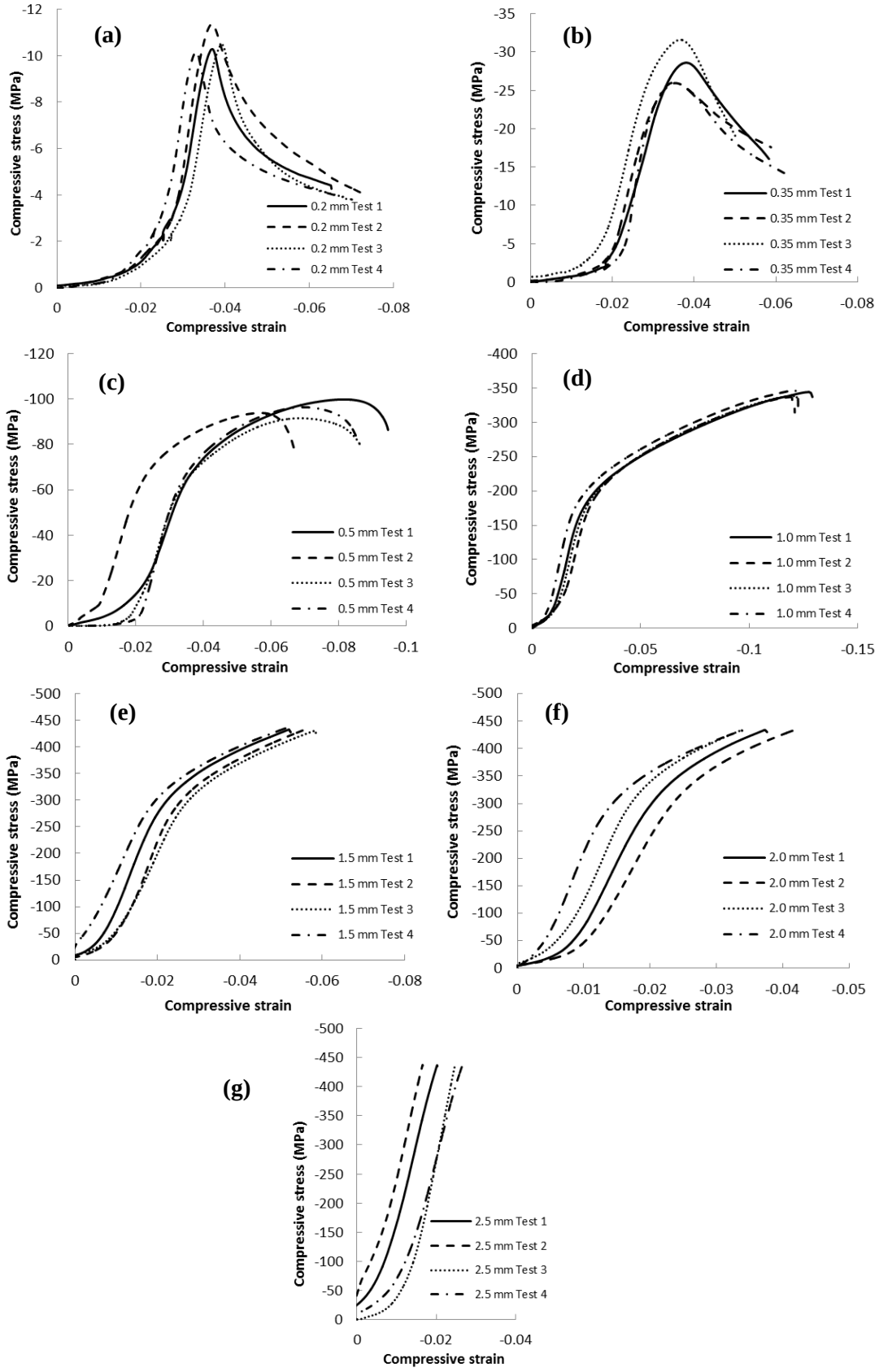

Figure 4.7 The experimental stress-strain relationship for each cellular structure (a) 0.2 mm (b) 0.35 mm (c) 0.5 mm (d) 1.0 mm (e) 1.5 mm (f) 2.0 mm (g) 2.5 mm.

Figure 4.7 compares the stress strain relationships for each of the test samples where it is evident that at the beginning of loading the curves are non-linear. This phenomenon has been observed elsewhere (McKown *et al*. 2008; Yan *et al*. 2012) and has been attributed to slight inaccuracies generated whilst removing the samples from the build plate and, or due to the unevenness of the top surface of the cellular structure. A more brittle failure was observed with the cellular structures possessing a strut size of less than 0.5 mm, as shown in Figures 4.7a and 4.7b. From the results, it is considered that the structure with a 1 mm strut size (Component 4) exhibited the most repeatable mechanical behaviour, as shown in Figure 4.7d.

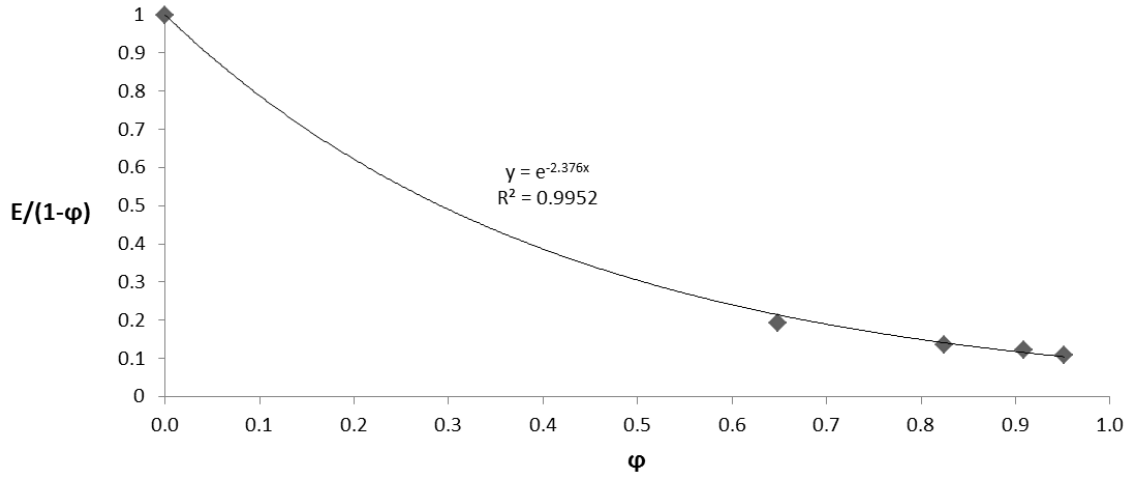

Figure 4.8 The curve that was used to derive the expression for predicting the effective elastic modulus based upon the experimental results.

The relationship between the effective elastic modulus and designed volumetric porosity has been analysed in Figure 4.8. From the experimental results, an expression has been proposed to predict the effective elastic modulus of square pore CoCrMo cellular structures where:

$$E_{eff} = E_s \left(1-\varphi\right) e^{(-2.376\varphi)} \tag{4.4}$$

Where E_s is the elastic modulus of the solid CoCrMo alloy that has been assumed as 200 GPa (Electro Optical Systems, 2010) and φ is the porosity. The derived expression has a coefficient of determination value (R^2) of 0.9952.

4.3.3 Finite element modelling

4.3.3.1 Predicting the effective elastic modulus of the cellular structures

Figure 4.9 compares the effective stiffness values obtained using the different methods. Correlation between the experimental and numerical results was poor. The numerical analysis overestimated the effective stiffness by a mean factor of 3.33 when comparing both sets of values.

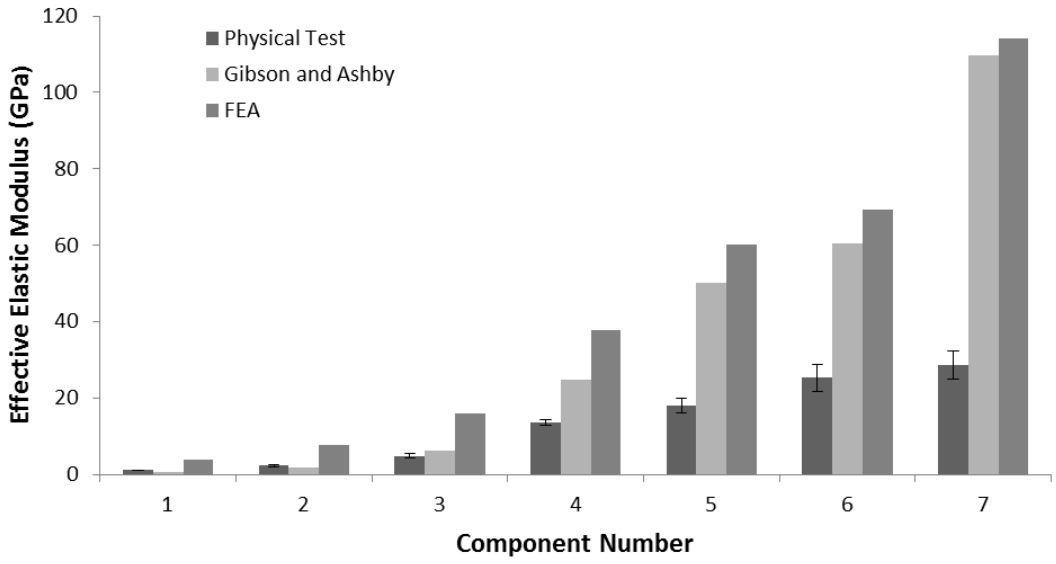

Figure 4.9 Comparison of the values for the elastic modulus for each method.

4.2.3.2 Finite element modelling of structural variation within a cellular structure

From the finite element model, 50% of the elements had their stiffness changed from 200 GPa to 0.02 GPa, in order to represent structural variation and heterogeneities within the cellular structure. This change resulted in an effective elastic modulus value of 5.37 GPa being calculated. When comparing this to a value of 16.03 GPa for the

ideal model, it shows an approximate 66% decrease in the structures stiffness when structural variation is modelled. The new stiffness value was also much closer to the mean experimental test value for Component 3, which was 4.79 GPa.

4.3.4 Analytical prediction of the structural stiffness

The effective elastic modulus for each design configuration was predicted using Equation 4.3. From Figure 4.10, the values obtained through the analytical prediction display a similar trend to the numerical results. Generally, the predicted values overestimate the stiffness of the structures when compared to the experimental data, this being concurred from other work (Parthasarathy *et al.*, 2010). A closer comparison was formed using the Gibson and Ashby method with the structures that were designed with porosity values of 80% and above, namely Components 1 - 3. This may be because the equation was originally derived to predict the effective elastic modulus of cellular structures and metal foams with porosities of 70% and above (Gibson and Ashby, 1997).

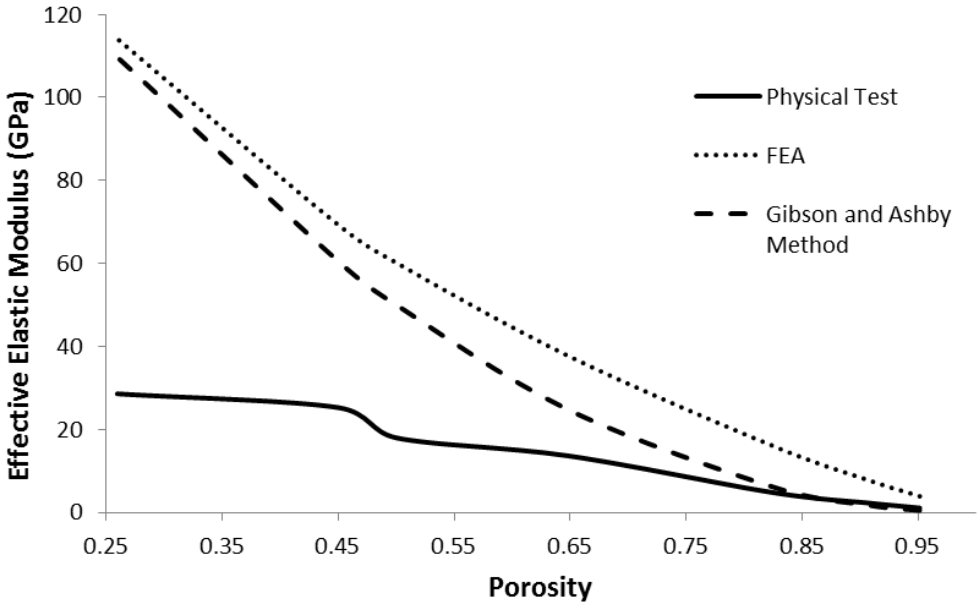

Figure 4.10 Comparison of the relationship between the effective elastic modulus and porosity.

4.4 Discussion

This chapter has investigated the compressive properties of square pore CoCrMo cellular structures that have been manufactured using SLM. Uniaxial compression testing was the chosen method of testing in this work and this was common within similar studies of this nature (Harrysson *et al*., 2008; Parthasarathy *et al*., 2011; Yan *et al*., 2012; Smith *et al*., 2013).

Tensile testing was considered as an alternative methodology. Examples of the manufactured test samples are shown in Figure 4.11. However, from visual inspection, fractures were evident between the connections of the individual struts and the main body of the specimen. It was considered that these defects were caused through the geometric mismatch between the strut and the main body of the specimen, thus creating concentrated areas of thermally induced stress. Therefore, from observing this phenomenon, no further work was performed on the tensile aspect of testing.

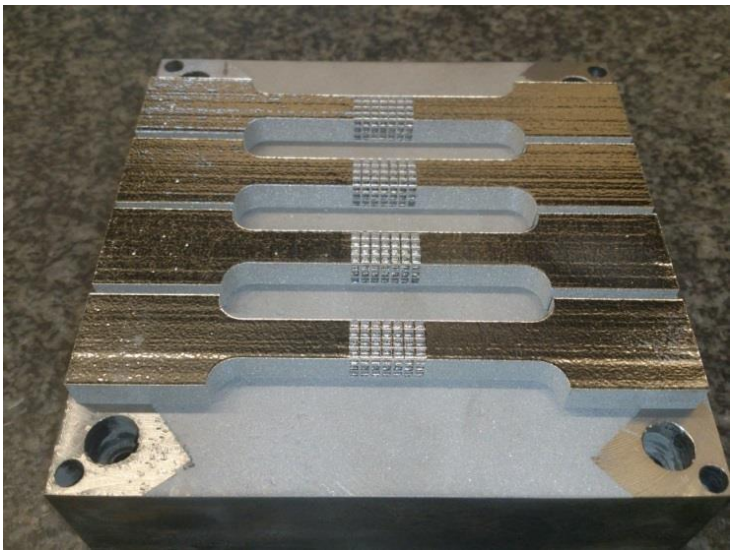

Figure 4.11 Tensile test specimens incorporating the cellular structure of Component 3.

The compressive elastic modulus and strength of femoral cortical and cancellous bone have previously been reported within the literature (Reilly and Burstein, 1975; Ohman *et al*., 2007). Elastic modulus values of 17 GPa and 2.73 GPa have been stated, with strength values of 193 MPa and 18 MPa being described for each bone type respectively. The values from Table 4.2 and the stress strain relationships in Figure 4.7 suggest that Components 2 and 5 provide cellular structures with stiffness and strength characteristics that are similar to the two types of femoral bone.

The experimental results agree with other published work, in that the stiffness and strength of the cellular structures are heavily dependent upon the volumetric porosity and strut size (Harrysson *et al*., 2008; Parthasarathy *et al*., 2011; Yan *et al*., 2012). From the literature review, this is the only study that has investigated the effective compressive properties of square pore CoCrMo cellular structures manufactured using SLM. In this instance, it has been difficult to compare the results with other published work.

The results however, were compared with those by Parthasarathy *et al.* (2011), who investigated the mechanical properties of square pore Ti-6Al-4V cellular structures with the same unit cell geometry as investigated in this work. A comparative calculation was performed by using the ratio between the elastic modulus of CoCrMo and Ti-6Al-4V in order to predict the expected difference in stiffness. A structure with similar porosity and strut size was compared however; a close correlation could not be achieved. A potential reason for this could be attributed to the displacement being measured using an extensometer in the current work, which can be assumed to be more accurate in comparison to measuring the displacement between the crossheads.

The correlation between the computational and experimental results was similar to other studies (Harrysson *et al*., 2008; Parthasarathy *et al*., 2011). Elsewhere, laser sintered

polycaprolactone square pore cellular structures have been analysed physically and numerically (Eshraghi and Das, 2010). A closer agreement was achieved between the experimental test and finite element analysis, with a 30% difference being observed. This provides an insight that the mechanical properties of polymeric additive manufactured components are more predictable when compared to metals. It is considered that the difference between experimental and numerical results in this chapter is attributed to the factors associated with the ALM of metals, concerning cell deformation and structural variation (Simone and Gibson, 1998; Parthasarathy *et al*., 2011; Smith *et al*., 2013).

It may be considered that the unit cell geometry investigated in this chapter is not ideal for SLM due to the horizontal struts creating downward facing unsupported surfaces. Structural variation was more evident in cellular structures that possessed strut sizes that were less than 0.5 mm. It is considered that the increased structural variation contributed to the more brittle failure of the more filigree cellular structures. Structural variation and an uneven surface finish have been observed with structures comprised of unit cell geometries that could be described as being more suitable for ALM, with respect to them not possessing horizontal downward facing surfaces (Harrysson *et al*., 2008; Yan *et al*., 2012; Smith *et al*., 2013).

Structural variations were applied to Component 3 in order to investigate what effect this had on the effective stiffness. The methodology employed was based upon the ANSYS element birth and death technique, where selected elements are multiplied by a stiffness reduction factor. The value of the stiffness reduction factor and quantity of elements selected was chosen to result in an effective elastic modulus value that was much closer to the experimental test for Component 3. ANSYS was used to unsystematically select elements within the structure, as it was not possible to determine

the exact distribution of the internal and external structural variations within the cellular structure itself. Changing the stiffness of 50% of the elements provided a stiffness value that was closer to the experimental test. In future work, the percentage and distribution of elements that are selected for stiffness reduction could be modelled more accurately if inspection methods such as μCT scanning were employed to identify the defects within the cellular structures. It is considered that the modelling technique used in this work has provided a suitable approach to help justify the theory that the compressive stiffness of additive manufactured square pore cellular structures is compromised through structural variation and heterogeneities that are inherently generated by the laser melting process.

In both the numerical and analytical aspects of this work, a mean value of 200 GPa was assumed for the elastic modulus of the fully dense CoCrMo (Electro Optical Systems, 2010). Elsewhere, the elastic modulus of EOS Cobalt Chrome MP1 has previously been reported as 198 GPa when manufactured using SLM with the same model of machine, processing parameters and build orientation as used in this work (Rivera *et al*., 2011). Therefore, the value of 200 GPa assumed in this work can be considered appropriate.

Equation 4.4 has been proposed to predict the stiffness of square pore CoCrMo cellular structures manufactured using SLM with a porosity of approximately 65% and above, based upon the experimental test results from this work. However, it should be mentioned that the equation has not been proposed as a universal design expression. When deriving Equation 4.4, the data for Components 5 to 7 was discarded. Only CoCrMo structures with a porosity of above 50% have been highlighted from this chapter for potential orthopaedic applications. This is partially based upon that the reviewed literature has concentrated on analysing cellular structures with a minimum volumetric porosity of 50% (Harrysson *et al*., 2008; Murr *et al*., 2010; Parthasarathy *et*

al., 2011; Li *et al*., 2012; Yan *et al*., 2012). Additionally, it is considered that cellular structures with low values of porosity behave like solid parts with isolated pores, as opposed to behaving like a cellular structure. It has been described that the transition between a cellular structure and a solid with isolated pores occurs when the relative density is approximately 0.3 or above (Gibson and Ashby, 1997).

4.5 Summary

This chapter has investigated the stiffness and strength characteristics of square pore CoCrMo cellular structures manufactured using SLM for potential orthopaedic applications. Within the discussed limitations, the main findings of the chapter can be summarised as follows:

- Square pore CoCrMo cellular structures manufactured using SLM have been presented, which have similar stiffness and strength characteristics when compared to femoral cortical and cancellous bone.
- The cellular structure with a 1 mm strut size and 64.8% volumetric porosity (Component 4) exhibited the most repeatable mechanical behaviour when subjected to uniaxial compression.
- Cellular structures with strut sizes smaller than 0.5 mm exhibited a more brittle failure mode when compared to the other structures.
- An expression has been proposed based upon the experimental test results to predict the effective elastic modulus of square pore CoCrMo cellular structures manufactured using SLM, with a volume based porosity of 65% and above.
- A finite element model has been proposed to help justify the theory that structural variation and heterogeneities can have a detrimental effect on the stiffness of cellular structures manufactured using SLM.

In the next chapter, the properties of the square pore cellular structures with a volumetric porosity of 50% and above are applied to vary the stiffness of monoblock CoCrMo femoral stems that are used in THA. The finite element method is used to investigate the load transfer to the periprosthetic femur when implanted with femoral stems that exhibit fully porous and functionally graded stiffness configurations.

Chapter 5 Finite element analysis of the periprosthetic femur

5.1 Introduction

This chapter addresses the development of finite element models for investigating the performance of CoCrMo femoral stems with varying stiffness configurations. One of the main aspects of this work was to investigate the potential advantages of incorporating cellular structures into the design of CoCrMo monoblock femoral stems.

Firstly, a finite element model of the intact femur was developed in order to provide a comparison with the implanted femur. The intact femur was then modified to accommodate a monoblock CoCrMo femoral stem that incorporated a selection of common design features.

The load transfer to the periprosthetic femur was then investigated where a fully dense CoCrMo stem was used as a benchmark for comparison with fully porous and functionally graded designs that offered different stiffness configurations. The fully porous and functionally graded designs were created by utilising the compressive properties of the CoCrMo cellular structures that were determined in the previous chapter. Certain cellular structures with a volumetric porosity of 50% and above were considered and modelled as continuum bodies by using the physically determined stiffness constants. Axially grading the stems stiffness was considered based upon the observations from previous work (Kuiper and Huiskes, 1997: Gong *et al*., 2012).

This work aims to hypothesise that incorporating the properties of square pore CoCrMo cellular structures into the design of a monoblock femoral stem can increase the periprosthetic stress and hence the mechanical stimulus within the femur, without compromising the strength of the bone itself.

5.2 Finite element analysis of the intact femur

5.2.1 Methods

The three dimensional geometry of a full left femur was taken from the 38 year old male cadaver that was used in the Visible Human Project (1994) at the US National Library of Medicine. A STL file of the femur was imported into Solidworks 2012 CAD software where a solid model of the femur was created. The distal region of the femur was cut away as the proximal portion of the femur was of interest. This provided a length of 285 mm, which was measured from the distal end of the femur to the top point of the femoral head. A STEP file of the femur was then imported into ANSYS 13.0 finite element software for analysis.

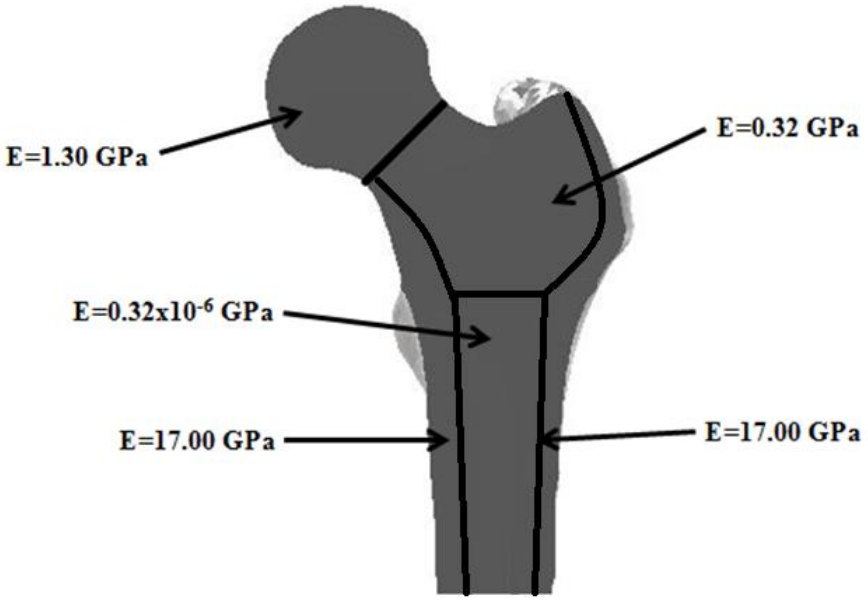

Figure 5.1 Schematic representation of the mechanical properties that were assumed in the finite element model for the intact femur.

The femur was meshed with 99,798 SOLID 185 four node tetrahedral elements and mesh sensitivity was studied until further mesh refinement changed the maximum von Mises stress in the femur by 5% or less. This resulted in an element size of 5 mm being used for the analysis.

Both bone types were modelled with linear isotropic behaviour (Yan *et al.*, 2011; Arabnejad Khanoki and Pasini, 2013). The material properties of the femur were manually controlled similar to the work of Wang *et al.* (1998), by selecting regions that corresponded to the different bone types, as shown in Figure 5.1. The mesh was adapted to maintain a cortical bone thickness of between 5 mm and 6 mm, which is thought to be representative for a male femur of the given age (Bousson *et al.*, 2000). The elastic modulus of cortical bone was chosen as 17 GPa, with the modulus of the two types of femoral cancellous bone being 1.30 GPa and 0.32 GPa (Wang *et al.*, 1998). The stiffness of the elements representing the bone marrow was modelled by using the same principle as the ANSYS EKILL command. The elements were originally meshed with the same elastic modulus of cancellous bone (E=0.32 GPa) and then their stiffness was multiplied by a reduction factor to the order of 1×10^{-6}. A Poisson's ratio of 0.3 was assumed for all materials throughout.

Table 5.1 The loads that were applied to the femur (Heller *et al.*, 2005).

Force	Medial-Lateral (N)	Superior-Inferior (N)	Anterior-Posterior (N)	Resultant (N)
Hip joint reaction	451.4	-1916.1	274.2	1987.6
Abductor muscle	-484.9	723.1	-35.9	871.4

The loading scenario was simplified by applying the hip joint reaction and abductor muscle force (Herrera *et al.*, 2007). The loading data was taken from Heller *et al.* (2005) in the single stance phase of gait, for a person walking with a body weight of 85.2 kg, which equates to 836 N. The hip joint reaction force was centred on the highest point of the femoral head and the abductor force was centred on the most lateral point of the greater trochanter (Bryan *et al.*, 2012). Both forces were evenly distributed over 20

nodes respectively and the components of both forces are shown in Table 5.1. The distal end of the femur was fully constrained to prevent rigid body motion.

5.2.2 Results

The stress distribution and displacement of the intact femur have been analysed in order to provide a comparison with the implanted femurs that are considered within this work. From Figure 5.2, it can be observed that the applied loading condition produced a bending stress distribution in the diaphysis of the femur, with higher stresses being observed on the medial and lateral surfaces when compared to the anterior and posterior surfaces of the femur.

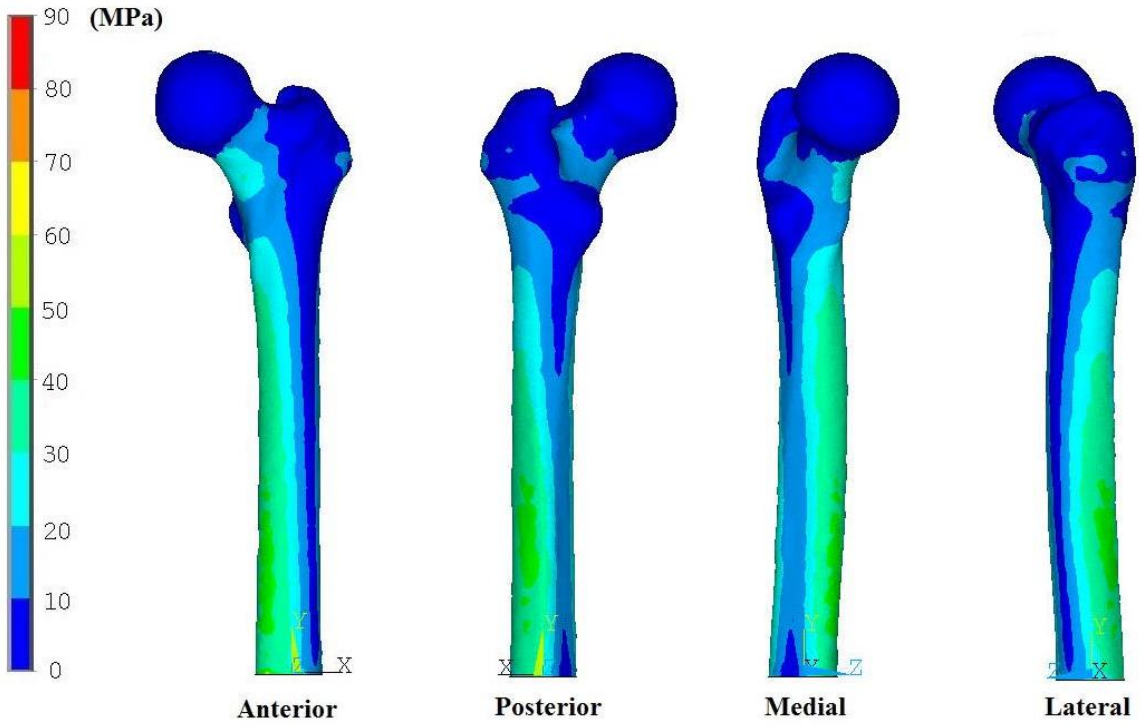

Figure 5.2 The von Mises stress distribution in the intact femur.

The maximum displacement values of the femoral head were 4.73 mm medially, 3.15 mm inferiorly and 6.52 mm anteriorly. From this, it is evident that the anterior displacement on the sagittal plane dominates in this analysis. It is thought that this is due to only the joint reaction and abductor force being applied to the femur. Other muscle forces such as the ilotibial tract and ilopsoas would need to be considered to correct this deformation (Taylor *et al*., 1996).

5.3 Finite element analysis of fully porous CoCrMo femoral stems

5.3.1 Methods

Numerical analysis was performed to investigate the load transfer to the periprosthetic femur when implanted with CoCrMo monoblock femoral stems that incorporated the mechanical properties of square pore cellular structures. The characteristics and mechanical properties of the cellular structures that have been utilised in this chapter are recalled and summarised in Table 5.2.

Table 5.2 Geometric and mechanical properties of the cellular structures.

Strut size (mm)	Pore size (mm)	Effective Elastic Modulus (GPa)	0.2% Compressive Yield Strength (MPa)
0.50	1.57	4.79	65.43
1.00	1.80	13.64	175.15
1.50	1.88	17.98	295.72

From the previous chapter, the cellular structures with a volumetric porosity of 50% and above were highlighted for potential orthopaedic applications. The cellular structures with a 0.20 mm and 0.35 mm (Components 1 and 2) strut size were not considered in this instance due to the more brittle failure (Figure 4.7a and b) and increased structural variation that was visually observed.

Five fully porous stiffness configurations were investigated and their performance was compared with a traditional fully dense CoCrMo stem. The investigated stiffness configurations are schematically shown in Figure 5.3 and are described below:

- **FDS,** a fully dense CoCrMo femoral stem with an elastic modulus of 200 GPa.
- **PS-1,** a fully porous stem with an elastic modulus of 17.98 GPa.
- **PS-2,** a fully porous stem with an elastic modulus of 13.64 GPa.
- **GPS-1,** a fully porous stem with elastic modulus values of 17.98 GPa and 13.64 GPa assigned to the proximal and distal regions respectively.
- **GPS-2,** a fully porous stem with elastic modulus values of 17.98 GPa and 4.79 GPa assigned to the proximal and distal regions respectively.
- **GPS-3,** a fully porous stem with elastic modulus values of 13.64 GPa and 4.79 GPa assigned to the proximal and distal regions respectively.

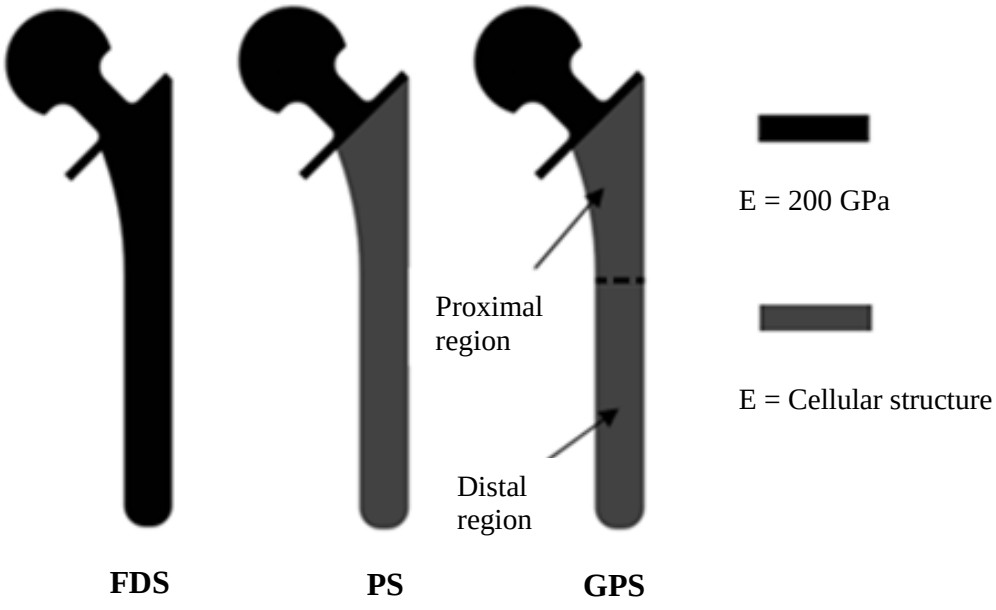

Figure 5.3 Schematic representation of the fully porous stiffness configurations.

5.3.1.1 Model geometry

The proximal region of the femur used for the intact analysis was modified using Solidworks 2012. The femoral head and neck region were cut away to provide a femoral neck angle of 135 degrees, which was similar to the anatomy of the intact femur. The internal cavity of the femur was created with an identical geometry to the femoral stem.

A femoral stem was designed using Solidworks 2012 to suit the anatomy of the proximal femur. The following general design features were incorporated:

- The stem geometry was designed in a similar manner to the VerSys Epoch FullCoat Hip System (Zimmer, 2013). The medial-proximal portion of the stem was designed with a curved geometry in order to achieve cortical fixation in the high diaphysis region local to the lesser trochanter.

- A collar was incorporated into the design to help improve the axial stability and prevent distal migration of the stem (Whiteside *et al*., 1988).

- The length of the femoral stem and diameter of the femoral head were chosen as 150 mm and 36 mm respectively. The femoral head size was chosen as a mid-range representation of common femoral head sizes (Hammerberg *et al*., 2010). The length is standard in the range of stem lengths listed by orthopaedic implant manufacturers.

- The femoral neck angle and femoral head offset were chosen as 135 degrees and 30 mm respectively, as this represented a close match to the anatomy of the intact femur. Anteversion of the femoral head was not accounted for in this instance.

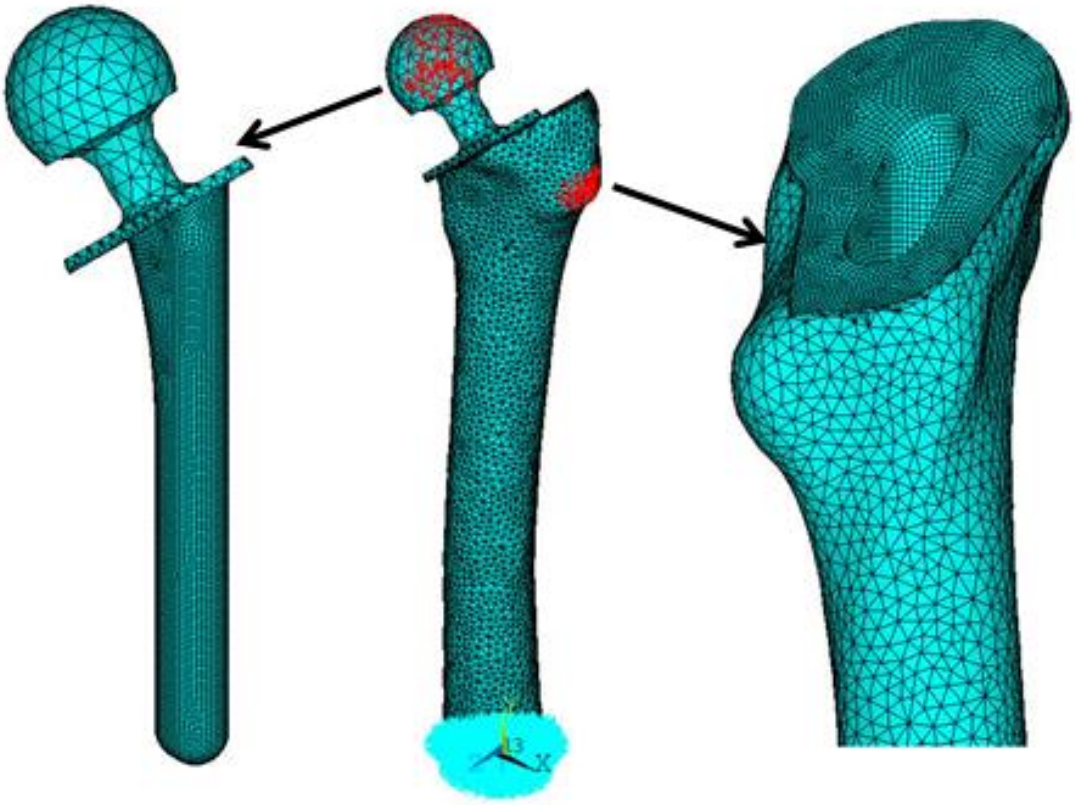

Figure 5.4 The finite element mesh of the implant and proximal femur.

5.3.1.2 Finite element mesh

The models were meshed typically with 329,777 SOLID 185 four node tetrahedral elements as shown in Figure 5.4. An element size of 5 mm was chosen to mesh the whole model initially. The bone-implant interface mesh was then refined with a 1mm element size following a mesh sensitivity study. Fully bonded surface to surface contact conditions were created to simulate ideal cementless fixation of the stem, by using CONTACT 174 and TARGET 170 elements.

5.3.1.3 Material properties and boundary conditions

The femur was assigned with the same material properties that were used for the analysis of the intact femur, with the exception that the femoral head/neck region of cancellous bone was not present in this model.

The femoral stems were modelled with linear isotropic behaviour. The elastic modulus of the fully dense CoCrMo was taken as 200 GPa (Electro Optical Systems, 2010). The stiffness constants for the square pore CoCrMo cellular structures were determined from the uniaxial compression tests that were performed in Chapter 4, as shown in Table 5.2. The cellular structures were modelled as continuum bodies that were assigned the elastic properties relating to the chosen cellular structure. The fully porous stems were modelled as one body and initially meshed with the properties of CoCrMo. The elements for the stem portion of the prosthesis were then selected with respect to a pre-defined coordinate system and the elastic modulus of the stem was adapted as required. In all scenarios, the femoral head and neck region of the implant was represented by fully dense CoCrMo (E=200GPa). A Poisson's ratio of 0.3 was assumed for all materials throughout. The applied boundary conditions were identical to the analysis of the intact femur and these are shown in Figure 5.5.

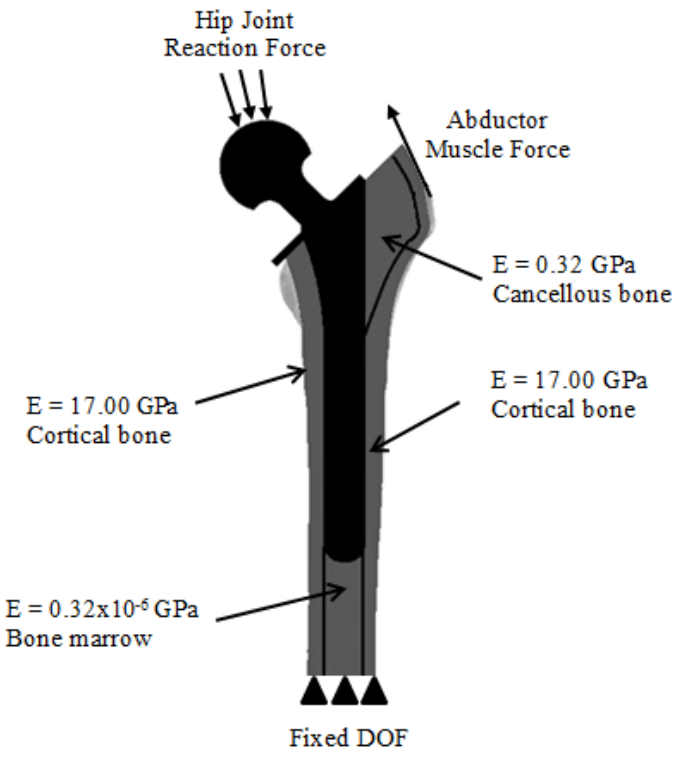

Figure 5.5 The material properties and applied boundary conditions for the finite element model.

5.3.2 Results

The displacement of the femoral head, von Mises and principal stresses in the proximal femur have been investigated throughout this chapter. The von Mises stress was compared with Gruens zones (Gruen *et al.*, 1979), as these have historically been used in clinical situations to measure periprosthetic bone density following THA, and thus provide an appropriate indicator of stress shielding. The von Mises stress was calculated at 28 nodal locations, at a distance of 2 mm from the bone-implant interface along the frontal plane of the femur, as shown in Figure 5.6. Four stress values for each zone were recorded and a mean value of von Mises stress was used for a comparative analysis. The maximum and minimum principal stresses in the femur were analysed to investigate whether there was any risk of failure in tension or compression.

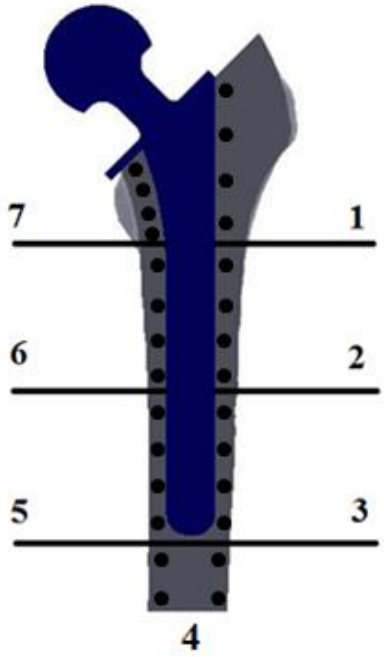

Figure 5.6 Gruens zones that were used to compare the von Mises stress. The black dots represent the approximate nodal locations where the stress was determined.

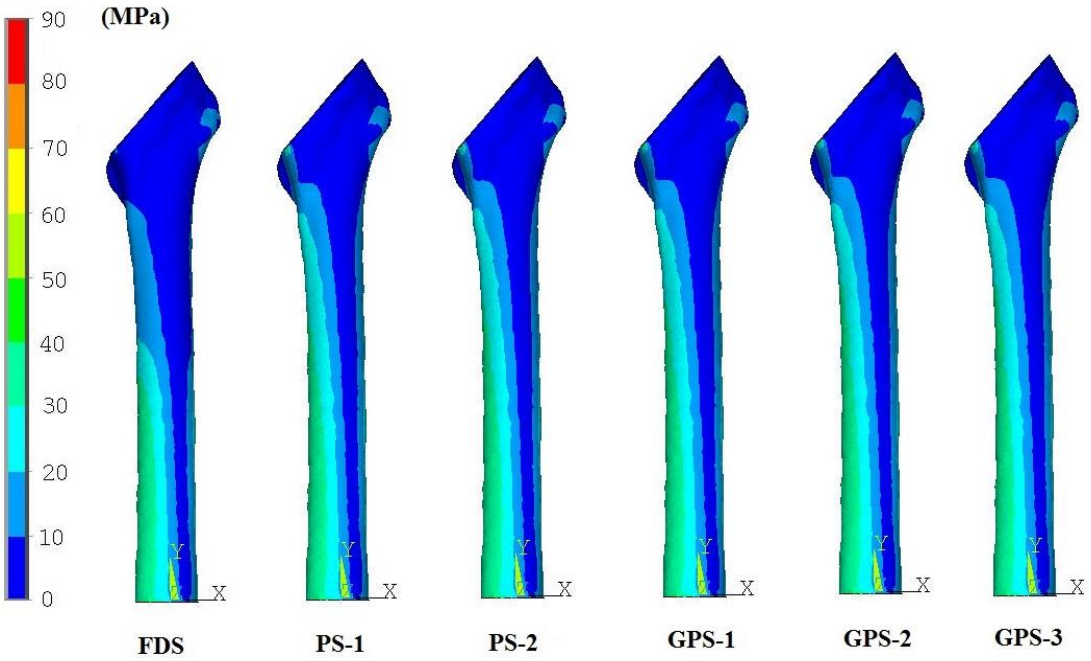

Figure 5.7 The anterior view of the von Mises stress distribution in the femur.

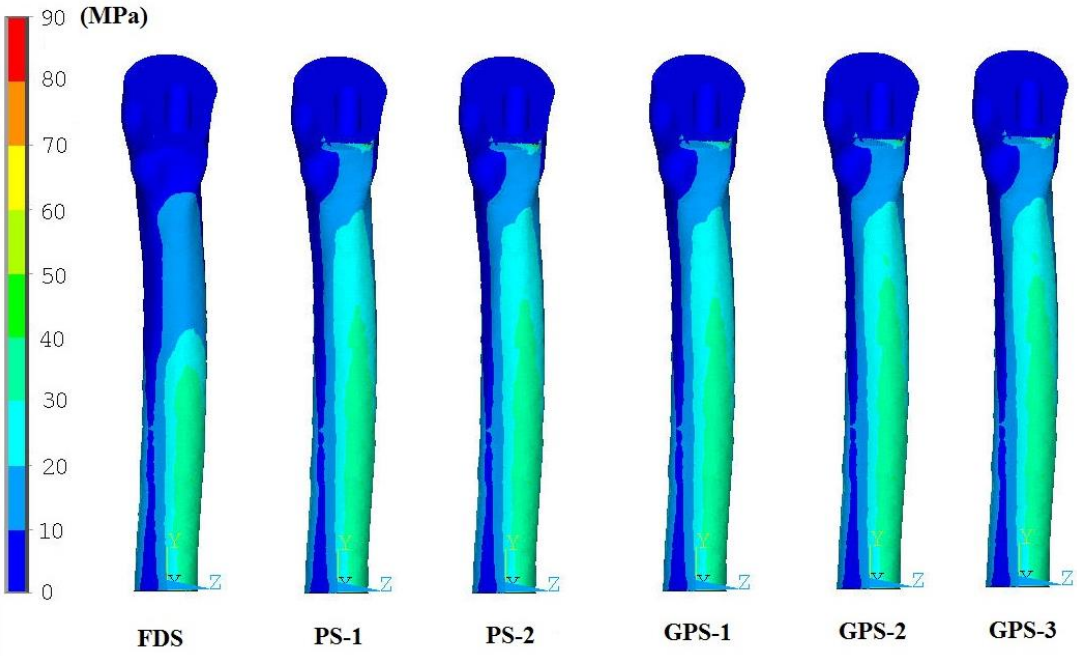

Figure 5.8 The medial view of the von Mises stress distribution in the femur.

Generally, from an anterior and medial perspective it can be observed that the fully porous stems provide higher von Mises stress values in the proximal femur when compared to the FDS, as shown in Figures 5.7 and 5.8. Additionally, from Figures 5.9

and 5.10, it is evident that the fully porous stems provide higher stress values in all of the Gruen zones when compared to the FDS, except for Zones 1 and 4.

In all cases, there was no noticeable difference in the stress distribution in Zone1, this is thought to be because the greater trochanteric region of the femur is mainly comprised of cancellous bone and is not highly stressed in its natural intact state, as shown in Figure 5.2. The lower stress values provided by the fully porous stems in Zone 4 indicates that more load is being transferred proximally. The maximum stress with each stem was evident in Zone 4 due to the femur being mainly subjected to bending in this analysis.

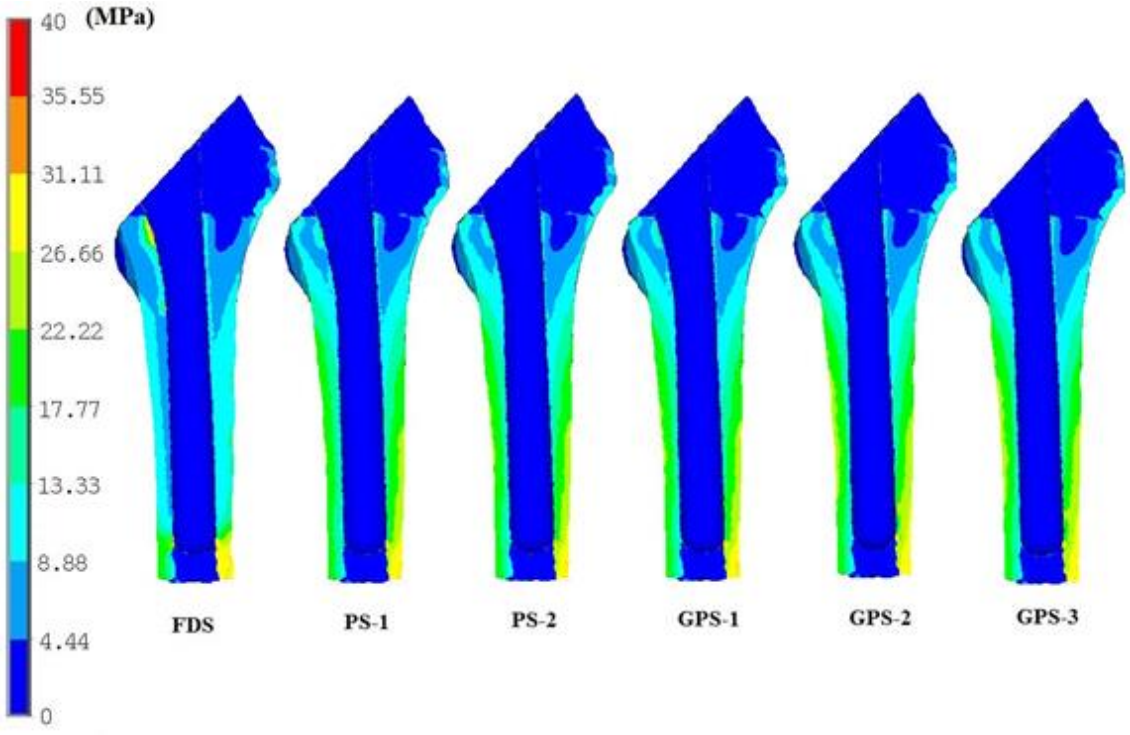

Figure 5.9 Cross sectional view along the frontal plane of the von Mises stress distribution in the periprosthetic femur.

The axially graded stems provided higher stress values in the medial Zones 5 and 6 when compared to the other fully porous stems. This shows that decreasing the stiffness in the distal portion of the stem can increase the stress values in the medial diaphysis

and metaphysis by approximately 50% and 93% respectively when compared to the FDS. Similar trends were observed in the lateral Zones 2 and 3 where by the stress values increased by approximately 50% in both zones. The fully porous stems provided on average a 44% increase in the stress value observed in Zone 7 when compared to the FDS.

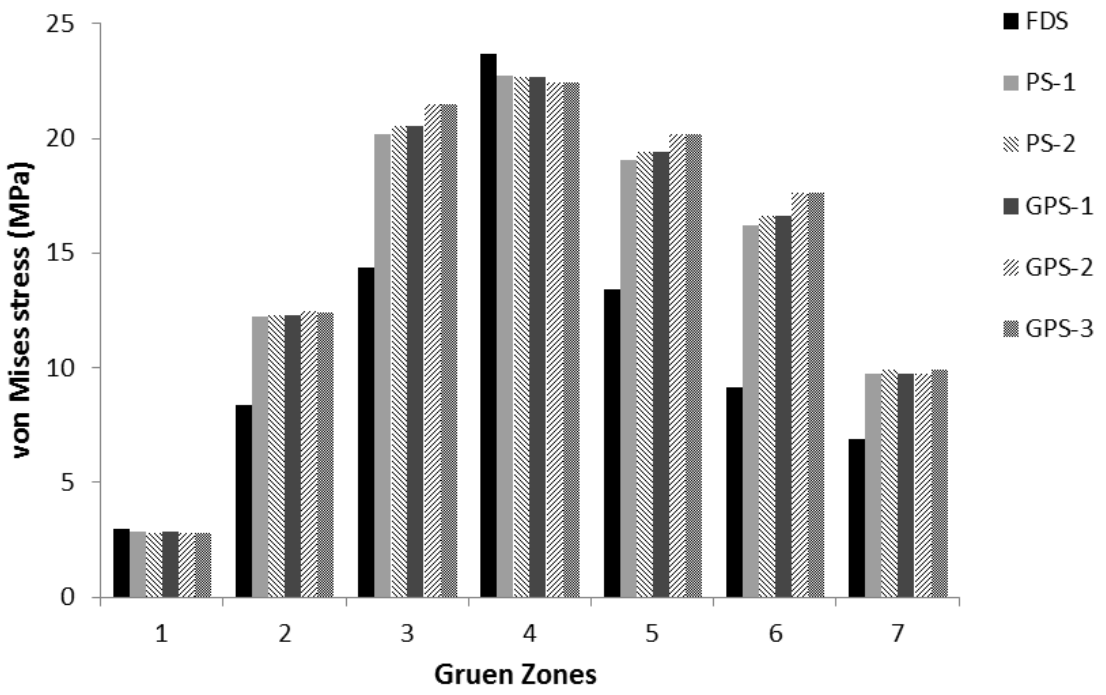

Figure 5.10 The von Mises stress in each Gruen zone.

The maximum and minimum principal stresses were observed in the cortical bone local to the distal tip of the prosthesis. The values presented in Table 5.3 indicate that the structural integrity of the femur would not be compromised in this instance. It was evident from the distribution of the principal stresses that the periprosthetic femur was mainly subjected to compression, with the medial-posterior cortex being subjected to tension.

Table 5.3 The peak maximum and minimum principal stresses that were observed in the femur.

Femoral stem	σ_1 (MPa)	σ_3 (MPa)
FDS	28.56	-24.68
PS-1	27.24	-25.04
PS-2	27.12	-25.11
GPS-1	27.12	-25.11
GPS-2	26.78	-25.32
GPS-3	26.78	-25.32

Table 5.4 The maximum displacement values of the femoral head.

Stiffness Configuration	Medial-Lateral Displacement (mm)	Superior-Inferior Displacement (mm)	Anterior-Posterior Displacement (mm)
FDS	-3.70	-0.93	2.49
PS-1	-4.13	-1.12	2.65
PS-2	-4.16	-1.14	2.66
GPS-1	-4.15	-1.13	2.66
GPS-2	-4.19	-1.15	2.67
GPS-3	-4.20	-1.15	2.68

Table 5.4 shows the maximum displacement values of the femoral head for the investigated stiffness configurations. Increased flexibility is gained in all three directions when the properties of the cellular structures are introduced into the femoral stem. From comparing the fully porous stems, the PS-2, GPS-1, GPS-2 and GPS-3 provide improved flexibility medial-laterally and anterior-posteriorly when compared to the PS-1, with smaller increases observed superior-inferiorly. Overall, it can be interpreted that the GPS-2 and GPS-3 provide the most flexible stiffness configurations. This flexibility is also comparable to the increased stress values and improved periprosthetic stress that can be observed from Figures 5.9 and 5.10.

5.4 Finite element analysis of CoCrMo femoral stems using a functionally graded approach

5.4.1 Methods

Six functionally graded stiffness configurations were investigated and their performance was compared with a traditional fully dense CoCrMo stem. The investigated stiffness configurations are schematically shown in Figure 5.11 and are described below:

- **FDS,** a fully dense CoCrMo femoral stem with an elastic modulus of 200 GPa.
- **PC-1,** 1 mm fully dense skin and a core with an elastic modulus of 17.98 GPa.
- **PC-2,** 1 mm fully dense skin and a core with an elastic modulus of 13.64 GPa.
- **PC-3,** 1 mm fully dense skin and a core with an elastic modulus of 4.79 GPa.
- **GPC-1,** 1 mm fully dense skin with an axially graded core. An elastic modulus of 17.98 GPa and 13.64 GPa was assigned to the proximal and distal regions respectively.
- **GPC-2,** 1 mm fully dense skin and an axially graded core. An elastic modulus of 17.98 GPa and 4.79 GPa was assigned to the proximal and distal regions respectively.
- **GPC-3,** 1 mm fully dense skin and an axially graded core. An elastic modulus of 13.64 GPa and 4.79 GPa was assigned to the proximal and distal regions respectively.

A 1 mm thick outer skin was selected for the functionally graded stems. This was based upon the results from the previous chapter, where the cellular structure with a 1 mm strut size exhibited the most repeatable mechanical behaviour.

The finite element model was identical to the model that investigated the fully porous stems, with the exception of the adapted design for the functionally graded femoral stems. The functionally graded stems were modelled as two continuum bodies in this instance. One body consisted of the femoral head, neck, collar and outer skin of the stem, whereas the other body represented the core. Therefore, the first body was meshed with CoCrMo material properties and the core was meshed with properties that were representative of the chosen cellular structures.

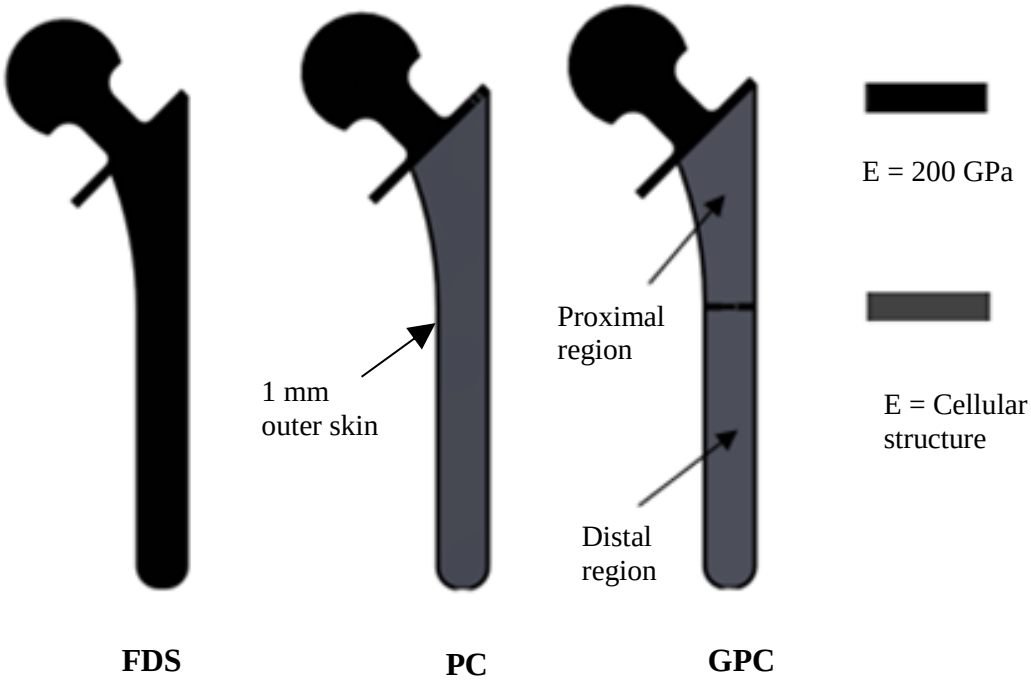

Figure 5.11 Schematic representation of the stiffness configurations.

5.4.2 Results

From observing Figures 5.12 and 5.13, it is evident that the functionally graded stems provide higher proximal stress values in both the anterior and medial views when compared to the FDS. Higher stress values were observed with the functionally graded stems when comparing the periprosthetic stress distribution as shown in Figure 5.14.

However, there was no noticeable difference in the stress distribution when comparing the functionally graded femoral stems.

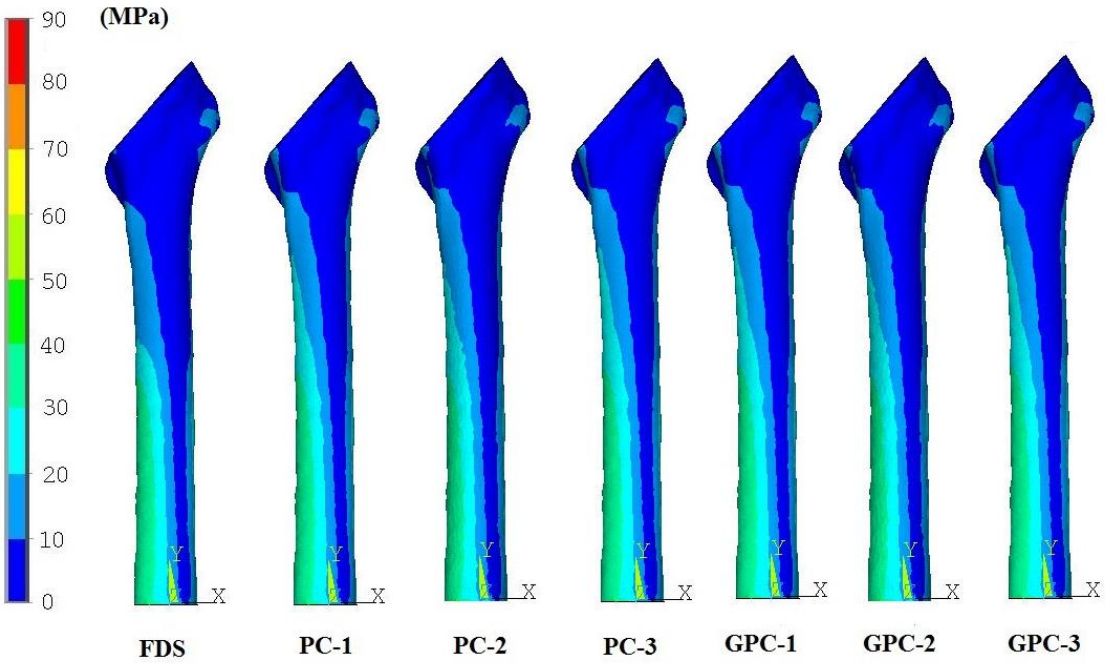

Figure 5.12 The anterior view of the von Mises stress distribution in the femur.

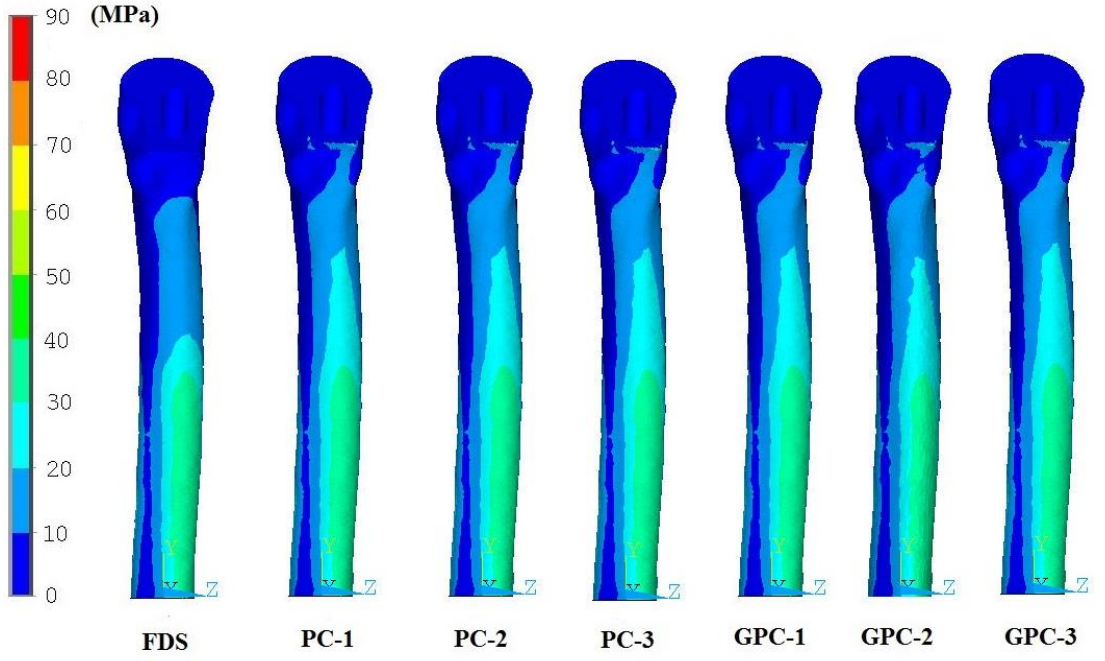

Figure 5.13 The medial view of the von Mises stress distribution in the femur.

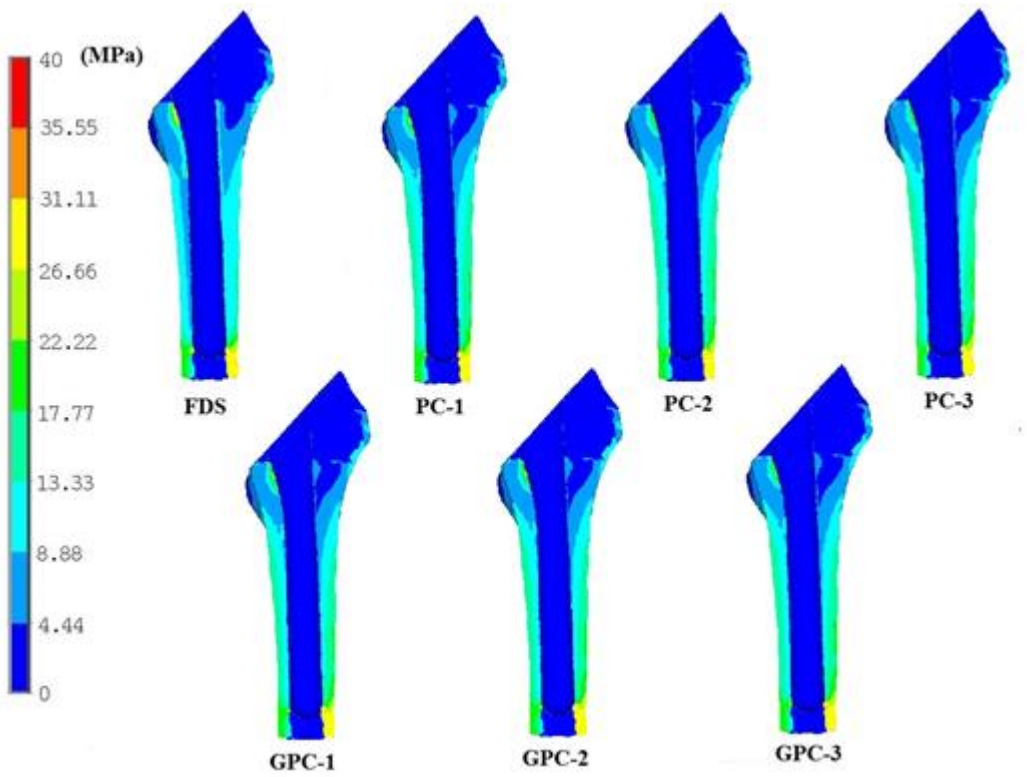

Figure 5.14 Cross sectional view along the frontal plane of the von Mises stress distribution in the periprosthetic femur.

Figure 5.15 shows the average von Mises stress values in each zone for each femoral stem modelled. The method for determining the stress values was identical to the method that was used for the fully porous stems. The functionally graded stems provided increased stress values of approximately 20% and 36% respectively in Zones 5 and 6 when compared to the FDS. Similar trends were observed in the lateral Zones 2 and 3 where the stress values increased by approximately 22% and 18% respectively. In Zone 7, it can be observed that the functionally graded stems provide an approximate 12% increase in the stress values in this zone when compared to the FDS.

The maximum and minimum principal stresses were again observed in the cortical bone local to the distal tip of the prosthesis. The values presented in Table 5.5 again indicate that the structural integrity of the femur would not be compromised in this instance.

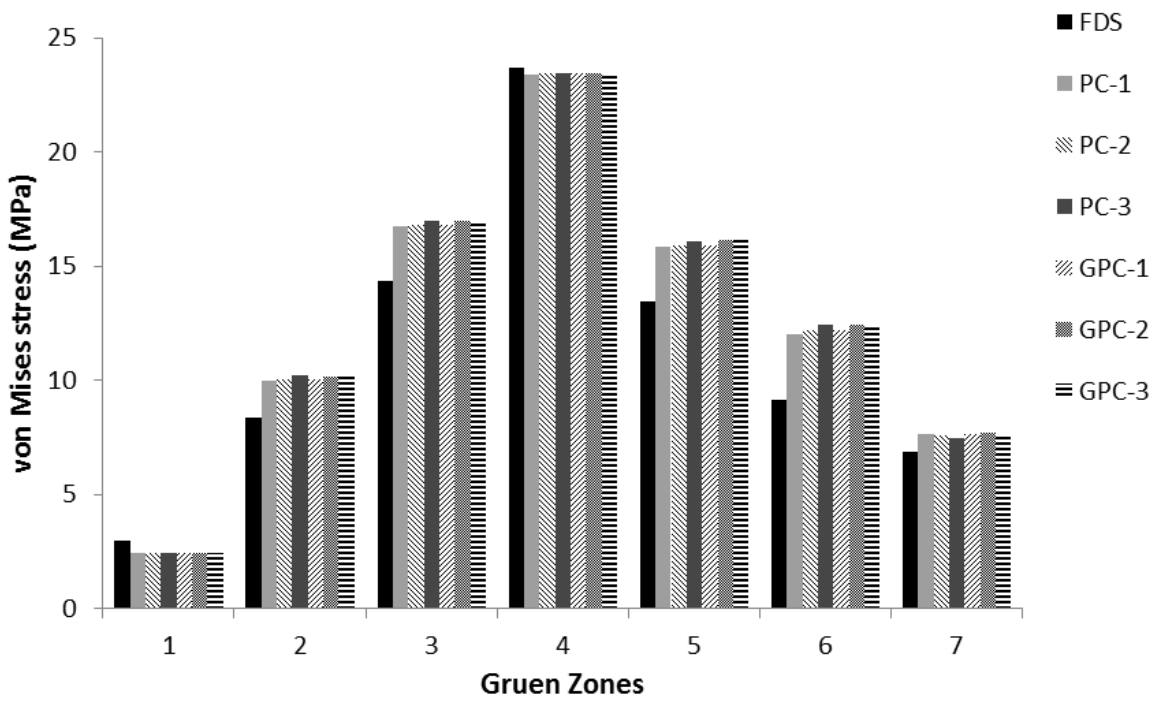

Figure 5.15 The von Mises stress in each Gruen zone.

Table 5.5 The peak maximum and minimum principal stresses that were observed in the femur.

Femoral stem	σ_1 (MPa)	σ_3 (MPa)
FDS	28.56	-24.68
PC-1	27.95	-25.09
PC-2	27.94	-25.09
PC-3	27.93	-25.08
GPC-1	27.94	-25.09
GPC-2	27.92	-25.09
GPC-3	27.92	-25.09

Table 5.6 shows the maximum displacement values of the femoral head for all of the stiffness configurations. Increased flexibility was evident in all three directions when the functionally graded stems were modelled. From comparing the functionally graded stems, it is evident that there is no significant difference in the flexibility of the stems.

Table 5.6 The maximum displacement values of the femoral head.

Stiffness Configuration	Medial-Lateral Displacement (mm)	Superior-Inferior Displacement (mm)	Anterior-Posterior Displacement (mm)
FDS	-3.70	-0.93	2.49
PC-1	-3.87	-1.01	2.55
PC-2	-3.88	-1.01	2.55
PC-3	-3.89	-1.02	2.55
GPC-1	-3.88	-1.01	2.55
GPC-2	-3.89	-1.02	2.55
GPC-3	-3.89	-1.02	2.55

5.5 Orthotropic material modelling

Human bone is a non-homogeneous and anisotropic material with mechanical properties that vary in accordance to the direction of loading. The elastic modulus of femoral cortical bone has been reported as 17 GPa and 11.5 GPa in the longitudinal and transverse axes respectively (Reilly and Burstein, 1975). In contrast to this, femoral stems that are currently utilised exhibit homogeneous and linear isotropic behaviour. This section of work theoretically investigates the influence of incorporating orthotropic material properties into the design of a monoblock CoCrMo femoral stem when using fully porous and functionally graded approaches.

5.5.1 Methods

The previous chapter did not physically investigate the mechanical properties of orthotropic cellular structures. Therefore, a comparison has been achieved by using the finite element method to estimate the material properties of cellular structures with both isotropic and orthotropic behaviour. The cellular structure with a 0.5 mm strut size and 82% volumetric porosity was utilised for this comparative analysis.

The material properties for the isotropic cellular structure were determined as in Chapter 4, by applying a 0.1% compressive strain to the top surface of the structure. The material properties for the orthotropic structure were calculated in compression and shear by applying 0.1% strains in different directions.

For an orthotropic material model, nine material constants are required, three elastic moduli *(E)*, three shear moduli *(G)* and three Poisson's ratios *(υ)*. These were calculated using the following general equations:

$$E = \frac{\sigma}{\varepsilon} = \frac{\left(\frac{F}{A}\right)}{\left(\frac{\Delta l}{l}\right)} = \frac{F}{0.001 \times A} \tag{5.1}$$

$$G = \frac{\tau}{\gamma} = \frac{\left(\frac{F}{A}\right)}{\left(\frac{\Delta l}{l}\right)} = \frac{F}{0.001 \times A} \tag{5.2}$$

$$\upsilon = -\frac{\varepsilon'}{\varepsilon} \tag{5.3}$$

Where F is the reaction force at the constrained face of the model, A is the cross sectional area of the component and ε' and ε are the transverse and longitudinal strain respectively.

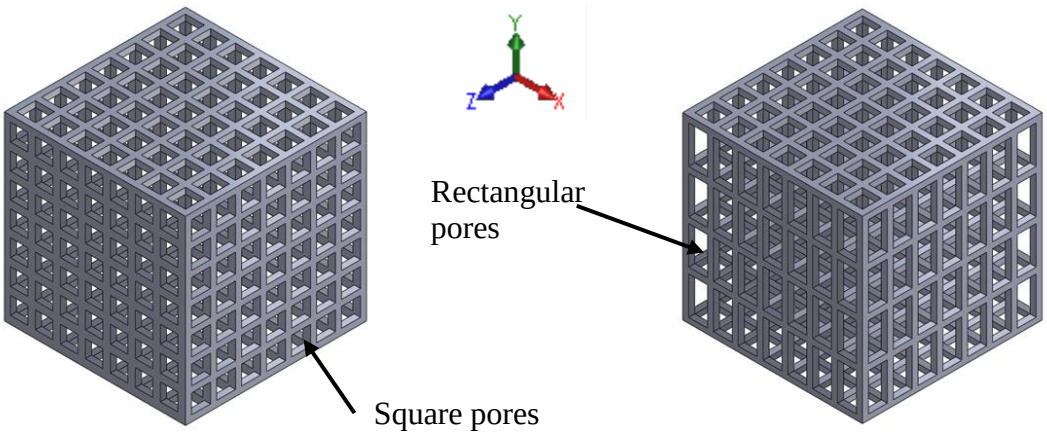

Isotropic structure
$E_x=E_y=E_z=$ 16.9 GPa

Orthotropic structure
$E_x = E_z =$ 11.3 GPa
$E_y =$ 16.9 GPa
$G_{xy}=G_{yz}=$ 0.58 GPa
$G_{xz}=$ 0.72 GPa
$\upsilon_{xy}=\upsilon_{yz} =$ 0.08
$\upsilon_{xz}=$ 0.11

Figure 5.16 The isotropic and orthotropic cellular structures and their calculated material properties.

Figure 5.16 shows the cellular structures and their respective material properties that were used for the numerical analysis. Four femoral stem stiffness configurations were investigated and their performance was compared with a traditional fully dense CoCrMo stem.

The investigated stiffness configurations are described below:

- **FDS**, a fully dense CoCrMo femoral stem (E=200 GPa).
- **PS**, a fully porous stem with isotropic behaviour (E=16.9 GPa).
- **OPS**, a fully porous stem with orthotropic behaviour (E=16.9 GPa longitudinally and E=11.3 GPa transversely).
- **PC**, 1 mm fully dense skin and a core with isotropic behaviour (E=16.9 GPa).
- **OPC**, 1 mm fully dense skin and a core with orthotropic behaviour (E=16.9 GPa longitudinally and E=11.3 GPa transversely).

The finite element model was identical to the model that was used to investigate the fully porous and functionally graded stems. In this instance, only the von Mises stress in the Gruen zones was used for a comparative analysis.

5.5.2 Results

Figure 5.17 shows the von Mises stress in the periprosthetic femur for each femoral stem modelled. As expected, the fully porous configurations provided higher stress values in the bone. When comparing the two fully porous stems, it was evident that orthotropic material properties can have a marginal influence on the load transfer to the proximal femur, as shown in Figure 5.18. The OPS femoral stem provided increases of 1.6%, 2.5% and 4.3% in the medial Gruen Zones 5, 6 and 7 respectively, when compared to the PS femoral stem. From the results, negligible differences in the stress values were observed between the PC and OPC functionally graded femoral stem designs.

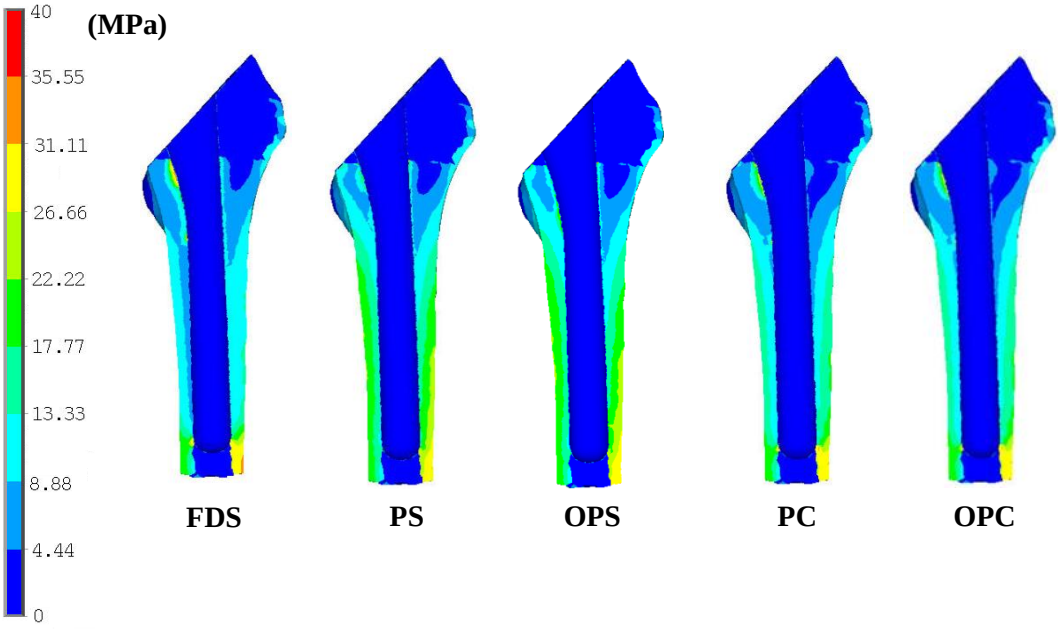

Figure 5.17 Cross sectional view along the frontal plane of the von Mises stress distribution in the periprosthetic femur.

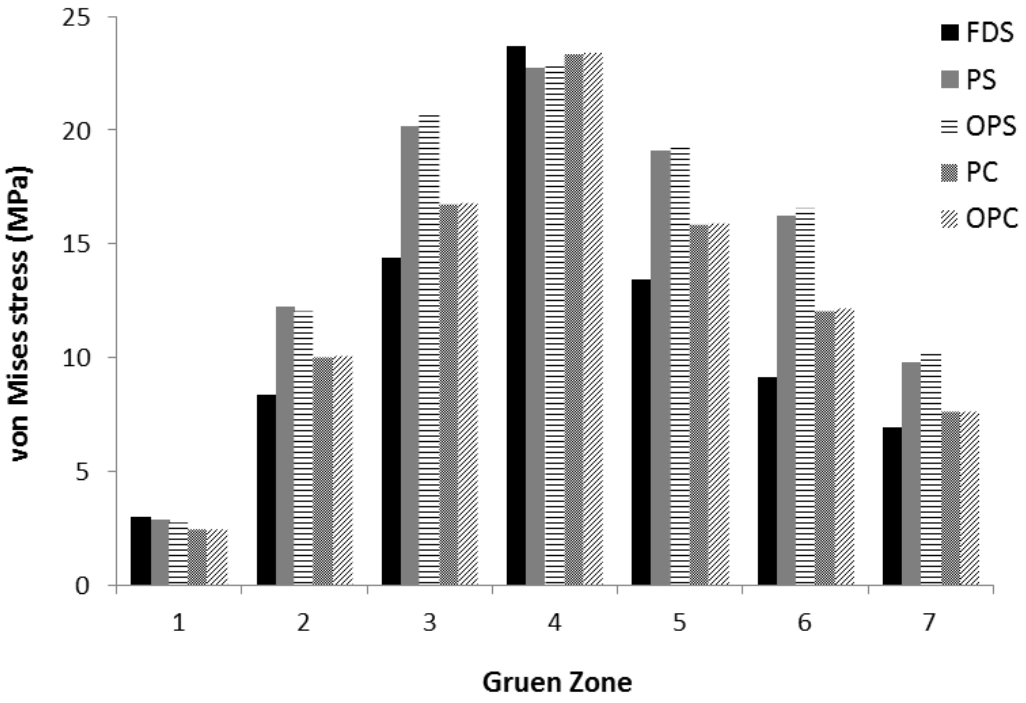

Figure 5.18 The von Mises stress in each Gruen zone.

5.6 Modelling the cellular structures with their idealised geometry

In sections, 5.3, 5.4 and 5.5 the cellular structures for the fully porous and functionally graded stems were represented as continuum bodies that were assigned a single value for the elastic modulus. This methodology was employed for two reasons. Firstly, in the previous chapter, the finite element method overestimated the stiffness of the square pore cellular structures by a mean factor of 3.33 when they were modelled with their idealised geometry. Secondly, limitations in computing power prevented the development of a finite element model by where the cellular structures of a fully porous or functionally graded stem could be modelled in their fully defined form. This section of work has modelled the cellular structures with their idealised geometry in order to justify the previously employed methodology. The two methodologies that were compared can be observed in Figure 5.19.

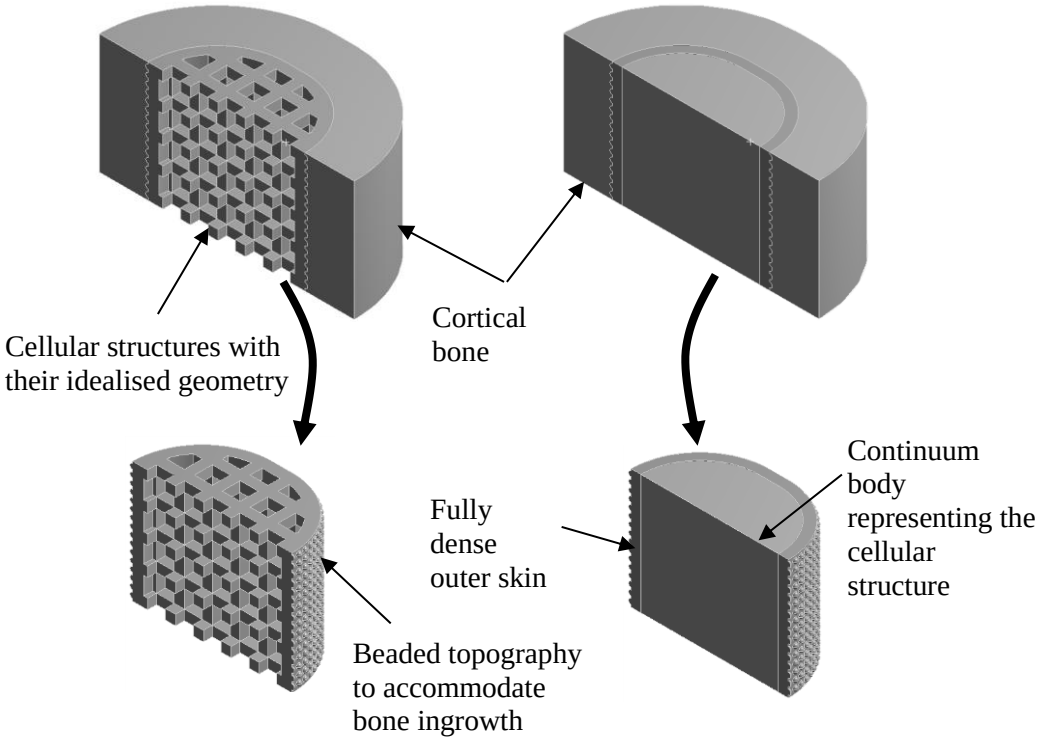

Figure 5.19 A comparison of the two modelling techniques used.

5.6.1 Methods

A three dimensional finite element model of a transverse section of the mid distal femoral stem and cortical bone was created using ANSYS Workbench 14.0. In this instance, the PC-2 functionally graded femoral stem was utilised for a comparative analysis. The bone and stem were meshed with four node tetrahedral elements. Mechanical interlocking was modelled at the bone-implant interface, to simulate fixation that is considered more replicative of in vivo conditions. All materials were modelled with linear elastic isotropic behaviour. The elastic modulus of the CoCrMo and cortical bone were taken as 200 GPa and 17 GPa respectively. In the continuum model, the core of the stem was assigned an elastic modulus of 13.64 GPa, which was relative to the cellular structure for the PC-2 femoral stem. A Poisson's ratio of 0.3 was assumed throughout. To reduce the size of the finite element model, only half of the transverse section was utilised, with symmetrical boundary conditions being applied.

The bottom surface of the bone was fully constrained and arbitrary displacements of 50 µm and 25 µm were applied simultaneously to the top surface of the stem medially and inferiorly for a comparative analysis.

5.6.2 Results

The load transfer and stress distribution in the bone is of primary interest in this chapter. From observing Figure 5.20, it is evident that the stress distribution in the cortical bone is similar for both of the finite element modelling techniques that were employed. The reaction force at the constrained face of the bone was compared, where the idealised model provided a force that was 7.5% larger than the continuum model. However, as expected the stress distribution in the stem was different when comparing the two methods.

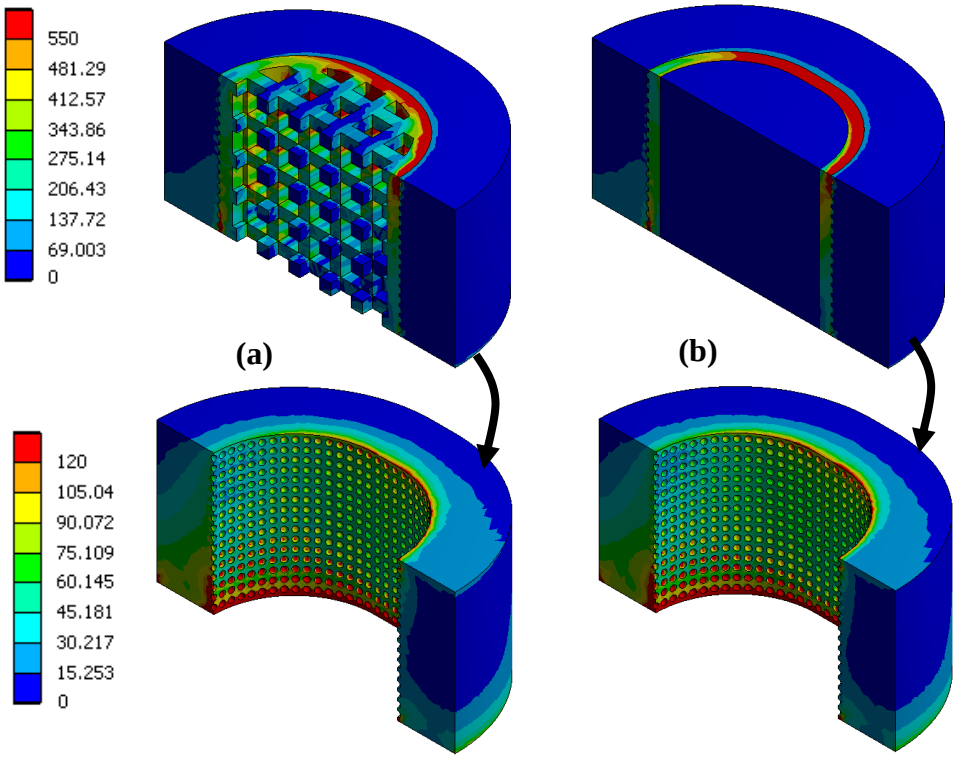

Figure 5.20 The von Mises stress distribution in the transverse assembly of the cortical bone and stem (MPa) (a) The idealised model (b) The continuum model.

5.7 Discussion

The finite element method has been used to investigate the mechanical behaviour of the proximal femur, when the compressive properties of square pore CoCrMo cellular structures have been incorporated into the design of a traditional monoblock femoral stem. In agreement with other published work, it was evident that more flexible stiffness configurations can increase the load transfer to the periprosthetic bone when compared to a traditional fully dense prosthesis (Harrysson *et al*., 2008; Yan *et al*., 2011; Gong *et al*., 2012; Arabnejad Khanoki and Pasini, 2013).

The periprosthetic stress values have been compared to the work of Hirata *et al*. (2013), where similar trends were observed in that the minimum and maximum stress values were found in Zones 1 and 4 respectively. The stress values were within the same order of magnitude and in both the medial and lateral zones, the stress values gradually decreased from the distal to proximal zones. It was difficult to compare exact stress values in the bone with other studies, as the stress distribution is dependent upon factors such as implant geometry, geometry of the femur and the distribution and values of material properties that are assumed in both the implant and the bone.

The results have shown that the fully porous stems are superior when compared to the fully dense and functionally graded stems, in relation to improving stress shielding characteristics. Upon examining the characteristics of the CoCrMo cellular structures used in this work, it is considered that the fully porous stems may not be suitable for in vivo use. Kienapfel *et al.* (1999) reviewed several studies and commented that the optimal pore size for bone ingrowth is between 0.1 mm and 0.4 mm. The pore size range for the cellular structures utilised lies between 1.57 mm and 1.88 mm. It is thought that pores of this size would encourage the ingrowth of fibrous tissue as opposed to new bone, and this would compromise the stability of the bone-implant

interface. The fully porous stems have been included in this work to investigate the effects of axial gradation and to provide a theoretical comparison with the functionally graded approach. Alternative design approaches will need to be considered to provide clinically suitable fully porous stems that utilise the cellular structures presented.

Femoral stems with orthotropic behaviour were considered and it was evident that the load transfer to the proximal-medial femur could be marginally improved with an orthotropic fully porous stem. These benefits were negated when the functionally graded approach was considered.

Decreasing the stiffness of cementless femoral stems can increase the risk of bone-implant interface failure through increased micromotion (Huiskes *et al*., 1992). In the main body of the numerical analysis, the interface stress was not analysed in depth, as the bone-implant interface was assumed to be perfectly bonded (Simoes and Marques, 2005; Harrysson *et al*., 2008; Boudeau *et al*., 2012; Gong *et al*., 2012; Arabnejad Khanoki and Pasini, 2013). From observing the stress values, the interface stability did not appear to be compromised. In addition to this, mechanical interlocking was modelled at the interface of the transverse section of the stem-bone assembly, in order to simulate fixation that is considered more replicative of in vivo conditions. Employing such a methodology for a full assembly would be computationally expensive as the transverse sectional model was meshed with 144,857 elements in this instance.

In the numerical analysis, assumptions have been made concerning the modelling of the bone types and CoCrMo cellular structures. The mechanical properties of the femur were distributed somewhat arbitrarily when compared to other studies that have used CT greyscale data to create more complex finite element models (Stiehl, 2009; Bryan *et al*., 2012). In reality, every case of THA is potentially different in terms of the anatomy and quality of the host bone. Therefore, it is thought that the approach used in this work

is appropriate for a comparative analysis where the stiffness configuration of the femoral stem was under investigation.

The CoCrMo cellular structures have been modelled as continuum bodies that were assigned with material properties that were determined from the uniaxial compression testing in Chapter 4. In contrast to this, a recent study by Wieding *et al*. (2013) successfully modelled square pore cellular titanium alloy bone scaffolds within a fractured femur explicitly. The length of the bone scaffold was one fifth of the length of the femoral stem used in this work, thus resulting in a much smaller finite element model. In addition, a recent study concluded that structural irregularities caused by ALM processes could have a significant effect on the mechanical properties of porous materials. It was subsequently suggested that structural variation should be implemented into finite element models (Campoli *et al*., 2013). Therefore, it is considered that the finite element modelling of additive manufactured cellular structures and hence a fully porous or functionally graded femoral stem is a complex topic that requires further attention.

To help justify the simplified modelling approach used in this work, a transverse section of a functionally graded femoral stem and cortical bone was selected as a region of interest. A portion of the implant was modelled with its idealised geometry and compared with the continuum approach. From the results, it can be interpreted that the simplified modelling technique used is reasonable and justified. However, these results are based upon a small region of the stem and bone assembly being modelled. It is considered that modelling the cellular structures as continuum parts is not sufficient to investigate the mechanical behaviour of the femoral stems. Physical testing is required to investigate the structural integrity and failure modes of the femoral stems manufactured using SLM.

Stress shielding following THA can lead to a reduction in bone mineral density around the femoral stem, with this being prevalent in the proximal-medial femur. Zone 7, which corresponds to the calcar and lesser trochanter of the femur, is often worst affected by stress shielding (Karachalios *et al*., 2004). Whilst not as flexible as the porous stems, the functionally graded stems did however improve the stress distribution in the medial and lateral periprosthetic Gruen zones when compared to their fully dense counterpart. It is evident that functionally graded stems can improve the load transfer to the periprosthetic femur and hence increase the mechanical stimulus in the bone without compromising its strength.

5.8 Summary

This chapter has used the finite element method to investigate the load transfer to the intact and implanted femur when using fully dense, fully porous and functionally graded CoCrMo monoblock femoral stems. Within the discussed limitations, the main findings of the chapter can be summarised as follows:

- Incorporating the mechanical properties of square pore CoCrMo cellular structures into the design of femoral stems can reduce stress shielding in the periprosthetic femur without compromising the strength of the bone.
- The fully porous stems with an axially graded stiffness (GPS-1, GPS-2 and GPS-3) were the most favourable designs for reducing stress shielding. In their current capacity, the fully porous stems exhibit pore sizes that are considered too large for biological fixation.
- The functionally graded stems provided a 20% (Zone 5), 36% (Zone 6) and 12% (Zone 7) increase in the von Mises stress in the proximal-medial femur, when compared to their fully dense counterpart. In this instance, there was no

noticeable difference observed when comparing the flexibility of the functionally graded stems (PC-1, PC-2 and PC-3).

- The 1 mm outer skin negated the benefits of axially grading the functionally graded stems stiffness, when compared to the fully porous stems.
- The continuum approach for modelling the square pore cellular structures is appropriate, but future research is recommended for the finite element modelling of additive manufactured cellular structures.

This chapter has highlighted the potential that laser melted CoCrMo femoral stems can have on improving the load transfer to the periprosthetic femur. Subsequently, the results have provided justification to investigate the mechanical behaviour of the functionally graded CoCrMo femoral stems. In the next chapter, the flexural behaviour of functionally graded femoral stems is investigated.

Chapter 6 The flexural behaviour of laser melted functionally graded CoCrMo femoral stems

6.1 Introduction

The load transfer to the periprosthetic femur could be improved when functionally graded CoCrMo femoral stems were considered. The stiffness of the functionally graded femoral stems has been shown to be similar when comparing the numerical results. It was also evident that axially grading the stiffness of the functionally graded stems was not beneficial for improving the periprosthetic load transfer.

This chapter investigates the mechanical behaviour of the functionally graded femoral stems (PC-1, PC-2 and PC-3) when subjected to cantilever bending. Physical tests were performed to determine the structural stiffness of the functionally graded stems when subjected to monotonic loading conditions. A traditional fully dense stem was manufactured and tested to provide a comparison with the functionally graded stems. Finite element analysis was performed to provide a comparison with the experimental results. In addition to this, the microstructure of the EOS Cobalt Chrome MP1 material was characterised using an optical laser scanning confocal microscope.

From the previously presented numerical results, the functionally graded stems should exhibit a similar mechanical behaviour, regardless of the cellular structure that populates the core. It was considered that utilising SLM to manufacture the functionally graded femoral stems would result in providing lightweight components that exhibit improved stiffness characteristics when compared to a traditional fully dense CoCrMo prosthesis.

6.2 Methods

6.2.1 Femoral stem design and manufacture

The femoral stem geometry from the previous chapter was utilised. In this instance, the flexural behaviour of the stem portion of the prosthesis was of interest. For economic purposes and ease of manufacture, the femoral neck and head region of the stem was removed from the design. Four different stiffness configurations for a femoral stem were investigated. Three designs were based upon the functionally graded approach (PC-1, PC-2 and PC-3), where the stems had a 1 mm thick fully dense CoCrMo outer skin that encased a porous core comprised of a square pore cellular structure. A fully dense CoCrMo stem (FDS) was also manufactured to act as a benchmark for comparison.

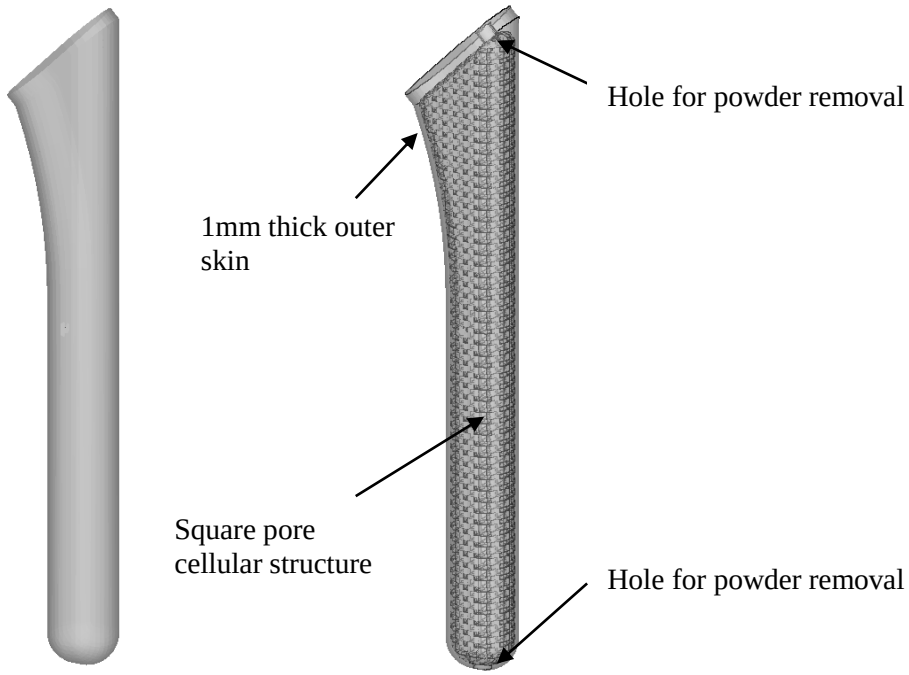

Figure 6.1 CAD models of a fully dense and functionally graded femoral stem.

Using Solidworks 2012, the fully dense stem was modelled as a single body whereas the functionally graded stems were modelled as two continuum bodies. In this instance, the two separate bodies were created to represent the outer skin and core of the stem. The unit cells that were representative of the cellular structures were also designed within the software. The CAD files were converted into an STL file format and imported into Materialise Magics 17.0 software. The structures module within Magics was used to generate the internal cellular structure for each of the functionally graded stems, by duplicating the appropriate unit cell geometry. The two bodies were then booleaned together to form one part. Typical solid models for the femoral stems are shown in Figure 6.1. Finally, the slice files for each component that contained the two dimensional cross sectional geometry of each layer were generated for manufacture.

Ten stems were manufactured in a single batch, one fully dense stem and three samples for each of the functionally graded configurations. The stems were manufactured from EOS Cobalt Chrome MP1 powder using the EOSINT M270 Xtended Direct Metal Laser Melting machine, with the same powder characteristics and operating parameters that were used in Chapter 4.

The material processing was performed in a nitrogen-based atmosphere with less than 0.1% oxygen present in the build chamber. Upon completion of the build, the excess powder located within the components was removed. The stems were stress relieved in an argon atmosphere at a temperature of 1050ºC for two hours and were left to cool in the furnace. The components were removed from the build plate using wire EDM. Each stem was weighed on calibrated digital scales that offered an accuracy of +/- 0.1 g and comparisons were noted between the functionally graded and fully dense stems.

6.2.2 Mechanical testing

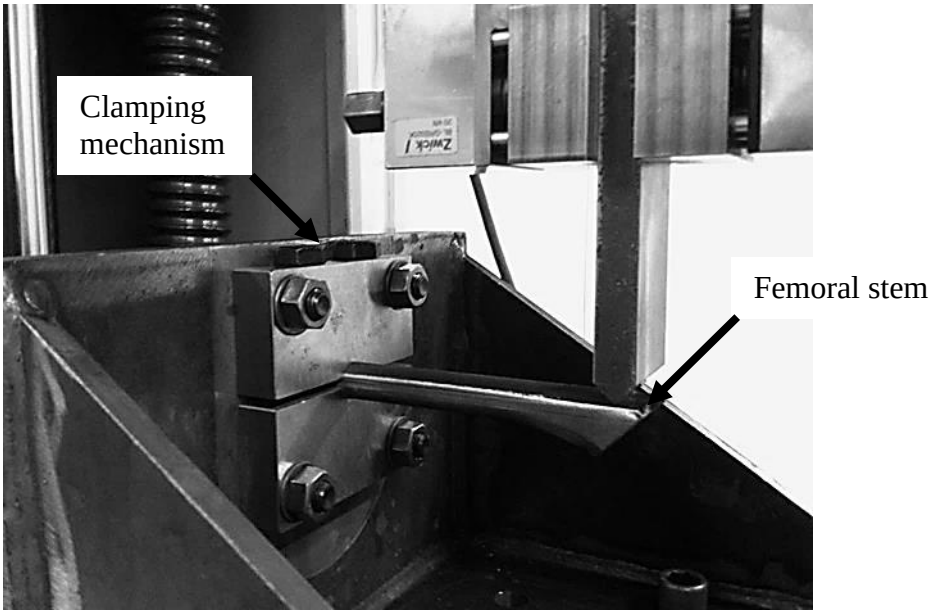

Figure 6.2 Cantilever bending test set up.

Cantilever bend tests were performed using a Zwick Roell 1474 materials testing machine having a maximum load capacity of 100 kN. The physical tests were performed to investigate the structural stiffness of each femoral stem. BS EN ISO 7438:2005 was referred to, and a bespoke test set up was designed and manufactured in order to eliminate any deformation that could occur within the test set up when loaded, as shown in Figure 6.2. The most distal 20 mm of the femoral stem was clamped and fully constrained within the test fixture, and the load was consistently applied at a distance of 140 mm from the distal tip of the stem. The components were loaded to failure by using a crosshead displacement speed of 2 mm/min. The real time force versus displacement data was recorded from the test machine in order to calculate the stiffness for each stem. Three samples for each of the functionally graded femoral stems were tested and the results from one fully dense stem were used as a benchmark for comparison.

6.2.3 Finite element modelling

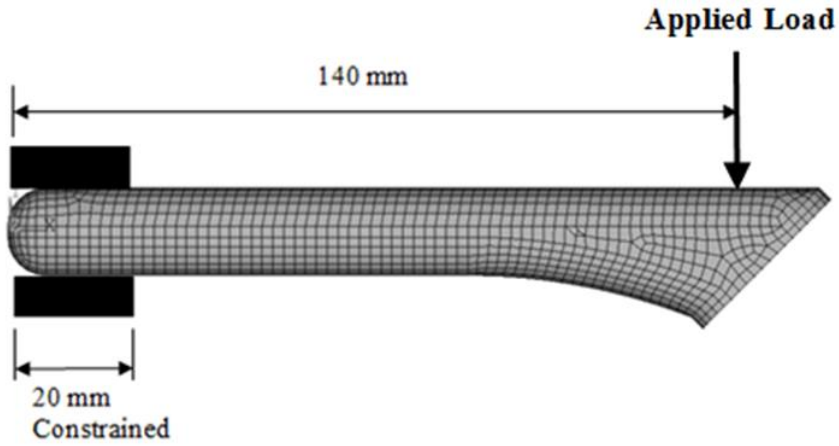

Figure 6.3 The finite element mesh and applied boundary conditions.

Three-dimensional finite element models were created using ANSYS 13.0 by importing the femoral stem geometries that were created in Solidworks 2012. The cellular structures were modelled as single continuum bodies, which were assigned material properties with respect to the chosen structure. The models were meshed using four node tetrahedral elements. Mesh sensitivity was studied until further mesh refinement changed the maximum von Mises stress in the stem by 5% or less. Boundary conditions were applied in order to replicate the physical test conditions as shown in Figure 6.3.

Table 6.1 Material properties assumed for the bilinear stress strain relationship.

Material	Elastic modulus (GPa)	Yield strength (MPa)	Tangent modulus (GPa)
Fully dense CoCrMo	200.00	600.00	29.41
PC-1 cellular structure	17.98	295.72	4.10
PC-2 cellular structure	13.64	175.15	1.66
PC-3 cellular structure	4.79	65.43	0.05

The fully dense CoCrMo alloy and cellular structures were both modelled with nonlinear material properties by using a bilinear isotropic hardening stress-strain relationship. The fully dense stem was assumed to have an elastic modulus of 200 GPa and a 0.2% offset yield strength of 600 MPa (Electro Optical Systems, 2010). The elastic modulus and yield strength of the cellular structures were previously determined in Chapter 4. The mean tangent modulus for each cellular structure was determined so that a bilinear stress-strain relationship could be utilised. A Poisson's ratio of 0.3 was assumed throughout for all materials and the material properties are summarised in Table 6.1. The force-displacement data for each femoral stem was obtained and stiffness values were calculated to form a comparison with the physical test data.

6.2.4 Microstructural characterisation of EOS Cobalt Chrome MP1

Horizontal (parallel to the build plate) and transverse samples (vertical to build plate) were cut away from a femoral stem for metallographic analysis by using wire EDM. The samples were mounted in a phenolic hot mounting resin by using an automatic mounting press. A series of Struers MD Piano, resin bonded diamond grinding discs were then used to grind the samples. Firstly, a 220 grade disc was used to obtain planeness, and then 500 and 1200 grade discs were subsequently used for fine grinding. The samples were polished using Struers 6 μm diamond paste, and finally, a colloidal silica mixture was used prior to etching.

Electrolytic etching was used to reveal the materials microstructure with a 10% oxalic acid aqueous solution. An Olympus LEXT (OLS 3000) optical laser scanning confocal microscope was used to characterise the materials microstructure and analyse porosity in its as-built, stress relieved condition.

6.3 Results

6.3.1 Femoral stem manufacture

The components can be observed in their as-built condition in Figure 6.4. Upon completion of the build, the components were inspected and there were no visible cracks or defects present on the outer surfaces of the stems. As expected with SLM, a somewhat rough surface finish was created due to the stair step effect that occurs when manufacturing curved geometries. After powder removal, each individual stem was weighed and the values are presented in Table 6.2. The functionally graded stems provided a 39% to 58% reduction in weight when compared to the fully dense stem.

Figure 6.4 Typical components on the build plate in their as-built condition.

6.3.2 Mechanical testing

The mean stiffness values for each design were calculated from the real time force versus displacement data and are summarised in Table 6.2. The typical force-displacement curve for each stiffness configuration can be compared from Figure 6.5. A reduction in stiffness of between 54.7% and 64.4% was achieved when the functionally graded approach was considered.

Table 6.2 The individual and mean values for stem weight and structural stiffness.

Femoral stem	Weight (g)	Mean weight (g)	Stiffness (N/mm)	Mean stiffness (N/mm)
FDS	230.00	230.00	869.94	869.94
PC1-1	141.00		397.18	
PC1-2	140.00	140.30	365.28	394.45
PC1-3	140.00		420.89	
PC2-1	119.00		348.75	
PC2-2	118.00	119.00	367.94	351.37
PC2-3	120.00		337.43	
PC3-1	98.00		313.72	
PC3-2	96.00	96.60	365.28	309.32
PC3-3	96.00		248.95	

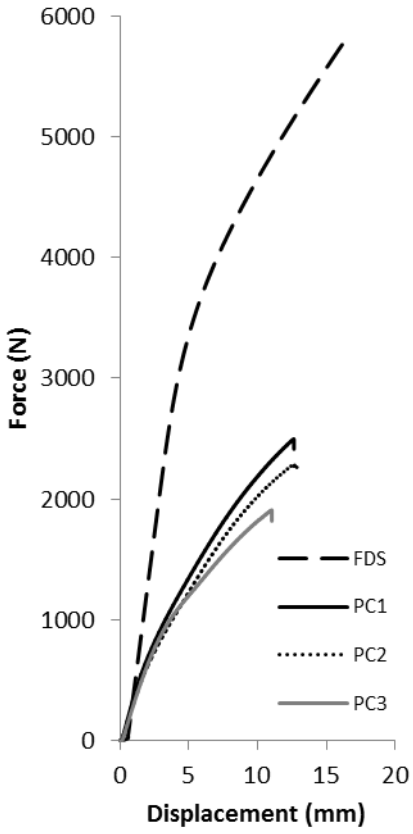

Figure 6.5 Typical force-displacement relationship for each femoral stem design.

Figure 6.6 compares the force-displacement relationship for each of the functionally graded stiffness configurations. The PC-1 and especially the PC-2 designs have similar trends and repeatability in terms of the mechanical behaviour. In contrast to this, the PC-3 design did not show reasonable repeatability and tended to fail with more unpredictable mechanisms. For instance, the sample PC3-2 fractured approximately half way down the length of the stem, whereas all of the PC-1 and PC-2 test samples fractured at the expected point of cantilever support. In addition, the sample PC3-3 fractured at a force that was 52% lower than the average force of the other two samples.

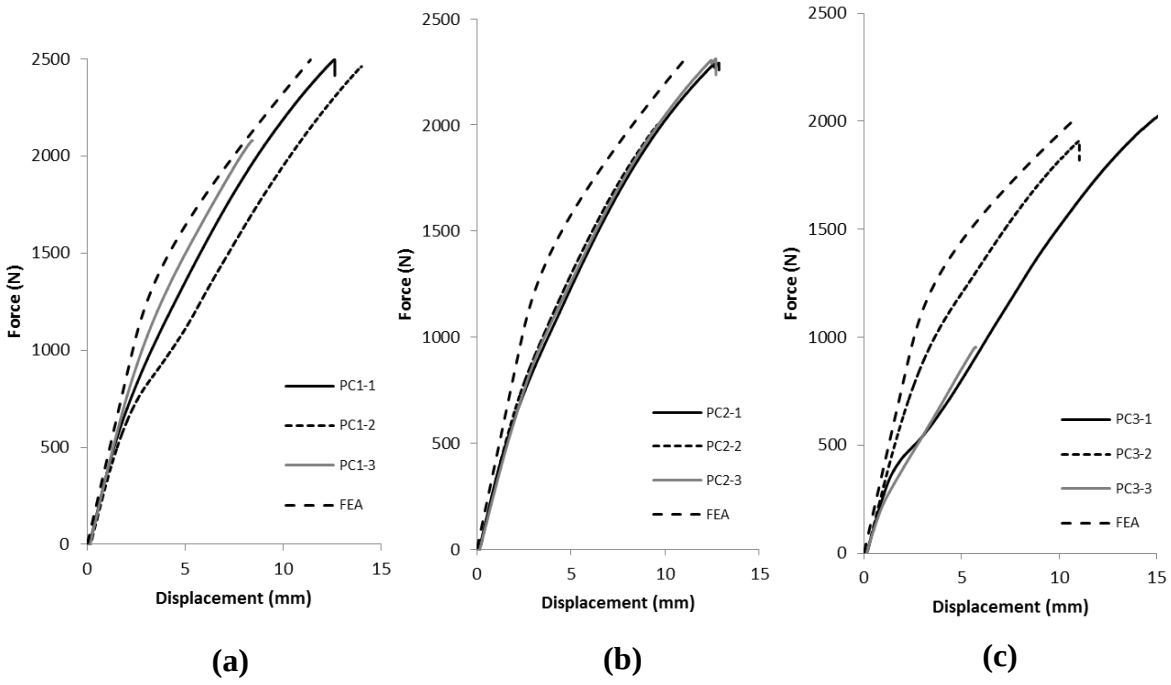

Figure 6.6 Force-displacement relationships for each of the functionally graded designs. (a) PC-1 (b) PC-2 (c) PC-3.

6.3.3 Finite element modelling

Stiffness values for each femoral stem were calculated from the force-displacement data that was generated from the finite element software. These have been summarised in Table 6.3.

Table 6.3 Comparison of the stiffness values obtained using physical testing and finite element analysis.

Femoral stem	Mean stiffness from physical test (N/mm)	Stiffness from numerical analysis (N/mm)	% Difference
FDS	869.94	911.14	4.7
PC-1	394.45	431.43	9.4
PC-2	351.57	419.25	19.2
PC-3	309.32	394.27	27.3

The numerical analysis overestimated the stiffness of the functionally graded stems by between 9.4% and 27.3% dependent upon the stiffness configuration. Figure 6.6 compares the numerically derived force-displacement relationship with the physical test for each functionally graded stem. It is considered that a reasonable agreement can be observed between the two methodologies, perhaps with the exception of the PC-3 design.

6.3.4 Microstructural characterisation of EOS Cobalt Chrome MP1

From Figure 6.7, it can be observed that the acid etching revealed a microstructure with a morphology that is typical for EOS Cobalt Chrome MP1 (Electro Optical Systems, 2009). Isolated pores were present in both the horizontal and transverse samples, as observed elsewhere (Rivera *et al*., 2011). The maximum pore size in both orientations was similar, with an average pore size of between 30 µm and 50 µm being measured throughout.

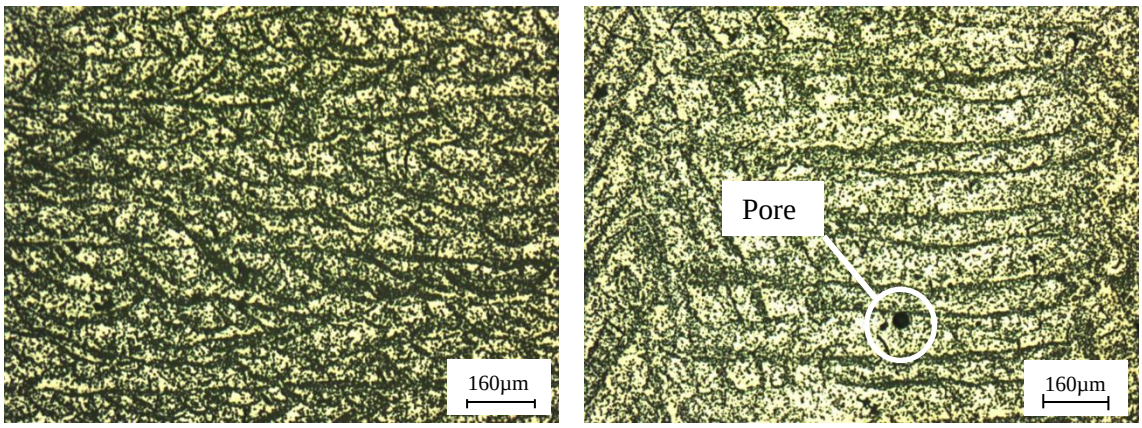

(a) **(b)**

Figure 6.7 Micrographs of the EOS Cobalt Chrome MP1. (a) Sample with transverse orientation (b) Sample with horizontal orientation.

6.4 Discussion

The literature review suggests that this is the first work to investigate the stiffness characteristics of such stems when subjected to cantilever bending. Three-point (Harrysson *et al.*, 2008) and four point (Brenne *et al.*, 2013) flexure testing has been utilised for determining the flexural characteristics of open cellular additive manufactured structures. In this instance, a cantilever bend test was used to compare the flexural behaviour of the different stiffness configurations when subjected to monotonic loading conditions. This methodology was employed to investigate the stiffness of the stems when loaded in what corresponded with the medial-lateral direction along the frontal plane of the human anatomy. Stress shielding of the proximal-medial femur can occur following THA (Karachalios *et al.*, 2004). Therefore, it is considered that investigating the flexural behaviour of the prostheses in what corresponds to the frontal plane of the anatomy, provides a suitable indicator of the stems ability to reduce stress shielding in this area.

It was hypothesised that the functionally graded approach employed in this work could provide lightweight femoral stems that exhibit improved stiffness characteristics when compared to a fully dense CoCrMo stem.

The results from this work have confirmed that laser melted functionally graded femoral stems are lighter and less stiff when compared to a traditional fully dense CoCrMo prosthesis. However, from the mechanical testing it can be interpreted that the PC-3 design would not be reliable in this instance. This provides an indication that SLM potentially has repeatability issues with manufacturing femoral stems that incorporate cellular structures with a strut size of 0.5 mm. It was observed in Chapter 4 that the strength of square pore cellular structures is dependent upon the strut size; this being concurred in this chapter and elsewhere (Parthasarathy *et al*., 2011).

From observing the physical test data of the PC-3 design, it can be assumed that internal structural defects were inherent with the manufacturing process. Further investigation would be needed to confirm this and to quantify the extent of the defects that are present. It is considered that a technology such as µCT scanning would be useful for the inspection of functionally graded femoral stems; such technology was not available for this research.

From the physical test results, the PC-2 design would be the recommended stiffness configuration. It is considered that this design provides a CoCrMo femoral stem with a stiffness that is comparable to that of a titanium alloy stem. This stem showed the greatest agreement and repeatability when comparing the force-displacement curves. This suggests that a functionally graded stem incorporating a square pore cellular structure with a 1 mm strut size is the most reliable design in relation to manufacturability and mechanical behaviour. This being concurred from the uniaxial compression testing that was performed in Chapter 4.

The femoral stem geometry utilised was designed to suit the anatomy of a given proximal femur (Visible Human Project, 1994). It is considered that variations in stem geometry or length would provide different stiffness values to what have been presented. However, it is thought that similar stiffness reduction ratios would be observed when comparing functionally graded and fully dense stems that offered a different geometry or length.

During running, the medial-lateral bending moments at locations that correspond to the periprosthetic femur have been reported to be 0.22 BWm (Edwards *et al*., 2008). The bending stress (σ) in the femoral stem can be approximated using the standard equation:

$$\sigma = \frac{My}{I} \tag{6.1}$$

Where M is the bending moment, y is the distance from the neutral axis to the point of interest and I is the second moment of area for the stem in the plane of bending. Considering the geometry of the femoral stem and a body weight of 836 N that was used in Chapter 5 for FEA, the maximum bending stress in the distal portion of the femoral stem was calculated to be 340 MPa, when subjected to loads generated by running.

The yield strength of EOS Cobalt Chrome MP1 is in the region of 600 MPa (Electro Optical Systems, 2010). Therefore, it is unlikely that the structural integrity of the PC-2 stem would be compromised even if it were subjected to severe loading conditions such as running. However, this is based upon the results of a sample size of three specimens only. In this instance, the sample size restriction was due to the limited build envelope size on the EOSINT M270 Xtended Direct Metal Laser Melting machine.

It is considered that any future testing of the functionally graded femoral stems should be more replicative of in vivo loading conditions and should consider the effect of cyclic loading. This would determine the fatigue life of such femoral stems, which is an important factor that governs the clinical use of orthopaedic implants. There is a small sample of published literature that has studied the fatigue characteristics of cellular structures manufactured using ALM. However, there does not appear to be any work that has physically investigated the fatigue characteristics of the material or stiffness configurations that are used in this work. Li *et al*. (2012), when performing compression fatigue testing on titanium alloy cellular structures, observed that the fatigue strength increased with an increasing relative density. Whereas, Brenne *et al*. (2013) found that the fatigue strength and energy absorption of titanium alloy structures manufactured using SLM was improved when the components were heat-treated and that areas of high strain local to the applied load were also observed within the struts. The authors subsequently suggested that these areas could be reinforced to create an equal load distribution within the structure.

The finite element models of the functionally graded stems were simplified by modelling the volume representing the cellular structure as a continuum body, with a single value being assigned for the elastic modulus. It is considered that a reasonable agreement was achieved between the physical testing and numerical analysis in this work, with the exception of the PC-3 design. Even so, if the stiffness value for the sample PC3-3 was removed from the data set, then a closer comparison would have been achieved between the physical test and numerical analysis. In this instance, the results show that the flexural behaviour of the functionally graded stems used in this work can be modelled with reasonable accuracy, without having to model the geometry of the cellular structures explicitly. This methodology will contribute towards reducing the size of finite element models and hence computational expense.

6.5 Summary

This flexural behaviour of functionally graded CoCrMo femoral stems manufactured using SLM have been investigated. Within the discussed limitations, the main findings of this chapter can be summarised as follows:

- SLM is capable of repeatedly manufacturing a functionally graded CoCrMo femoral stem (PC-2) that is 48% lighter and 60% more flexible than a traditional fully dense stem. This provides a CoCrMo femoral stem with a stiffness that is comparable to that of a titanium alloy stem.
- Concerning repeatability, the preferred strut size for laser melted square pore CoCrMo cellular structures is 1 mm. SLM could not repeatedly manufacture femoral stems that incorporated a cellular structure with a strut size of 0.5 mm (PC-3).
- Cellular structures were modelled as continuum parts where a reasonable correlation was achieved between the numerical analysis and physical test data, indicating that this simplified approach is suitable for modelling the behaviour of femoral stems that incorporate cellular structures in their designs.

This chapter has shown the potential of utilising SLM to manufacture lightweight femoral stems with improved stiffness characteristics. There are concerns associated with the repeatability of the manufacturing process for producing stems with cellular structures that incorporate strut sizes that are equal to 0.5 mm. In the next chapter, factors that can affect the manufacturability and mechanical behaviour of femoral stems produced using SLM are investigated.

Chapter 7 The manufacturability of laser melted functionally graded CoCrMo femoral stems

7.1 Introduction

In the previous chapter, a functionally graded stem incorporating a square pore cellular structure with a 1 mm strut size (PC-2) was proposed as the best performing design. There was less repeatability observed with the femoral stems that utilised the 0.5 mm (PC-3) and 1.5 mm (PC-1) cellular structures. An investigation is needed to consider factors that are associated with the manufacturability and mechanical behaviour of laser melted functionally graded CoCrMo femoral stems.

Thermally induced residual stresses can affect the quality of components produced using laser melting processes (Mercelis and Kruth, 2006). Considering this, a preliminary investigation has been performed to measure the effect of residual stress in the functionally graded stems.

From the literature and previous results, it is reasonable to assume that internal structural defects and stress raisers could be present at connections between the cellular structure and the outer skin of the stems. Two functionally graded femoral stems were examined using a Scanning Electron Microscope (SEM) facility, in order to identify any internal structural defects and potential areas of stress concentration.

The square pore cellular structures investigated in this thesis so far have possessed downward facing surfaces that are not considered ideal for ALM. In this chapter, for comparison, a femoral stem has been manufactured with a square pore cellular structure that is orientated at 45 degrees with respect to the build platform, and hence self-supporting.

Additional factors that are considered to affect the manufacturability of laser melted functionally graded femoral stems are discussed in terms of the removal of unprocessed/partially melted powder, part orientation and post processing.

7.2 Femoral stem design and manufacture

In order to investigate the manufacturability of laser melted functionally graded femoral stems, the GPC-2 design from Chapter 5 was utilised throughout this chapter. Once again, the stem portion of the prosthesis was of interest. However, in this instance the collar was included in the stem design.

The stem was designed using Solidworks 2012 and consisted of three continuum bodies. The three separate bodies were created to represent the outer skin/collar and the proximal and distal cores of the stem. The same unit cells were used as in the previous chapter to generate the cellular structures. The CAD files were converted into an STL file format and imported into Materialise Magics 17.0 software.

The structures module within Magics was used to generate the internal cellular structure for each of the functionally graded stems, by duplicating the appropriate unit cell geometry. For each stem, the three bodies were then booleaned together to form one part. Two stems were designed for manufacture and were different when considering the orientation of the cellular structure. One design possessed horizontal struts that were parallel to the build platform and the other with struts that were orientated at 45 degrees with respect to the build platform. In this instance, support structures were required due to the inclusion of the collar in the femoral stem design. The models that were used to manufacture the femoral stems are shown in Figure 7.1. Finally, the slice files that contained the two dimensional cross sectional geometry of each layer were generated for manufacture.

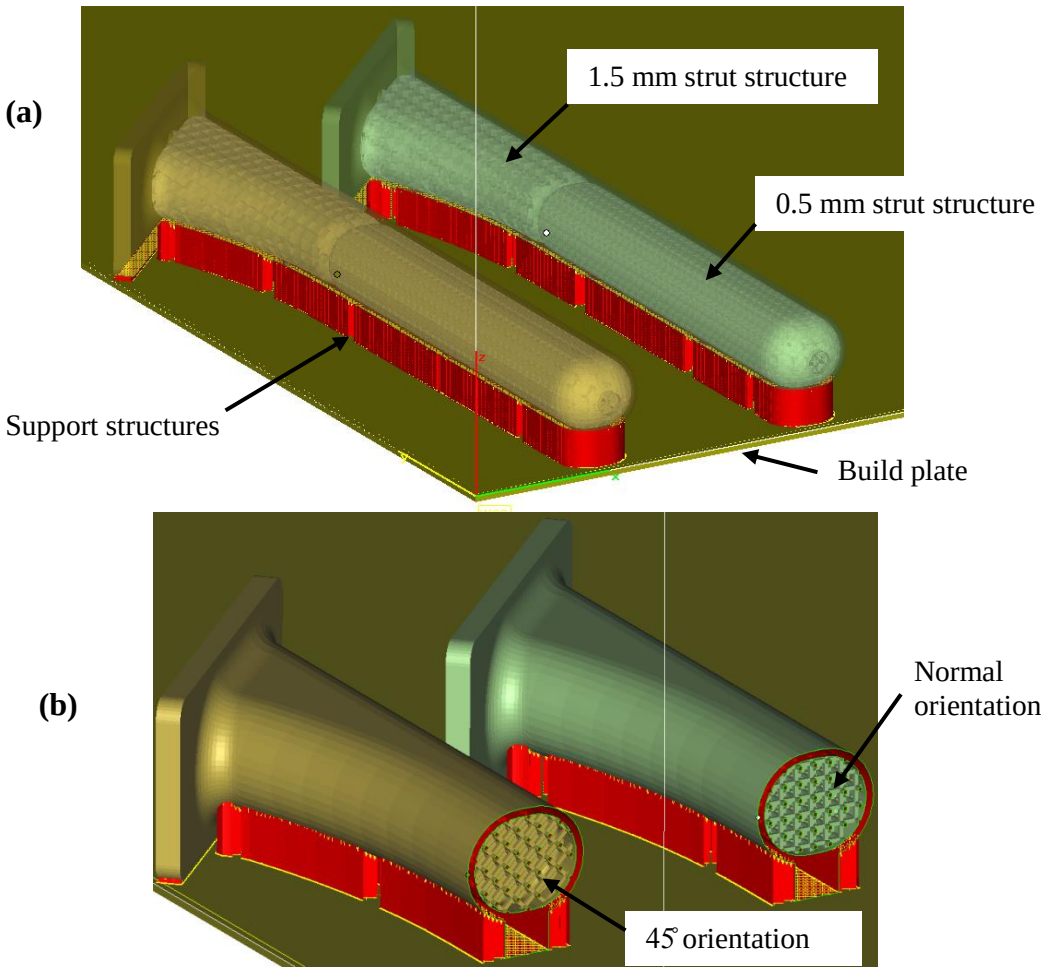

Figure 7.1 (a) Transparent full view of both femoral stems (b) Sectional view of both stems showing the orientation of the cellular structures.

The two stems were manufactured from the EOS Cobalt Chrome MP1 powder using the EOSINT M270 Xtended Direct Metal Laser Melting machine, with the same powder characteristics and operating parameters as used in Chapters 4 and 6. Upon completion of the build, the excess powder located within the components was removed. In this instance, the components were not stress relieved as no mechanical testing was being performed, and the effects of residual stress were being investigated. The components in their as-built condition are shown in Figure 7.2.

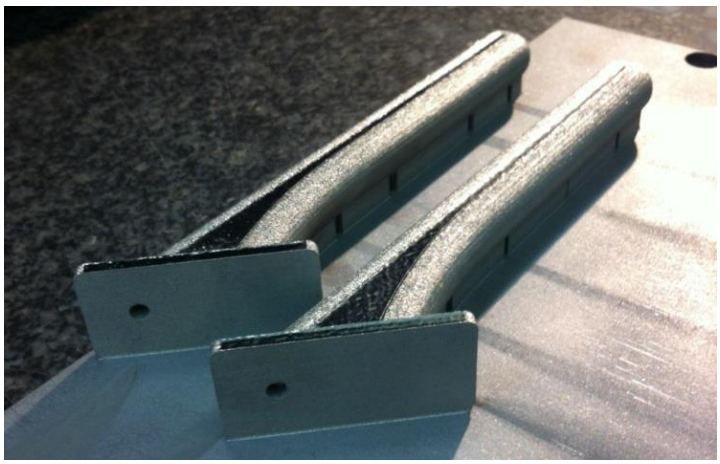

Figure 7.2 The femoral stems on the build plate in their as-built condition.

7.3 Residual stress

7.3.1 Methods

Following manufacture and powder removal, the build plate was located on a Merlin Co-ordinate Measuring Machine (CMM). Four dots were marked on the top surface of each femoral stem at identical locations where co-ordinates were measured, as shown in Figure 7.3.

A Renishaw PH10M motorised indexing probe head was then used to determine the initial co-ordinate (Z_1) at each location on the top surface of the femoral stems. Following this, the stems were located on the EDM facility, which was used to slice the stems in half. Cutting started from the distal tip of the stem and was set to travel a distance of 140 mm, this left 10 mm of the proximal stem intact. The build plate was then removed from the EDM facility, relocated on the CMM and the new co-ordinate (Z_2) at each location was recorded. The new value was then subtracted from the initial value (Z_2-Z_1) in order to provide an indication of stress induced stem deformation.

Location	Z_1	Z_2	Z_2-Z_1
1A	18.227	18.275	0.048
1B	18.164	18.660	0.496
1C	18.167	19.344	1.177
1D	18.212	20.214	2.002
2A	18.282	18.455	0.173
2B	18.182	18.730	0.548
2C	18.152	19.420	1.268
2D	18.187	20.419	2.232

Z_1 = Initial co-ordinate prior to EDM

Z_2 = Final co-ordinate following EDM

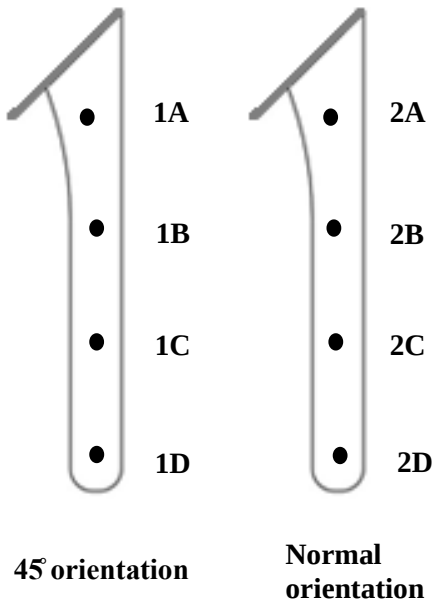

Figure 7.3 The measured co-ordinates and locations that were selected to measure the deformation of the femoral stems.

7.3.2 Results and discussion

Figure 7.3 presents the results that were obtained using the CMM. The results show that residual stress was more prominent in the stem with the normal orientated cellular structures. A 13% average increase was observed in the deformation when comparing the two stems. When comparing the individual locations, the biggest difference was observed between 1A and 2A, indicating that the 1.5 mm cellular structure with normal orientation was in a higher stress state than the structure with a 45 degree orientation.

It would have been beneficial to perform a comparison with a fully dense stem of identical geometry; however, restrictions in material quantity prevented this. Figure 7.4 shows the fully dense stem that was manufactured in the previous chapter. It can be observed that residual stresses have caused warping and deformation that has lifted the tip of the stem from the build plate.

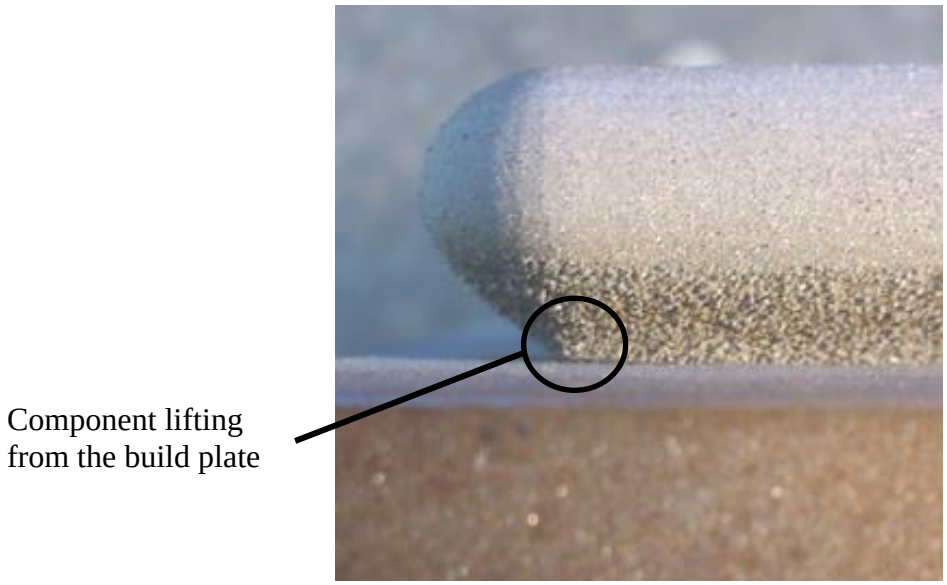

Figure 7.4 The effect of residual stress on a fully dense stem.

It can be observed that residual stress is more prominent in fully dense stems when compared to stems that have porosity incorporated into their designs. It is surmised that functionally graded designs are more suitable for laser melting processes. Less material and thinner wall sections are utilised and less material is affected by the high temperature gradients that are responsible for the generation of the thermally induced stresses.

It may be construed that designs with porosity will self-stress relieve due to the movement and distortion of the internal cellular structures. However, there is a caveat in that this may promote micro crack formation within the cellular structure or at the interface between the cellular structure and the outer skin of the femoral stem.

7.4 Internal structural defects

7.4.1 Methods

Work was undertaken to inspect the internal characteristics of the functionally graded femoral stems using a SEM facility. This has been done to identify internal structural defects or areas of stress concentration that could potentially contribute to the failure of the prostheses.

To prepare the samples, the stems were completely sliced in half parallel to the build plate using wire EDM. The stems were then removed from the build plate by making another pass with the wire. Four regions on each stem were selected to provide a range of specimens where the characteristics could be examined for both of the cellular structures at different orientations, as shown in Figure 7.5.

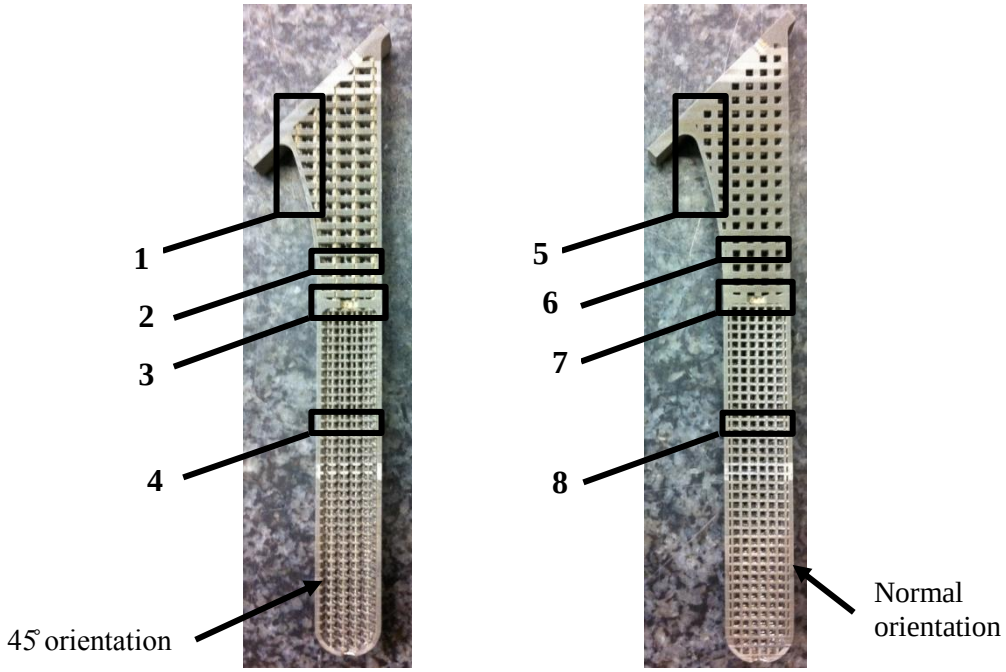

Figure 7.5 The locations that were selected for sample preparation.

Wire EDM was used to cut away the samples from the femoral stem halves. Samples 1, 3, 5 and 7 were chosen for inspection in the frontal plane of the stem, with Samples 2, 4, 6 and 8 being selected for inspection transversely.

The samples were mounted in resin, ground and polished using the same methodology as employed in the previous chapter. The samples were inspected at regular intervals throughout the grinding and polishing process by using an optical microscope. This was done to verify the quality of the preparation work and to ensure that the samples were suitable for inspection using SEM. In this instance, microstructural characterisation was not performed therefore etching was not required.

The samples were arranged to allow for their tracking within the SEM chamber and images were taken at varying magnification by using a Zeiss EVO 50EP SEM facility, in order to identify internal structural defects and areas of stress concentration.

7.4.2 Results and discussion

SEM was used to inspect the femoral stems at different regions of interest. Stress raisers and defects were assumed to be present at the connections between the cellular structures and the outer skin. This was based upon the unpredictable failure of the PC-3 femoral stem that was observed in the previous chapter.

No cracks were identified at the interface between the cellular structure and the 1 mm outer skin across the entire sample selection, Figure 7.6 provides an example of this. The images identified sharp corners at the interface, as shown in Figure 7.6a. Whilst there were no cracks identified, it is still considered that these sharp corners may act as stress raisers if the stems were to be subjected to cyclic loading conditions.

(a)

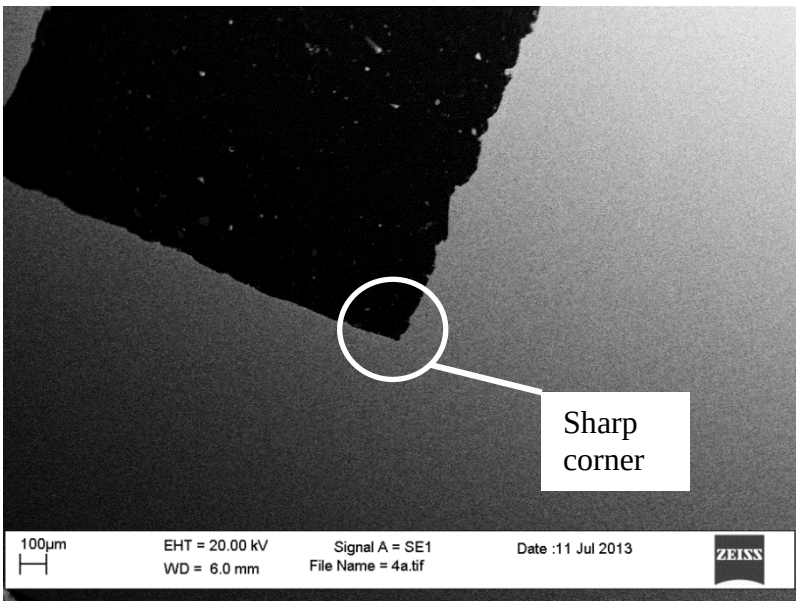

(b)

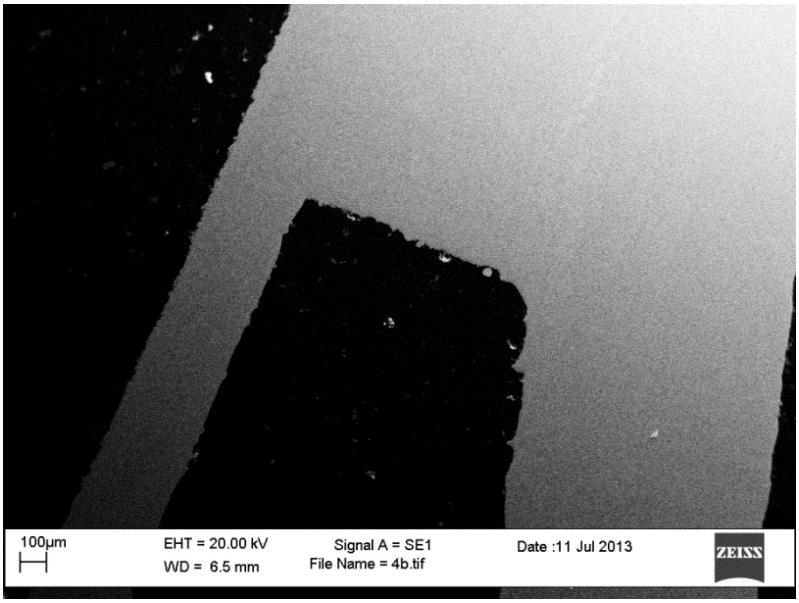

Figure 7.6 (a) SEM image from Sample 6 (b) SEM image from Sample 1.

Cracks were identified from the SEM in Samples 3 and 7, which corresponded to the transitional region between the 0.5 mm and 1.5 mm cellular structures for both stems. In both instances, the cracks were identified at a connection between a 0.5 mm strut and the 2.0 mm thick cross section that was used to create the transition between the two cellular structures. From the images in Figure 7.7, the cracks were identified at connections where acute angles were observed. It is considered that these acute angles produce stress raisers and that thermally induced stresses associated with SLM have

caused cracks to initiate and propagate during the build process. Therefore, any connections with acute angles are a concern for the manufacturability and structural integrity of laser melted functionally graded femoral stems.

(a)

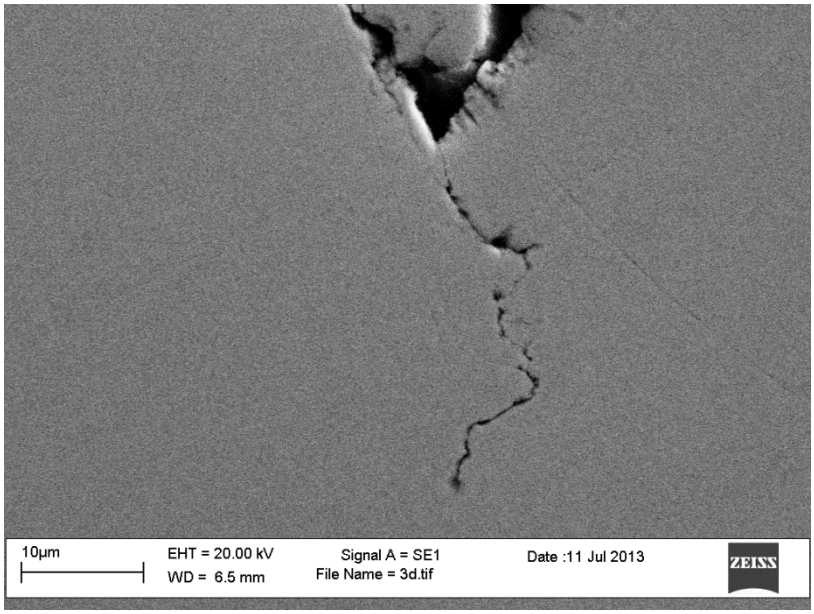

(b)

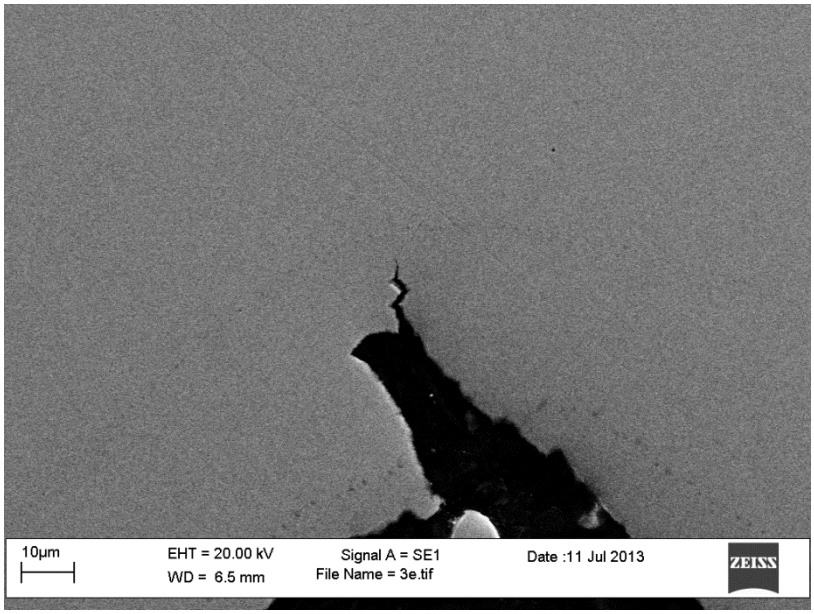

Figure 7.7 (a) SEM image from Sample 7 (b) SEM image from Sample 3.

It is considered that the areas of stress concentration are created through the design approach and more specifically the software that has been used to generate the cellular structures within the functionally graded designs. The structures module within Materialise Magics 17.0 has been utilised in this research and this software does not have the capability to create fillets where cellular struts connect to other cross sections. Additionally, to use a manual modelling approach is considered troublesome, due to the number of connections that are present in each functionally graded design. The same software has been utilised in other studies that have investigated alternative orthopaedic implant designs when considering fully porous approaches using Ti-6Al-4V and no problems were discussed (Harrysson *et al*., 2008; Murr *et al*., 2010).

There were no defects identified at connections between the cellular structures and the 1 mm outer skin. There were cracks identified at connections between 0.5 mm struts and the 2.0 mm cross section, this being concurred in Chapter 4, where a similar phenomenon was observed with the manufacture of the tensile specimens. This provides an indication that a geometric mismatch to the order of four is a concern for manufacturing CoCrMo components using SLM.

From the results, it can be interpreted that the unpredictable failure of the PC-3 stem in the previous chapter is more attributed to heterogeneities within the cellular structure, as opposed to defects at the interface. This has been based upon a limited number of samples and it is considered that a technology such as µCT scanning would provide a more accurate method for inspecting the functionally graded femoral stems that have been investigated in this work.

7.5 Orientation of the cellular structure

7.5.1 Methods

Four transverse sections, two from each design were cut away from the femoral stem halves using wire EDM. This provided one sample for each respective strut size and orientation, the sample selection is shown in Figure 7.8. Samples 1 and 2 were from the cellular structure with a 45 degree orientation, possessing respective strut sizes of 1.5 mm and 0.5 mm. Whereas, Samples 3 and 4 were from the cellular structure with normal orientation, possessing respective strut sizes of 1.5 mm and 0.5 mm.

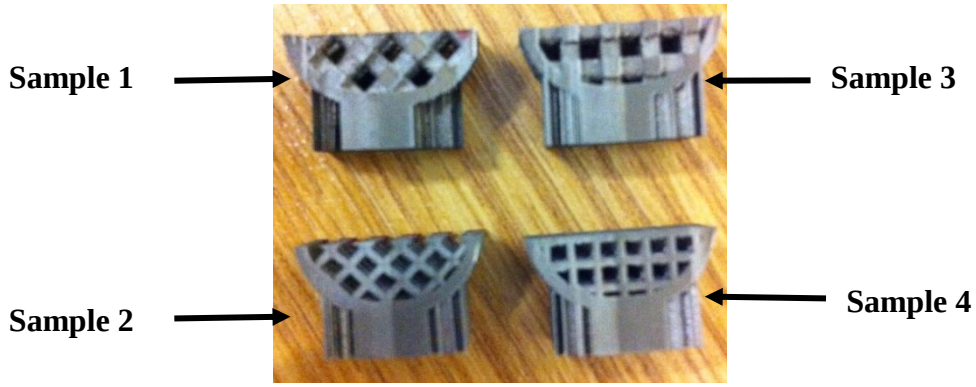

Figure 7.8 The cellular structure samples that were selected for inspection.

An Olympus LEXT (OLS 3000) optical laser scanning confocal microscope was used to visually inspect the struts and measure the strut thickness at five randomly selected locations within each sample. Three measurements were taken along the length of each measured strut to account for structural variation. A mean value for the thickness of each individual strut was then determined. Finally, the overall mean value and standard deviation for each strut thickness and orientation was calculated for a comparative analysis.

7.5.2 Results and discussion

Table 7.1 presents the measured strut thickness for each sample at the randomly selected locations. In all cases, it can be considered that the mean values show a reasonable correlation with the designed strut thickness, for both orientations.

Table 7.1 Measured strut thickness for each sample (* marks a horizontal strut). The standard deviation is shown next to the mean values (*n=5*).

Sample number	Strut	Orientation to the build plate	Designed strut thickness (mm)	Measured strut thickness (mm)	Mean thickness (mm)
1	A	45°	1.50	1.59	1.53 +/-0.069
	B			1.44	
	C			1.48	
	D			1.59	
	E			1.57	
2	A	45°	0.50	0.45	0.50 +/-0.037
	B			0.48	
	C			0.54	
	D			0.53	
	E			0.51	
3	A	Parallel	1.50	1.49	1.45 +/-0.074
	B			1.52	
	C			1.49	
	D			1.35*	
	E			1.39*	
4	A	Parallel	0.50	0.52	0.50 +/-0.020
	B			0.49	
	C			0.51	
	D			0.49*	
	E			0.47*	

In Samples 3 and 4, a reduction in the designed thickness was observed in the horizontal struts. This was most prevalent in the 1.5 mm cellular structure where a 7.3% to 10% reduction in strut thickness was measured. The reduction in the measured thickness of the horizontal struts may be attributed to the metal powder not being able to support itself in the powder bed, thus reducing the thickness of the horizontal downward facing struts. Such differences were not observed in Sample 1 where the mean strut thickness was 2% higher than the designed value. Overall, this conflicts with Parthasarthy *et al*. (2011) who reported that the difference between the designed and measured strut thickness increased as the strut size decreased. However, the referred published work is different in that the whole cubes containing the square pore titanium alloy cellular structures were orientated at 45 degrees with respect to the build platform.

The orientation of the square pore cellular structures utilised are not ideal for ALM due to them possessing downward facing surfaces that are parallel to the build platform. Chapters 4, 6 and other published work has identified that such structures can be produced using ALM techniques (Parthasarathy *et al*., 2011; Emmelmann *et al*., 2011). However, structural irregularities have been observed, which have been found to have a detrimental effect on the mechanical properties of additive manufactured cellular structures (Harrysson *et al*., 2008; Parthasarathy *et al*., 2011; Smith *et al*., 2013). Considering this, a femoral stem was manufactured with a cellular structure that was orientated at 45 degrees with respect to the build platform. This was performed to visually investigate the characteristics of a self-supporting structure and to provide a comparison with the cellular structures that have been investigated in the previous chapters.

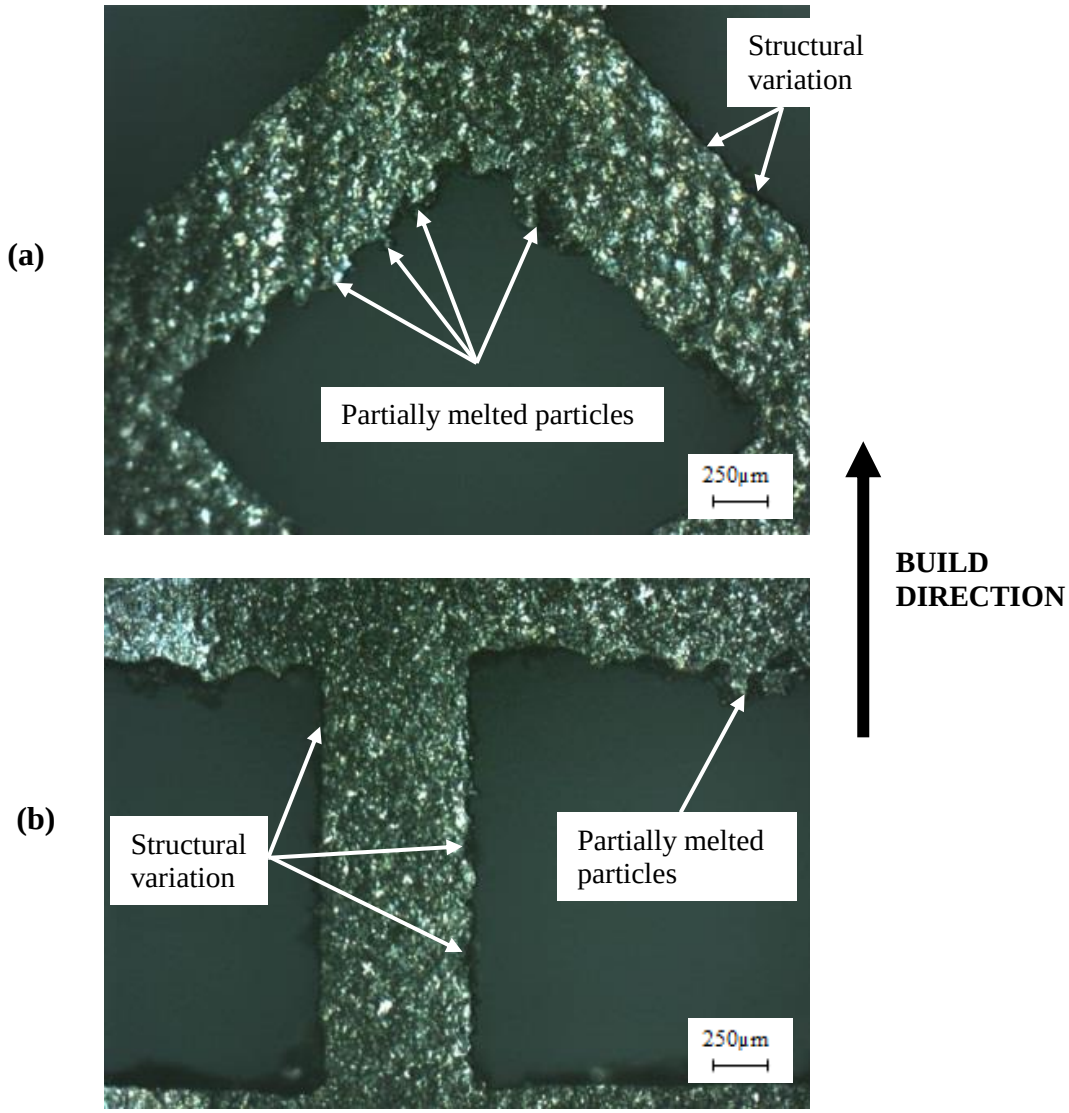

Figure 7.9 Micrographs of the cellular structures. (a) 0.5 mm cellular structure with 45 degree orientation (b) 0.5 mm cellular structure with normal orientation.

Figure 7.9 compares the two orientations of the 0.5 mm cellular structure. From the images, it is evident that structural variation and irregularities are present in both samples. This concurs with other work that has investigated additive manufactured cellular structures with alternative unit cell geometries that may be considered more suitable for ALM (Harrysson *et al*., 2008; Murr *et al*., 2010; Yan *et al*., 2012; Smith *et al*., 2013). The 45 degree orientation may adhere to ALM design guidelines but the same issues with structural variation and heterogeneities are still present within the square pore cellular structures.

The observations made are based upon a visual inspection using a limited selection of samples. It is proposed that further physical testing and finite element analysis would be needed to investigate the mechanical behaviour of the 45 degree orientated structure. This would determine any potential benefits of utilising them when compared to the normal orientated cellular structure that has been investigated in the bulk of this research.

7.6 Additional factors

In addition to the previous sections of work, it is believed that there are additional factors associated with the manufacturability of laser melted CoCrMo femoral stems that require some attention. The removal of unprocessed/partially melted powder particles and part orientation/post processing have been highlighted as factors and are discussed below.

7.6.1 Removal of unprocessed and partially melted powder

The deposition of cobalt and chromium ions in the blood stream can result in the aseptic loosening of orthopaedic implants, and cause necrosis of the bone and surrounding soft tissue (Gruber *et al*., 2007). In this instance, femoral stems would have to be designed and manufactured so that any unprocessed and partially melted powder would not cause contamination in the bloodstream.

The functionally graded stems for this work have been designed with two holes for powder removal. From visual inspection and through measuring the weight of the stems, it can be claimed that the unprocessed powder has been removed successfully following manufacture. In contrast to this, Figures 7.6, 7.7 and 7.9 show the presence of partially melted powder particles that are inherent with the additive manufacture of metallic cellular structures.

It is standard practice for the partially melted particles to be removed as part of the post processing operations. However, this is not straight forward when considering internal or closed cellular structures. It is considered that techniques such as extrusion honing could be utilised to remove these particles, but there would be a risk of depositing the honing medium within the stem and therefore potentially creating a separate problem. One suggestion is to manufacture and insert plugs into the powder removal holes and then seal them using a welding process. It is considered that this would eliminate any risks of releasing metal debris in the form of unprocessed and partially melted powder particles into the blood stream.

7.6.2 Part orientation and post processing

Cobalt chrome alloys are often used in orthopaedic applications because of their hardness and ability to take a smooth polished surface finish (Marti, 2000). Due to the the hardness and toughness of CoCrMo, machining and polishing can be labour intensive, time consuming and hence expensive (Zeng and Blunt, 2013). This is a key factor when considering the feasibility of producing CoCrMo femoral stems using SLM.

The femoral stems for this work have been manufactured without the femoral head so that less material is used and the build height is minimised. In Chapter 6, support structures were not required for manufacturing purposes, as the collar was not included in the design. Subsequent stems were made with the collar and therefore support structures were required, as shown in Figure 7.10.

Standard supports for cobalt chrome parts were used as well as a solid support for anchoring the components to the build plate. The standard supports that are generated in Materialise Magics 17.0 for cobalt chrome cannot be removed easily by hand. Therefore, these support structures would have to be machined as part of the component

post processing. This would be time-consuming due to the poor machinability and high costs associated with processing cobalt chrome alloys.

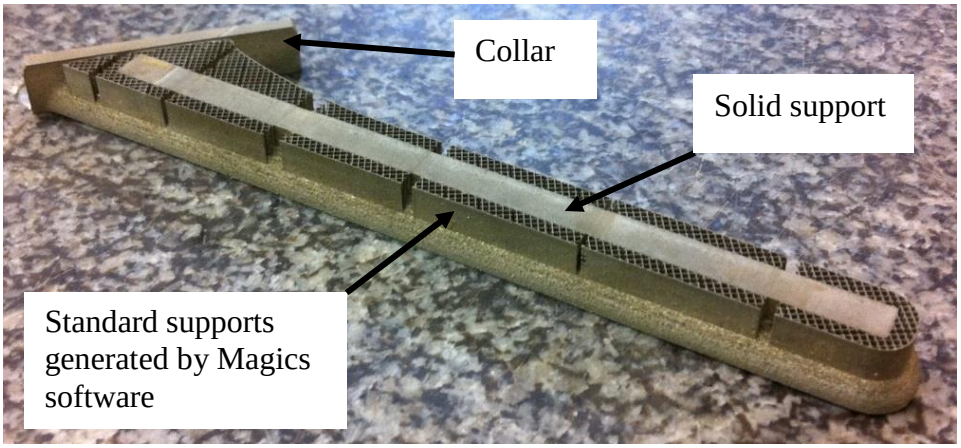

Figure 7.10 The underside of a femoral stem and the support structures that were used for manufacture.

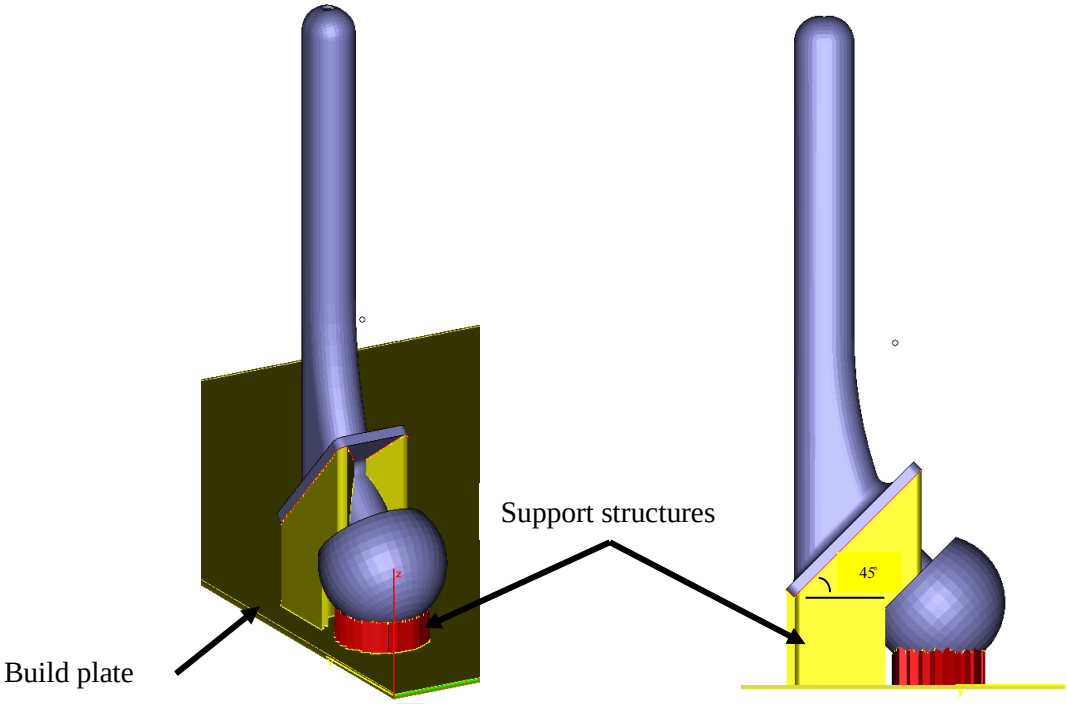

Figure 7.11 The vertical orientation of the femoral stem with the automatically generated support structures.

If a full femoral stem was to be manufactured using SLM, vertical orientation of the component in the build chamber is proposed. Figure 7.11 shows a femoral stem virtually positioned on a build plate, with the support structures that were automatically generated using Materialise Magics 17.0. In this instance, it considered that the bulk of the structures that are supporting the collar of the stem could be removed. This is because the downward facing surface of the collar is orientated at 45 degrees with respect to the build plate and is self-supporting according to ALM design guidelines.

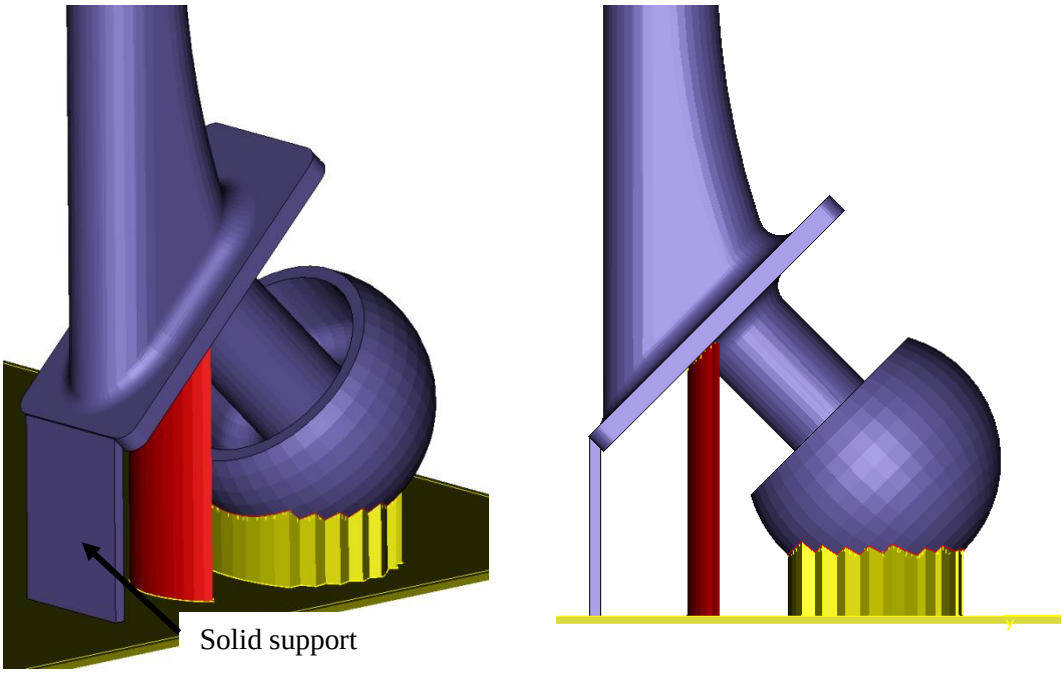

Figure 7.12 Modified support structures that would be utilised for manufacture.

Figure 7.12 shows the modified support structures. This was achieved through changing the threshold value in the software, so that only surfaces that were inclined at angles of less than 45 degrees were supported. Additionally, a solid support was positioned on the corner of the collar in order to provide additional support and anchoring to the build plate.

It is considered that the proposed part orientation and support methodology is justified in that the majority of the post processing would be performed on the femoral head,

which would require polishing in order to meet clinical requirements. There would also be minimal post processing of the stem portion of the prosthesis and this would enable the manufacture of fully porous or functionally graded stems with a porous surface topography that could accommodate biological fixation.

7.7 Summary

The manufacturability of laser melted functionally graded CoCrMo femoral stems has been investigated. Within the discussed limitations, the main findings of this chapter can be summarised as follows:

- It has been indicated that functionally graded femoral stems are less affected by residual stress when compared to fully dense stems. The stem that incorporated the cellular structure with a 45 degree orientation appeared to be more favourable for reducing residual stress.
- There were no defects observed between the cellular structures and 1 mm thick outer skin. However, the sharp corners at the interface connections are a future concern for fatigue failure.
- Micro cracks were identified where acute angles were observed at connections between 0.5 mm struts and the 2.0 mm thick cross section. It is recommended that such geometric mismatches should be avoided in future designs.
- Structural variation appears to be equally evident when comparing the two orientations of the square pore cellular structures. Physical testing and numerical analysis is recommended to determine the mechanical properties of square pore cellular structures with a 45 degree orientation.
- The post processing of functionally graded CoCrMo femoral stems is a key economical factor associated with the manufacturability. This is based upon the poor machinability and costs associated with machining cobalt chrome alloys.

In the next chapter, femoral stem designs are proposed and justified based upon the results and observations that have been presented in this thesis.

Chapter 8 Design proposals

8.1 Introduction

This work has employed experimental and numerical methods to investigate the mechanical behaviour and manufacturability of CoCrMo femoral stems that can be manufactured using SLM. Subsequently, this chapter proposes femoral stem designs that are justified from the results and observations from this work.

In Chapter 5, it was highlighted that the pore size range of the cellular structures studied in this work would encourage the ingrowth of fibrous tissue as opposed to new bone at the interface. In this respect, the fully porous femoral stems were assumed not to be clinically suitable, as the stability of the bone-implant interface could be compromised.

Given this, a functionally graded stiffness configuration has been utilised and its versatility has been shown by proposing designs for cemented or cementless THA. A hypothetical design for a fully porous stem that considers an alternative functionally graded approach has also been proposed.

8.2 Functionally graded CoCrMo stem

The results from Chapters 4 and 6 show that a square pore CoCrMo cellular structure exhibiting a 1 mm strut size and 64.8% volumetric porosity could be manufactured using SLM with a repeatable mechanical behaviour, when subjected to both uniaxial compression and cantilever bending loading conditions. This is evident from the stress-stain and force-displacement relationships presented in Figures 4.7d and 6.6b respectively. Additionally, this cellular structure was found to be beneficial for stiffness matching as it provided effective mechanical properties that were close to femoral

cortical bone, where values of 13.64 GPa and 175.15 MPa were determined for the effective elastic modulus and 0.2% compressive yield strength respectively.

The PC-2 functionally graded stiffness configuration utilised the cellular structure described above and has therefore been proposed as the most favourable design. It was considered that this functionally graded femoral stem possessed the versatility to be utilised for either cemented or cementless THA.

8.2.1 Cemented stem

Figure 8.1 shows the proposed design for cemented fixation. Shot peening and light polishing post-processing operations would be required to improve the as-built surface finish and to remove partially melted powder particles from the outer surface of the stem. It is considered that a suitable surface finish could be obtained for cemented fixation, given the material's ability to take a smooth surface finish (Marti, 2000).

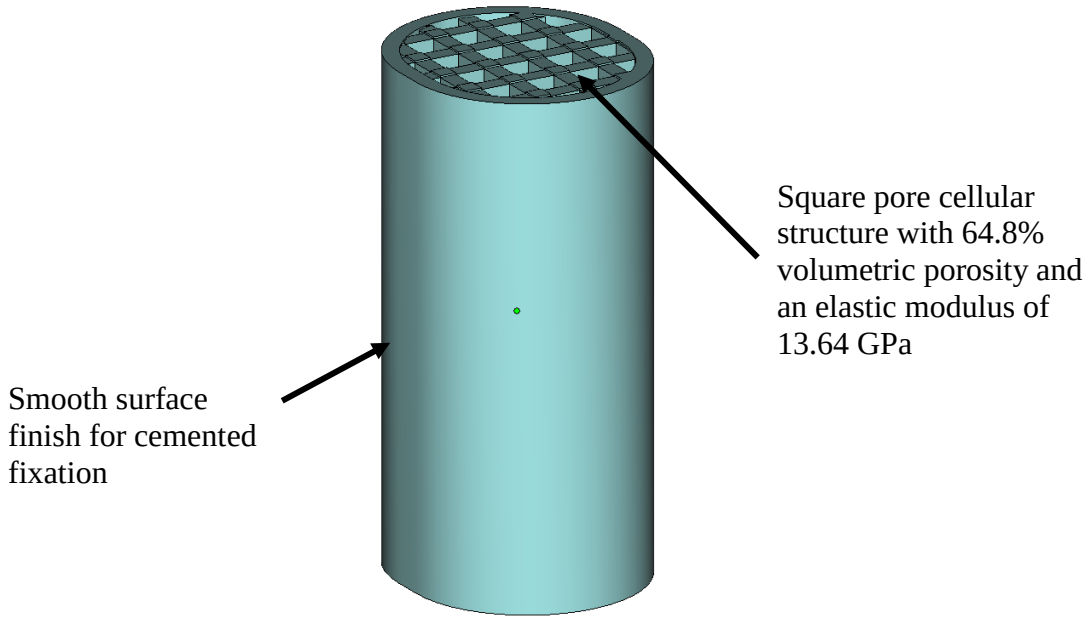

Figure 8.1 CAD model showing a cross section of the proposed cemented stem.

8.2.2 Cementless stem

Figure 8.2 shows the proposed design for cementless fixation. A beaded porous topography has been designed onto the outer surface of the femoral stem, to provide an interface condition that can accommodate bone ingrowth. In this instance, a square porous topography with 0.5 mm pore and bead sizes has been utilised to provide an example. However, the geometry, size and distribution of the pores/beads could be adapted in order to optimise the biological fixation of the stem, and hence implant stability.

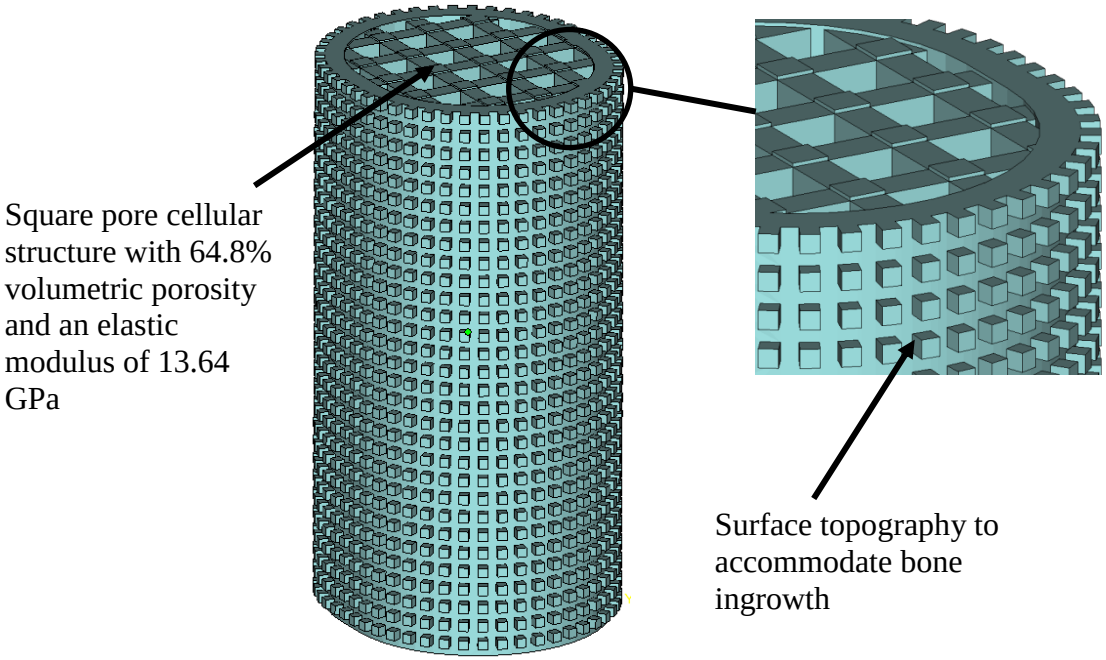

Figure 8.2 CAD model showing a cross section of the proposed cementless stem.

8.3 Alternative fully porous design

As discussed previously, the pore size range investigated in this research is not ideal for accommodating biological fixation at the bone-implant interface. From the numerical analysis performed in Chapter 5, it was evident that the load transfer to the periprosthetic femur was much improved when the fully porous stiffness configurations

were considered. Given this, an alternative fully porous design has been hypothetically proposed as shown below in Figure 8.3.

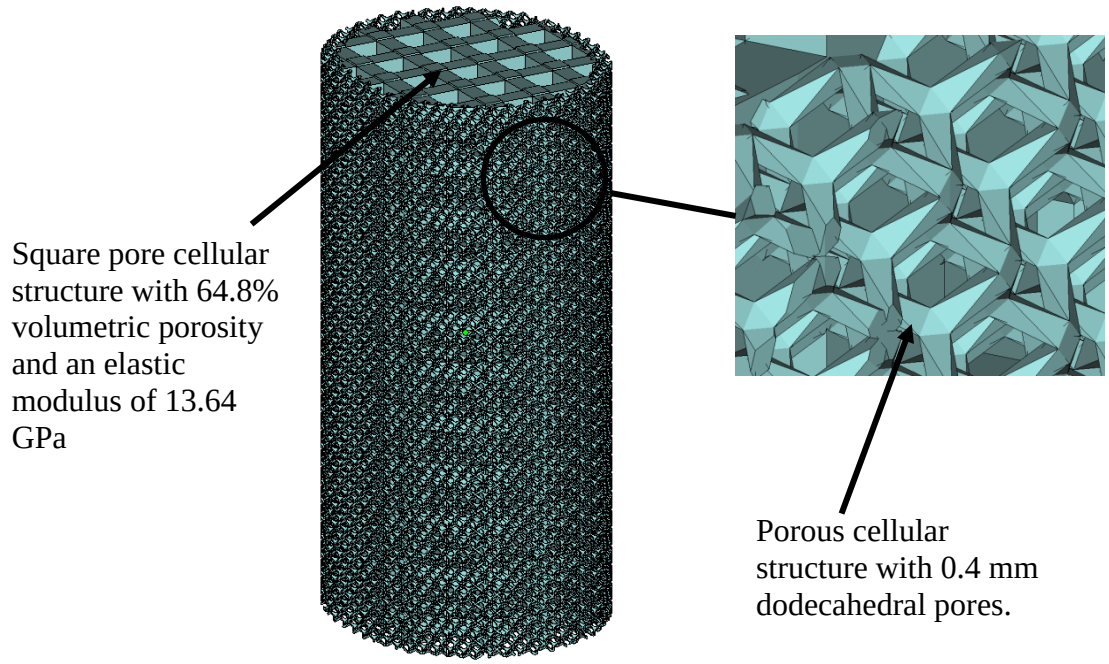

Figure 8.3 CAD model showing a cross section of the proposed fully porous stem.

The fully porous design utilises an alternative functionally graded approach by combining two cellular structures with different densities and unit cell geometries. The core is comprised with the same square pore cellular structure as used with the previous cemented and cementless designs. In this instance though, a more filigree cellular structure has been utilised in order to provide clinically suitable surface characteristics that will accommodate bone ingrowth. A unit cell with dodecahedral pores was selected from the structures library located within Materialise Magics 17.0 software. In this instance, the cellular structure was characterised with 0.2 mm and 0.4 mm strut and pore sizes respectively. It is considered that the proposed hypothetical design has the potential to offer a fully porous femoral stem with a similar stiffness and strength to femoral cortical bone, coupled with an interconnected porous surface topography that can accommodate bone ingrowth.

8.4 Discussion

This chapter has presented alternative CoCrMo femoral stem designs that can be manufactured using SLM. A functionally graded femoral stem (PC-2) has been proposed and justified from experimental data, which is 48% lighter and 60% more flexible than a traditional fully dense CoCrMo prosthesis. The functionally graded stem is inherently stiffer than the fully porous configurations that were investigated in Chapter 5. However, favourable stress shielding characteristics were evident when the functionally graded stem was compared to its bulk metallic counterpart. Additionally, it is considered that the functionally graded stem provides a versatile design that could be potentially utilised for cemented or cementless fixation.

The proposed functionally graded design has been justified from the results of mechanical tests that have applied monotonic loading conditions. Future testing would need to consider cyclic loading in order to determine the fatigue characteristics of the stem when subjected to dynamic loads.

A fully dense titanium alloy femoral stem has previously been manufactured using SLM with an interconnected cellular surface topography (Harrison *et al*., 2013). The results showed that the stem had potential to improve the primary stability of the implant when compared to other traditional surface coatings. It is considered that the cementless stem proposed in Figure 8.2 would provide similar conditions at the bone-implant interface. However, the design proposed from this research is different in offering a CoCrMo femoral stem with stiffness characteristics that can potentially alleviate stress shielding in the periprosthetic femur.

From the functionally graded design, it was observed that the 1 mm fully dense outer skin restricts the load transfer to the bone. In order to increase the flexibility of the

functionally graded stem, it may be beneficial to reduce the thickness of the outer skin. This would need to be approached with caution, given the discussed repeatability issues associated with manufacturing thinner wall sections and struts.

A clinically suitable fully porous femoral stem would be more desirable for reducing periprosthetic stress shielding. In this instance, a hypothetical design for a fully porous femoral has been proposed. The design shown in Figure 8.3 could provide a femoral stem with effective mechanical properties that are similar to femoral cortical bone, whilst exhibiting clinically suitable interface characteristics that have the potential to accommodate bone ingrowth. It is considered that such a design could be realised using SLM. However, there are concerns associated with the removal of powder from such small pores and the unpredictable and brittle failure of more filigree cellular structures.

Modular designs that utilise a titanium alloy stem have often been the preferred choice for THA, due to their relatively low stiffness, and due to the individual customisation that they offer the patient (Sporer and Paprosky, 2006). The negative factors associated with modular designs in relation to the failure of the taper junction (Sotereanos *et al*., 2013) and the identification of adverse soft tissue reactions (Langton *et al*., 2012) have provided recent and ongoing concerns.

It can be construed that the functionally graded femoral stem presented from this research, highlights the potential of a laser melted monoblock CoCrMo stem for cemented and cementless THA, which is 48% lighter and 60% more flexible than its bulk metallic counterpart is. Additionally, the concerns that are associated with modular designs are eliminated when monoblock stems are considered.

Chapter 9 Conclusions and future work

This thesis has investigated the adoption of SLM for manufacturing lightweight CoCrMo femoral stems with improved stiffness characteristics. It was hypothesised that alternative femoral stem designs could be realised using SLM, which could contribute towards alleviating stress shielding in the periprosthetic femur, without compromising the strength of the bone itself. Physical and analytical methods were used to study the mechanical behaviour and manufacturability of CoCrMo cellular structures and femoral stems with varying stiffness configurations.

9.1 Main findings of the research

The main findings of this research are chapter specific and have been summarised in the respective chapters throughout this thesis. However, the section below aims to synthesise the main findings of this research in relation to the aim and objectives that were presented in the introduction of this thesis.

The main findings from the physical aspects of the work can be summarised as follows:

- Square pore CoCrMo cellular structures can be manufactured using SLM with compressive properties that are close to human bone. Thus, stiffness matching strategies between the femoral stem and the femur can be investigated.
- A cellular structure with a 1 mm strut size and 64.8% volumetric porosity exhibited the most repeatable mechanical behaviour when subjected to both uniaxial compression and cantilever bending.
- There are concerns associated with the more brittle failure and repeatable manufacturability of square pore cellular structures that incorporate a strut size of 0.5 mm or less.

- SLM can repeatedly manufacture a functionally graded CoCrMo femoral stem that is 48% lighter and 60% more flexible than its bulk metallic counterpart is.
- Geometric variation within the CoCrMo cellular structures creates heterogeneities that have a detrimental effect on the structural stiffness and strength.
- Incorporating cellular structures into the designs of CoCrMo femoral stems has a positive effect in reducing the presence of thermally induced residual stresses.
- Micro cracks were identified within the functionally graded femoral stems at structural connections where a geometric mismatch to the order of 4 was observed.

The main findings from the numerical and analytical aspects of the work can be summarised as follows:

- The finite element method overestimated the stiffness of the square pore cellular structures by a mean factor of 3.33, when subjected to uniaxial compression.
- A closer agreement was obtained between the experimental and numerical results, when structural variation was incorporated into the finite element model of a square pore cellular structure subjected to uniaxial compression.
- The load transfer to the periprosthetic femur was improved when the mechanical properties of the CoCrMo cellular structures were utilised. The mechanical stimulus within the periprosthetic femur was increased without compromising the strength of the bone.
- The proposed functionally graded stem (PC-2) provided increased stress values of 20%, 36% and 12% in the medial Gruen zones 5, 6 and 7 respectively when compared to a traditional stem. Similar trends were observed in the lateral Gruen

zones 2 and 3 by where the stress values increased by approximately 22% and 18% respectively.

- A simplified continuum approach was utilised to model the cellular structures when incorporated into the femoral stems. This was justified from observing the von Mises stress distribution in the cortical bone when comparing a region of interest that modelled the cellular structures with their idealised geometry.
- A reasonable correlation was observed in the flexural stiffness of the stems when comparing the numerical and experimental results.

9.2 Implications of the research

The positive effect that more flexible femoral stems can have on alleviating stress shielding is already known. Previous studies have shown that additive manufactured titanium alloy femoral stems have the potential to improve the load transfer to the periprosthetic femur (Harrysson *et al*., 2008; Arabnejad Khanoki and Pasini, 2013). In agreement with this, the results from this research concur with those findings. Additionally, the work of Harrison *et al.* (2013) has also highlighted the potential of utilising SLM for producing a surface topography that can improve the stability of a titanium alloy femoral stem. It can be construed that SLM has the potential to manufacture femoral stems with improved stiffness characteristics whilst maintaining the bone-implant interface stability. It is evident that previous research has focused upon investigating titanium alloys. The research presented in this thesis is considered the first collective body of work to investigate the potential application of CoCrMo femoral stems that can be manufactured using SLM.

Traditional CoCrMo femoral stems possess an elastic modulus that is in the region of 200 GPa. These stems have previously shown undesirable stress shielding characteristics in numerical studies (Harrysson *et al*., 2008; Yan *et al*., 2011). For this

reason, titanium alloys are often considered due to their lower stiffness, where the elastic modulus of Ti-6Al-4V is in the region of 115 GPa. However, the concerns associated with modular femoral stem designs have supported the direction of the research presented in this thesis.

This work has highlighted the potential adoption of SLM for realising the design of a CoCrMo stem that offers more flexibility when compared to a bulk metallic CoCrMo femoral stem. A functionally graded design has been proposed for cemented or cementless THA, which is 48% lighter and 60% more flexible than a traditional CoCrMo prosthesis. This provides a CoCrMo femoral stem with a stiffness that is comparable to a titanium alloy. Thus, it is considered that an alternative design for a CoCrMo femoral stem has been presented with improved stress shielding characteristics that can potentially eliminate the risks associated with titanium alloy modular designs.

9.3 Limitations of the research

The research presented in this thesis offers a study that has combined two topical areas of research; these being femoral stem biomechanics and ALM. As a direct consequence of this methodology, the research encountered a number of limitations that should be considered.

Assumptions were made when developing the finite element models used throughout this thesis. In Chapter 5, the material properties of the femur were divided into regions to represent the cortical bone, cancellous bone and bone marrow. However, every case of THA is potentially unique, concerning the anatomy and quality of the proximal femur. It is considered that the employed methodology was suitable for a comparative analysis where the load transfer to the femur was of interest.

With the exception of Chapter 4, the square pore cellular structures were modelled as continuum bodies that were assigned physically determined material properties. Computational power restricted the development of a finite element model where the cellular structures of a full femoral stem could be modelled with their idealised geometry. As a result, the simplified continuum approach used in this work was considered justified. In Chapter 5, a region of interest was modelled to compare the continuum and idealised approach, and in Chapter 6, a reasonable correlation was observed between the numerical and experimental results for flexure.

The mechanical testing that was performed in Chapters 4 and 6 utilised monotonic loading conditions. Previously, it has been estimated that the hip joint can be subjected to in excess of 1 million gait cycles every year (Morlock *et al*., 2001). It may be perceived that the effects of cyclic loading should have been investigated. However, before cyclic loading can be considered, it is thought that the mechanical behaviour of the cellular structures and femoral stems when subjected to monotonic loads needed to be understood first.

Square pore cellular structures with a normal orientation were mechanically tested, both individually and when incorporated into functionally graded femoral stems. Thus, a single unit cell geometry was considered in this work. It may have been beneficial to consider alternative unit cell geometries for adapting the stiffness of the femoral stems. However, square pore cellular structures were selected because they can be designed and modelled with manual techniques. Therefore, the research was not dependent upon the use of specialist software packages for designing and analysing the cellular structures.

The recommendations and observations regarding the manufacturability of laser melted CoCrMo femoral stems have been based upon producing components without the

femoral neck and head region of the implant. It is considered that the manufacturing process could realise the production of a full femoral stem. However, restrictions and constraints in the availability of the raw material prevented the manufacture of a full femoral stem in this research.

9.4 Future work

In order to further the understanding and develop the research presented in this thesis, the following areas of research are proposed for future work:

Femoral stem manufacture – A full functionally graded femoral stem should be manufactured to meet clinical requirements. This would further the understanding of adopting laser melting technology for the manufacture of functionally graded CoCrMo femoral stems.

Physical testing - It is considered that any future testing of the functionally graded femoral stems should be more replicative of in vivo loading conditions. Therefore, a stem could be inserted into a cadaveric or synthetic femur and be mechanically loaded under in vitro conditions.

Fatigue analysis – Femoral stem failure often occurs due to years of full weight bearing activities. The effects of cyclic loading or dynamic stress should be considered in order to determine the fatigue life of the femoral stems.

Cellular structures – A single unit cell geometry was considered in this thesis. Future investigation is recommended to analyse the mechanical behaviour and manufacturability of cellular structures with alternative unit cell geometries and orientations.

Fully porous designs – Fully porous designs are more favourable for reducing stress shielding. It would be beneficial for a clinically suitable fully porous femoral stem to be designed and manufactured using SLM with the required structural integrity. Future investigation should be considered to analyse the mechanical behaviour and manufacturability of the fully porous stem that was hypothetically proposed.

References

Aebli, N., Krebs, J., Schwenke, D., Stich, H., Schawalder, P. and Theis, J. (2003) Degradation of hydroxyapatite on a well functioning femoral component. *Journal of Bone and Joint Surgery (Br),* **85-B**(4), pp.499-503.

Arabnejad Khanoki, S. and Pasini, D. (2013) Fatigue design of a mechanically biocompatible lattice for a proof-of-concept femoral stem. *Journal of the Mechanical Behaviour of Biomedical Materials,* **22,** pp.65-83.

Aubault, M., Druon, J., Le Nail, L. and Rosset, P. (2013) Outcomes at least 10 years after cemented PF® (Zimmer) total hip arthroplasty: 83 cases. *Orthopaedics & Traumatology: Surgery & Research,* **99,** pp.S235-S239.

Bacchewar, P., Singhal, S. and Pandey, P. (2007) Statistical modelling and optimization of surface roughness in the selective laser sintering process. *Proceedings of the Institution of Mechanical Engineers, Part B: Journal of Engineering Manufacture,* **221**(1), pp.35-52.

Bergmann, G., Deuretzbacher, G., Heller, M., Graichen, F., Rohlmann, A., Strauss, J. and Duda, G. N. (2001) Hip contact forces and gait patterns from routine activities. *Journal of Biomechanics,* **34**(7), pp.859-871.

Bergmann, G., Graichen, F. and Rohlmann, A. (1993) Hip joint loading during walking and running, measured in two patients. *Journal of Biomechanics,* **26**(8), pp.969-990.

Bergmann, G., Graichen, F., Siraky, J., Jendrzynski, H. and Rohlmann, A. (1988) Multichannel strain gauge telemetry for orthopaedic implants. *Journal of Biomechanics,* **21**(2), pp.169-176.

Bertol, L. S., Junior, W. K., Silva, F. P. D. and Aumund-Kopp, C. (2010) Medical design: Direct metal laser sintering of Ti-6Al-4V. *Materials and Design,* **31**(8), pp.3982-3988.

Bertollo, N., Matsubara, M., Shinoda, T., Chen, D., Kumar, M. and Walsh, W. R. (2011) Effect of surgical fit on integration of cancellous bone and implant cortical bone shear strength for a porous titanium. *The Journal of Arthroplasty,* **26**(7), pp.1000-1007.

Bever, M. B. and Duwez, P. E. (1972) Gradients in composite materials. *Materials Science and Engineering,* **10,** pp.1-8.

Bobyn, J., Cameron, H., Abdulla, D., Pilliar, R. and Weatherly, G. (1982) Biologic fixation and bone modelling with an unconstrained total knee prosthesis. *Current Orthopaedics and Related Research,* **166,** pp.301-312.

Bobyn, J., Pilliar, R., Cameron, H. and Weatherly, G. (1980) The optimum pore size for the fixation of porous-surfaced metal implants by the ingrowth of bone. *Clinical Orthopaedics and Related Research,* **150,** pp.263-270.

Bobyn, J., Stackpool, G., Hacking, S., Tanzer, M. and Krygier, J. (1999) Characteristics of bone ingrowth and interface mechanics of a new porous tantalum biomaterial. *Journal of Bone and Joint Surgery (Br),* **81-B**(5)**,** pp.907-14.

Boudeau, N., Liksonov, D., Barriere, T., Maslov, L. and Gelin, J. C. (2012) Composite based on polyetheretherketone reinforced with carbon fibres, an alternative to conventional materials for femoral implant: Manufacturing process and resulting structural behaviour. *Materials & Design,* **40,** pp.148-156.

Bousson, V., Bergot, C., Meunier, A., Barbot, F., Parlier-Cuau, C., Laval-Jeantet, A.-M. and Laredo, J.-D. (2000) CT of the mid-diaphyseal femur: Cortical bone mineral density and relation to porosity. *Radiology,* **217**(1), pp.179-187.

Brenne, F., Niendorf, T. and Maier, H. J. (2013) Additively manufactured cellular structures: Impact of microstructure and local strains on the monotonic and cyclic behaviour under uniaxial and bending load. *Journal of Materials Processing Technology,* **213**(9), pp.1558-1564.

British Standards Institution (2005) BS EN ISO 7438:2005. *Metallic materials – Bend test*. London: BSI.

British Standards Institution (2011) BS ISO 13314:2011. *Mechanical testing of metals – ductility testing – compression test for porous and cellular metals.* London: BSI.

British Standards Institution (2012) BS EN ISO 9513:2012. *Metallic materials. Calibration of extensometer systems used in uniaxial testing.* London: BSI.

Brown, B., Smallwood, R., Barber, D., Lawford, P. and Hose, D. (1998) *Medical Physics and Biomedical Engineering*. 1st ed. San Val.

Bryan, R., Nair, P. B. and Taylor, M. (2012) Influence of femur size and morphology on load transfer in the resurfaced femoral head: A large scale, multi-subject finite element study. *Journal of Biomechanics,* **45**(11), pp.1952-1958.

Campoli, G., Borleffs, M. S., Amin Yavari, S., Wauthle, R., Weinans, H. and Zadpoor, A. A. (2013) Mechanical properties of open-cell metallic biomaterials manufactured using additive manufacturing. *Materials & Design*, **49,** pp.957-965.

Cansizoglu, O., Harrysson, O., Cormier, D., West, H. and Mahale, T. (2008) Properties of Ti–6Al–4V non-stochastic lattice structures fabricated via electron beam melting. *Materials Science and Engineering: A,* **492**(1-2), pp.468-474.

Cash, D., Bayer, J., Logan, K. and Wimhurst J. (2010) The Exeter Trauma Stem: Early results of a new cemented Hemiarthroplasty for femoral neck fracture. *British Journal of Medical Practitioners*, **3**, p. 303.

Cheah, C., Chua, C., Leong, K. and Chua, S. (2003) Development of a tissue engineering scaffold structure library for rapid prototyping. Part 1: Investigation and Classification. *The International Journal of Advanced Manufacturing Technology,* **21,** pp.291-301.

Cook, S., Walsh, K. and Haddad, R. J. (1985) Interface mechanics and bone growth into porous Co-Cr-Mo alloy implants. *Clinical Orthopaedics & Related Research,* **193,** pp.271-280.

Cowin, S. C. and Hegedus, D. H. (1976) Bone Remodelling I: A theory of adaptive elasticity. *Journal of Elasticity,* **6**(3), pp.313-326.

Crowninshield, R. D., Johnston, R. C., Andrews, J. G. and Brand, R. A. (1978) A biomechanical investigation of the human hip. *Journal of Biomechanics,* **11**(1-2), pp.75-85.

Dorr, L., Absatz, M., Gruen, T., Saberi, M. and Doerzbacher, J. (1990) Anatomic porous replacement hip arthroplasty: First 100 consecutive cases. *Seminars in arthroplasty*, **1**(1), pp.77 - 86.

Ebrahimi, H., Rabinovich, M., Vuleta, V., Zalcman, D., Shah, S., Dubov, A., Roy, K., Siddiqui, F. S., H. Schemitsch, E., Bougherara, H. and Zdero, R. (2012) Biomechanical

properties of an intact, injured, repaired, and healed femur: An experimental and computational study. *Journal of the Mechanical Behaviour of Biomedical Materials,* **16,** pp.121-135.

Edwards, W. B., Gillette, J. C., Thomas, J. M. and Derrick, T. R. (2008) Internal femoral forces and moments during running: Implications for stress fracture development. *Clinical Biomechanics,* **23**(10), pp.1269-1278.

Electro Optical Systems. (2005) EOSINT M250 Xtended, M270 Basic Operation Manual.

Electro Optical Systems. (2010) Material Data Sheet EOS Cobalt Chrome MP1.

Electro Optical Systems. (2009) Whitepaper: Materials for Direct Metal Laser Sintering. p. 7.

Emmelmann, C., Scheinemann, P., Munsch, M. and Seyda, V. (2011) Laser additive manufacturing of modified implant surfaces with osseointegrative characteristics. *Physics Procedia,* **12,** Part A, pp.375-384.

Eshraghi, S. and Das, S. (2010) Mechanical and microstructural properties of polycaprolactone scaffolds with one-dimensional, two-dimensional, and three-dimensional orthogonally oriented porous architectures produced by selective laser sintering. *Acta Biomaterialia,* **6**(7), pp.2467-2476.

Espana, F. L. A., Balla, V. K., Bose, S. and Bandyopadhyay, A. (2010) Design and fabrication of CoCrMo alloy based novel structures for load bearing implants using laser engineered net shaping. *Materials Science and Engineering: C,* **30**(1), pp.50-57.

Geesink, R., De Groot, K. and Klein, C. (1988) Bonding of bone to apatite coated implants. *Journal of Bone and Joint Surgery (Br)*, **70-B**(1), pp.17-22.

Gibson, L. and Ashby, M. (1997). *Cellular Solids: Structures and Properties*. 2nd ed. Cambridge. Cambridge University Press.

Gil, L., Bruhl, S., Jimenez, L., Leon, O., Guevara, R. and Staia, M. (2006) Corrosion performance of the plasma nitrided 316L stainless steel. *Surface and Coatings Technology*, **201**(7), pp.4424-4429.

Gomez, P. F. and Morcuende, J. A. (2005) Early attempts at hip arthroplasty: 1700s to 1950s. *The Iowa orthopaedic journal*, **25,** pp.25-29.

Gong, H., Wu, W., Fang, J., Dong, X., Zhao, M. and Guo, T. (2012) Effects of materials of cementless femoral Stem on the functional adaptation of bone. *Journal of Bionic Engineering*, **9**(1), pp.66-74.

Gruber, F. W., Böck, A., Trattnig, S., Lintner, F. and Ritschl, P. (2007) Cystic lesion of the groin due to metallosis: A rare long-term complication of metal-on-metal total hip arthroplasty. *The Journal of Arthroplasty*, **22**(6), pp.923-927.

Gruen, T. A., Mcneice, G. M. and Amstutz, H. C. (1979) "Modes of failure" of cemented stem-type femoral components: A radiographic analysis of loosening. *Clinical Orthopaedics and Related Research*, **141,** pp.17-27.

Gu, D. and Shen, Y. (2009) Balling phenomena in direct laser sintering of stainless steel powder: Metallurgical mechanisms and control methods. *Materials & Design*, **30**(8), pp.2903-2910.

Hammerberg, E. M., Wan, Z., Dastane, M. and Dorr, L. D. (2010) Wear and range of motion of different femoral head sizes. *The Journal of Arthroplasty,* **25**(6), pp.839-843.

Harrison, N., Mchugh, P. E., Curtin, W. and McDonnell, P. (2013) Micromotion and friction evaluation of a novel surface architecture for improved primary fixation of cementless orthopaedic implants. *Journal of the Mechanical Behaviour of Biomedical Materials,* **21,** pp.37-46.

Harrysson, O. L. A., Cansizoglu, O., Marcellin-Little, D. J., Cormier, D. R. and West II, H. A. (2008) Direct metal fabrication of titanium implants with tailored materials and mechanical properties using electron beam melting technology. *Materials Science and Engineering: C,* **28**(3), pp.366-373.

Hearn, S. L., Bicalho, P. S., Eng, K., Booth Jr, R. E., Hozack, W. J. and Rothman, R. H. (1995) Comparison of cemented and cementless total hip arthroplasty in patients with bilateral hip arthroplasties. *The Journal of Arthroplasty,* **10**(5), pp.603-608.

Heller, M. O., Bergmann, G., Deuretzbacher, G., Dürselen, L., Pohl, M., Claes, L., Haas, N. P. and Duda, G. N. (2001) Musculo-skeletal loading conditions at the hip during walking and stair climbing. *Journal of Biomechanics,* **34**(7), pp.883-893.

Heller, M. O., Bergmann, G., Kassi, J. P., Claes, L., Haas, N. P. and Duda, G. N. (2005) Determination of muscle loading at the hip joint for use in pre-clinical testing. *Journal of Biomechanics,* **38**(5), pp.1155-1163.

Herrera, A., Panisello, J. J., Ibarz, E., Cegoñino, J., Puértolas, J. A. and Gracia, L. (2007) Long-term study of bone remodelling after femoral stem: A comparison between dexa and finite element simulation. *Journal of Biomechanics,* **40**(16), pp.3615-3625.

Hirata, Y., Inaba, Y., Kobayashi, N., Ike, H., Fujimaki, H. and Saito, T. (2013) Comparison of mechanical stress and change in bone mineral density between two types of femoral implant using finite element analysis. *The Journal of Arthroplasty,* **28**(10), pp.1731-1735.

Huiskes, R., Ruimerman, R., Van Lenthe, G. and Janssen, J. (2000) Effects of mechanical forces on maintenance and adaption of form in trabecular bone. *Nature,* **405,** pp.704-706.

Huiskes, R., Weinans, H., Grootenboer, H. J., Dalstra, M., Fudala, B. and Slooff, T. J. (1987) Adaptive bone-remodelling theory applied to prosthetic-design analysis. *Journal of Biomechanics,* **20**(11-12), pp.1135-1150.

Huiskes, R., Weinans, H. and Rietbergen, B. (1992) The relationship between stress shielding and bone resorption around total hip stems and the effects of flexible materials. *Clinical Orthopaedics and Related Research,* **274,** pp.124-134.

Hwang, K.-T., Kim, Y.-H., Kim, Y.-S. and Choi, I.-Y. (2012) Total hip arthroplasty using cementless grit-blasted femoral component: A minimum 10-year follow-up study. *The Journal of Arthroplasty,* **27**(8), pp.1554-1561.

Karachalios, T., Tsatsaronis, C., Efraimis, G., Papadelis, P., Lyritis, G. and Diakoumopoulos, G. (2004) The long-term clinical relevance of calcar atrophy caused by stress shielding in total hip arthroplasty: A 10-year, prospective, randomized study. *The Journal of Arthroplasty,* **19**(4), pp.469-475.

Kavanagh, B. F., Wallrichs, S., Dewitz, M., Berry, D., Currier, B., Ilstrup, D. and Coventry, M. B. (1994) Charnley low-friction arthroplasty of the hip: Twenty-year results with cement. *The Journal of Arthroplasty,* **9**(3), pp.229-234.

Kerner, J., Huiskes, R., Van Lenthe, G., Weinans, H., Van Rietbergen, B., Engh, C. and Amis, A. (1999) Correlation between pre-operative periprosthetic bone density and post-operative bone loss in THA can be explained by strain adaptive remodelling. *Journal of Biomechanics,* **32**(7), pp.695-703.

Kienapfel, H., Sprey, C., Wilke, A. and Griss, P. (1999) Implant fixation by bone ingrowth. *The Journal of Arthroplasty,* **14**(3), pp.355-368.

Kröger, H., Venesmaa, P., Jurvelin, J., Miettinen, H., Suomalainen, O. and Alhava, E. (1998) Bone density at the proximal femur after total hip arthroplasty. *Clinical Orthopaedics and Related Research,* **352,** pp.66-74.

Kruth, J.P., Froyen, L., Van Vaerenbergh, J., Mercelis, P., Rombouts, M. and Lauwers, B. (2004) Selective laser melting of iron-based powder. *Journal of Materials Processing Technology,* **149**(1-3), pp.616-622.

Kuiper, J. and Huiskes, R. (1997) Mathematical optimization of elastic properties: Application to cementless hip stem design. *Journal of Biomechanical Engineering,* **119**(2), pp.166-174.

Langton, D., Sidaginamale, R., Lord, J., Nargol, A. and Joyce, T. (2012) Taper junction failure in large-diameter metal-on-metal bearings. *Bone and Joint Research,* **1**(4), pp.56-63.

Levy, G. N., Schindel, R. and Kruth, J. P. (2003) Rapid manufacturing and rapid tooling with Layer Manufacture (LM) technologies: State of the art and future perspectives. *CIRP Annals - Manufacturing Technology,* **52**(2), pp.589-609.

Li, S. J., Murr, L. E., Cheng, X. Y., Zhang, Z. B., Hao, Y. L., Yang, R., Medina, F. and Wicker, R. B. (2012) Compression fatigue behaviour of Ti–6Al–4V mesh arrays fabricated by electron beam melting. *Acta Materialia,* **60**(3), pp.793-802.

Mai, K. T., Verioti, C. A., Casey, K., Slesarenko, Y., Romeo, L. and Colwell Jr, C. W. (2010) Cementless femoral fixation in total hip arthroplasty. *American Journal of Orthopaedics,* **39**(3), pp.126-130.

Maloney, W., Jasty, M., Burke, D., O'Connor, D., Zalenski, E., Bragdon, C. and Harris, W. (1989) Biomechanical and histologic investigation of cemented total hip arthroplasties: A study of autopsy retrieved femurs after in vivo cycling. *Clinical Orthopaedics,* **249,** pp.129-140.

Manley, M., Capello, W., D'antonio, J., Eddin, A., Rudolph, G. and Geesink, M. (1998) Fixation of acetabular cups without cement in Total Hip Arthroplasty. A comparison of three different implant surfaces at a minimum duration of follow up of five years. *Journal of Bone and Joint Surgery (Am),* **80**(8), pp.1175-1185.

Marti, A. (2000) Cobalt-base alloys used in bone surgery. *Injury,* **31,** (Supplement 4), pp.D18-D21.

McKee, G. and Watson-Farrar, J. (1966) Replacement of arthritic hips by the McKee-Farrar prosthesis. *Journal of Bone & Joint Surgery, British Volume,* **48-B**(2), pp.245-259.

McKown, S., Shen, Y., Brookes, W., Sutcliffe, C., Cantwell, W., Langdon, G., Nurick, G. and Theobald, M. (2008) The quasi-static and blast loading response of lattice structures. *International Journal of Impact Engineering,* **35**(8), pp.795-810.

McMinn (2012) Proximal femur image [online]. [Accessed 12 December 2012]. Available at: <http://www.mcminncentre.co.uk >.

Meftah, M., John, M., Lendhey, M., Khaimov, A., Ranawat, A. S. and Ranawat, C. S. (2013) Safety and efficiency of non-cemented femoral fixation in patients 75 years of age and older. *The Journal of Arthroplasty*, **28**(8), pp.1378-1380.

Mercelis, P. and Kruth, J.-P. (2006) Residual stresses in selective laser sintering and selective laser melting. *Rapid Prototyping Journal*, **12**(5), pp.254-265.

Mont, M. A., Yoon, T.-R., Krackow, K. A. and Hungerford, D. S. (1999) Clinical experience with a proximally porous-coated second-generation cementless total hip prosthesis: Minimum 5-year follow-up. *The Journal of Arthroplasty*, **14**(8), pp.930-939.

Morlock, M., Schneider, E., Bluhm, A., Vollmer, M., Bergmann, G., Müller, V. and Honl, M. (2001) Duration and frequency of every day activities in total hip patients. *Journal of Biomechanics,* **34**(7), pp.873-881.

Mumtaz, K. and Hopkinson, N. (2009) Top surface and side roughness of Inconel 625 parts processed using selective laser melting. *Rapid Prototyping Journal,* **15**(2), pp.96-103.

Murr, L., Gaytan, S., Medina, F., Lopez, H., Martinez, E., Machado, B., Hernandez, D., Martinez, L., Lopez, M. and Wicker, R. (2010) Next-generation biomedical implants using additive manufacturing of complex, cellular and functional mesh arrays. *Philosophical Transactions of the Royal Society A: Mathematical, Physical and Engineering Sciences,* **368,** pp.1999-2032.

Murr, L. E., Quinones, S. A., Gaytan, S. M., Lopez, M. I., Rodela, A., Martinez, E. Y., Hernandez, D. H., Martinez, E., Medina, F. and Wicker, R. B. (2009) Microstructure

and mechanical behavior of Ti-6Al-4V produced by rapid-layer manufacturing, for biomedical applications. *Journal of the Mechanical Behaviour of Biomedical Materials,* **2**(1), pp.20-32.

National Joint Registry (2013) *10th Annual Report* [online]. National Joint Registry for England, Wales and Northern Ireland. [Accessed 10 October 2013]. Available at: <http://www.njrcentre.org.uk>.

Niinomi, M. (2002) Recent metallic materials for biomedical applications. *Metallurgical and Materials Transactions A,* **33**(3), pp.477-486.

Niinomi, M. (2008) Mechanical biocompatibilities of titanium alloys for biomedical applications. *Journal of the Mechanical Behaviour of Biomedical Materials,* **1**(1), pp.30-42.

Nishino, T., Mishima, H., Kawamura, H., Shimizu, Y., Miyakawa, S. and Ochiai, N. (2013) Follow-up results of 10–12 years after total hip arthroplasty using cementless tapered stem — Frequency of severe stress shielding with synergy stem in Japanese patients. *The Journal of Arthroplasty,* **28**(10), pp.1736-1740.

Öhman, C., Baleani, M., Perilli, E., Dall'ara, E., Tassani, S., Baruffaldi, F. and Viceconti, M. (2007) Mechanical testing of cancellous bone from the femoral head: Experimental errors due to off-axis measurements. *Journal of Biomechanics,* **40**(11), pp.2426-2433.

Oshkour, A. A., Osman, N.A., Bayat, M., Afshar, R. and Berto, F. (2014) Three-dimensional finite element analyses of functionally graded femoral prostheses with different geometrical configurations. *Materials & Design,* **56,** pp.998-1008.

Parsons, I. and Sonnabend, D. (2004) What is the role of joint replacement surgery? *Best Practice and Research. Clinical rheumatology*, **18**(4), pp.557-572.

Parthasarathy, J., Starly, B. and Raman, S. (2011) A design for the additive manufacture of functionally graded porous structures with tailored mechanical properties for biomedical applications. *Journal of Manufacturing Processes*, **13**(2), pp.160-170.

Parthasarathy, J., Starly, B., Raman, S. and Christensen, A. (2010) Mechanical evaluation of porous titanium (Ti6Al4V) structures with Electron Beam Melting (EBM). *Journal of the Mechanical Behaviour of Biomedical Materials*, **3**(3), pp.249-259.

Pedersen, D., Brand, R., Cheng, C. and Arora, J. (1987) Direct comparison of muscle force predictions using linear and nonlinear programming. *Journal of Biomechanical Engineering*, **109**(3), pp.192-199.

Phillips, T., Messieh, S. and Mcdonald, P. (1990) Femoral stem fixation in hip replacement. A biomechanical comparison of cementless and cemented prostheses. *Journal of Bone and Joint Surgery (Br)*, **72-B**(3), pp.431-434.

Pilliar, R., Lee, J. and Maniatopoulos, C. (1986) Observations on the effect of bone ingrowth into porous-surfaced implants. *Clinical Orthopaedics and Related Research***, 208,** pp.108-113.

Pompe, W., Worch, H., Epple, M., Friess, W., Gelinsky, M., Greil, P., Hempel, U., Scharnweber, D. and Schulte, K. (2003) Functionally graded materials for biomedical applications. *Materials Science and Engineering: A*, **362**(1-2), pp.40-60.

Reilly, D. T. and Burstein, A. H. (1975) The elastic and ultimate properties of compact bone tissue. *Journal of Biomechanics*, **8**(6), pp.393-405.

Ring, P. (1968) Complete replacement arthroplasty of the hip by the Ring prosthesis. *Journal of Bone and Joint Surgery (Br),* **50,** pp.720-731.

Rivera, S., Panera, M., Miranda, D. and Varela, F. J. B. (2011) Development of dense and cellular solids in CoCrMo alloy for orthopaedic applications. *Procedia Engineering,* **10,** pp.2979-2987.

Roberts, I. A., Wang, C. J., Esterlein, R., Stanford, M. and Mynors, D. J. (2009) A three-dimensional finite element analysis of the temperature field during laser melting of metal powders in additive layer manufacturing. *International Journal of Machine Tools and Manufacture,* **49**(12-13), pp.916-923.

Robertson, D. M., Pierre, L. S. and Chahal, R. (1976) Preliminary observations of bone ingrowth into porous materials. *Journal of Biomedical Materials Research,* **10**(3), pp.335-344.

Ryan, G., McGarry, P., Pandit, A. and Apatsidis, D. (2009) Analysis of the mechanical behaviour of a titanium scaffold with a repeating unit-cell substructure. *Journal of Biomedical Materials Research Part B: Applied Biomaterials,* **90B**(2), pp.894-906.

Ryan, G., Pandit, A. and Apatsidis, D. P. (2006) Fabrication methods of porous metals for use in orthopaedic applications. *Biomaterials,* **27**(13), pp.2651-2670.

Sallica-Leva, E., Jardini, A. L. and Fogagnolo, J. B. (2013) Microstructure and mechanical behaviour of porous Ti–6Al–4V parts obtained by selective laser melting. *Journal of the Mechanical Behaviour of Biomedical Materials,* **26,** pp.98-108.

Shi, J. (2007) *Finite element analysis of total knee replacement considering gait cycle load and malalignment*. Ph.D. Thesis, University of Wolverhampton.

Simões, J. A. and Marques, A. T. (2005) Design of a composite hip femoral prosthesis. *Materials & Design,* **26**(5), pp.391-401.

Simone, A. E. and Gibson, L. J. (1998) The effects of cell face curvature and corrugations on the stiffness and strength of metallic foams. *Acta Materialia,* **46**(11), pp.3929-3935.

Smith, M., Guan, Z. and Cantwell, W. J. (2013) Finite element modelling of the compressive response of lattice structures manufactured using the selective laser melting technique. *International Journal of Mechanical Sciences,* **67,** pp.28-41.

Smith, S. W., Estok, D. M. and Harris, W. H. (1998) Total hip arthroplasty with use of second-generation cementing techniques. An eighteen-year-average follow-up study. *The Journal of Bone & Joint Surgery,* **80**(11), pp.1632-1640.

Sotereanos, N. G., Sauber, T. J. and Tupis, T. T. (2013) Modular Femoral Neck Fracture After Primary Total Hip Arthroplasty. *The Journal of Arthroplasty,* **28**(1), pp.196.e7-196.e9.

Sporer, S. M. and Paprosky, W. G. (2006) (iii) Cementless femoral revision: The role of monoblock versus modular stems. *Current Orthopaedics,* **20**(3), pp.171-178.

Stamp, R., Fox, P., O'Neill, W., Jones, E. and Sutcliffe, C. (2009) The development of a scanning strategy for the manufacture of porous biomaterials by selective laser melting. *Journal of Materials Science: Materials in Medicine,* **20**(9), pp.1839-1848.

Stiehl, J. B. (2009) Long-term periprosthetic remodelling in THA shows structural preservation. *Clinical Orthopaedics and Related Research,* **467**(9), pp.2356-2361.

Strano, G., Hao, L., Everson, R. M. and Evans, K. E. (2013) Surface roughness analysis, modelling and prediction in selective laser melting. *Journal of Materials Processing Technology,* **213**(4), pp.589-597.

Stryker (2013). Stryker [online]. [Accessed 20 January 2014]. Available at: <http://www.stryker.com/enus/products/Orthopaedics/HipReplacement/Primary/Cemented/ExeterCemented/index.htm>.

Taylor, M. E., Tanner, K. E., Freeman, M. A. R. and Yettram, A. L. (1996) Stress and strain distribution within the intact femur: Compression or bending? *Medical Engineering & Physics,* **18**(2), pp.122-131.

Terrier, A. (1999) *Adaption of bone to mechanical stress: Theoretical model, experimental identification and orthopaedic application.* Ph.D. Thesis, Swiss Federal Institute of Technology.

Thompson, C.W. and Floyd, R.T. (2011) *Manual of Structural Kinesiology*. 18th ed. McGraw Hill Higher Education.

Turner, C. H., Cowin, S. C., Rho, J. Y., Ashman, R. B. and Rice, J. C. (1990) The fabric dependence of the orthotropic elastic constants of cancellous bone. *Journal of Biomechanics,* **23**(6), pp.549-561.

Viceconti, M., Baleani, M., Squarzoni, S. and Tonil, A. (1997) Fretting wear in a modular neck hip prosthesis. *Journal of Biomedical Materials Research,* **35**(2), pp.207-216.

Viceconti, M., Muccini, R., Bernakiewicz, M., Baleani, M. and Cristofolini, L. (2000) Large-sliding contact elements accurately predict levels of bone-implant micromotion relevant to osseointegration. *Journal of Biomechanics,* **33**(12), pp.1611-1618.

Visible Human Project (1994). US National Library of Medicine [online]. [Accessed 20 December 2012]. Available at: <http://www.nlm.nih.gov>.

Wang, C. J., Yettram, A. L., Yao, M. S. and Procter, P. (1998) Finite element analysis of a Gamma nail within a fractured femur. *Medical Engineering & Physics,* **20**(9), pp.677-683.

Wang, Y., Shen, Y., Wang, Z., Yang, J., Liu, N. and Huang, W. (2010) Development of highly porous titanium scaffolds by selective laser melting. *Materials Letters,* **64**(6), pp.674-676.

Weber, J. N. and White, E. W. (1972) Carbon-metal graded composites for permanent osseous attachment of non-porous metals. *Materials Research Bulletin,* **7**(9), pp.1005-1016.

Weidenhielm, L. R. A., Mikhail, W. E. M., Nelissen, R. G. H. H. and Bauer, T. W. (1995) Cemented collarless (Exeter-CPT) versus cementless collarless (PCA) femoral components: A 2- to 14-year follow-up evaluation. *The Journal of Arthroplasty,* **10**(5), pp.592-597.

Weinans, H., Huiskes, R. and Grootenboer, H. J. (1992) The behaviour of adaptive bone-remodelling simulation models. *Journal of Biomechanics,* **25**(12), pp.1425-1441.

Wheeless, C.R. (2011) Textbook of Orthopaedics [online]. [Accessed 11 February 2014]. Available at: <http://www.wheelessonline.com/ortho/anatomy_of_femur>.

Whiteside, L.A., Amador, D., and Russell, K. (1988) The effects of the collar on total hip femoral component subsidence. *Clinical Orthopaedics and Related Research,* **231,** pp.120-126.

Whiteside, L. A. (1989) The effect of stem fit on bone hypertrophy and pain relief in cementless total hip arthroplasty. *Clinical Orthopaedics and Related Research,* **247,** pp.138-147.

Wieding, J., Souffrant, R., Mittelmeier, W. and Bader, R. (2013) Finite element analysis on the biomechanical stability of open porous titanium scaffolds for large segmental bone defects under physiological load conditions. *Medical Engineering & Physics,* **35**(4), pp.422-432.

Wiles, P. (1958) The surgery of the osteoarthritic hip. *British Journal of Surgery,* **45,** pp.488-497.

Wirth, A. J., Goldhahn, J., Flaig, C., Arbenz, P., Müller, R. and Van Lenthe, G. H. (2011) Implant stability is affected by local bone microstructural quality. *Bone,* **49**(3), pp.473-478.

Wolff, J. L. (1986) The law of bone remodelling. *Springer, Berlin*.

Yan, C., Hao, L., Hussein, A. and Raymont, D. (2012) Evaluations of cellular lattice structures manufactured using selective laser melting. *International Journal of Machine Tools and Manufacture,* **62,** pp.32-38.

Yan, W., Berthe, J. and Wen, C. (2011) Numerical investigation of the effect of porous titanium femoral prosthesis on bone remodelling. *Materials & Design,* **32**(4), pp.1776-1782.

Zeng, S. and Blunt, L. (2013) Experimental investigation and analytical modelling of the effects of process parameters on material removal rate for bonnet polishing of cobalt chrome alloy. *Precision Engineering,* **38**(2), pp. 348-355.

Zimmer (2013) Product information: Versys Epoch Full Coat Hip Stem [online]. [Accessed 5 April 2013]. Available at: <http://www.zimmer.com >.

Related publications

Journals

Hazlehurst, K., Wang, C. and Stanford, M. (2013) The potential application of a Cobalt Chrome Molybdenum femoral stem with functionally graded orthotropic structures manufactured using Laser Melting technologies. *Medical Hypotheses,* **81**(6), pp.1096-1099.

Hazlehurst, K., Wang, C. J. and Stanford, M. (2013) Evaluation of the stiffness characteristics of square pore CoCrMo cellular structures manufactured using laser melting technology for potential orthopaedic applications. *Materials & Design,* **51**, pp.949-955.

Hazlehurst, K., Wang, C.J. and Stanford, M. (2014) A numerical investigation into the influence of the properties of cobalt chrome cellular structures on the load transfer to the periprosthetic femur following total hip arthroplasty. *Medical Engineering and Physics,* **36**, pp. 458-466.

Hazlehurst, K., Wang, C.J. and Stanford, M. (2014) An investigation into the flexural characteristics of functionally graded cobalt chrome femoral stems manufactured using selective laser melting. *Materials & Design,* **60**, pp.177-183.

Conference

Hazlehurst, K., Wang, C.J. and Stanford, M. (2013) *A numerical investigation into the application of an orthotropic porous structure for a femoral stem manufactured using laser melting technology*. In: 19th Congress of the European Society of Biomechanics, 25-28 August 2013, Patras, Greece.